A SYSTEMATIC STUDY OF SELF-DISCHARGE MECHANISMS IN CARBON-BASED, AQUEOUS ELECTROLYTE ELECTROCHEMICAL CAPACITORS

by

Alicia M. Oickle

Submitted in partial fulfilment of the requirements
for the degree of Doctor of Philosophy

at

Dalhousie University
Halifax, Nova Scotia
January 2013

DALHOUSIE UNIVERSITY

DEPARTMENT OF CHEMISTRY

The undersigned hereby certify that they have read and recommend to the Faculty of Graduate Studies for acceptance a thesis entitled "A Systematic Study of Self-discharge Mechanisms in Carbon-based, Aqueous Electrolyte Electrochemical Capacitors" by Alicia M. Oickle in partial fulfilment of the requirements for the degree of Doctor of Philosophy.

Dated: January 21, 2013

External Examiner: _____

Research Supervisor: _____

Examining Committee: _____

_____

_____

Departmental Representative: _____

DALHOUSIE UNIVERSITY

DATE: January 21, 2013

AUTHOR: Alicia M. Oickle

TITLE: A Systematic Study of Self-discharge Mechanisms in Carbon-based, Aqueous Electrolyte Electrochemical Capacitors

DEPARTMENT OR SCHOOL: Department of Chemistry

DEGREE: PhD CONVOCATION: May YEAR: 2013

_____

Signature of Author

TABLE OF CONTENTS

LIST OF TABLES

LIST OF FIGURES

ABSTRACT

This work focused on the study of self-discharge mechanisms of carbon electrochemical capacitor electrodes in 1.0 M H_2SO_4 electrolyte. Electrochemical capacitors have an increasingly important role in the future of energy storage for specific applications due to their high cycle lives, high power capabilities and the ability to use environmentally friendly materials. Remediation of the occurrence of self-discharge – the loss of charge over time when left in open-circuit configuration – must take place before electrochemical capacitors can be used more widely as this diminished potential results in a reduction of stored energy. By examining the now poorly understood causes and mechanisms of self-discharge, beneficial modifications to the electrochemical capacitors systems can be made, improving device performance.

Three-electrode electrochemical set-ups were used to separate self-discharge mechanisms on the negative and positive electrodes. Various electrode and electrolyte reactions were investigated in relation to self-discharge, including Fe-contamination reaction, electrolyte decomposition, oxygen-reduction, carbon oxidation, and carbon surface group development. All experiments were conducted on porous carbon electrodes. It was determined that Fe-contamination increased self-discharge on both carbon electrodes at concentrations $>10^{-3}$ M, and that previously developed planar kinetic models applied to these porous systems. Electrolyte decomposition did not result in increased self-discharge on either electrode. Electrolyte oxygen content must be minimized as oxygen is believed to undergo reduction to hydrogen peroxide on the negative-electrode, resulting in an increase in self-discharge. The carbon electrodes used in this work must be cycled prior to energy storage as the capacitance varies greatly with continued cycling, and the lack of cycling results in increased self-discharge. Additionally, interest in the carbon electrode's surface functionalities resulted in the standardization of the Boehm titration.

LIST OF ABBREVIATIONS AND SYMBOLS USED

Abbreviations

BET	Brunauer-Emmett-Teller theory
EC	Electrochemical Capacitor
ICP-MS	Inductively Coupled Plasma Mass Spectrometry
KHP	Potassium Hydrogen Phthalate
n_{CSF}	Moles of Carbon Surface Functionality
OCP	Open-Circuit Potential
PANI	Polyaniline
PPy	Polypyrrole
PTFE	Polytetrafluoroethylene
RHE	Reversible Hydrogen Electrode
SD	Self-discharge
SHE	Standard Hydrogen Electrode
SSCE	Saturated Sodium Calomel Electrode

Symbols

α	Symmetry factor
A	Area of electrode
c_o	Initial concentration
C	Capacitance
C_{diff}	Differential capacitance
D	Diffusion coefficient
d	Distance between electrode and ions in double-layer
ε	Dielectric constant
ε_o	Permittivity of a vacuum
E^o	Standard reduction potential
F	Faraday's constant, Farad
h	Hour

i_o	Exchange current density
I	Current
m	Mass
ν	Sweep rate
N	Number of electrodes used for standard deviation calculations
P	Power
q	Charge density
Q	Charge
R	Universal gas constant, Resistance
R_s	Solution resistance
σ	Standard deviation
s	Second
τ	Integration constant in equation 7
t	Time
T	Temperature
V	Voltage, Potential
$V_{applied}$	Applied potential
V_{final}	Final potential in self-discharge
V_i	Initial voltage
V_{loss}	Potential lost on open-circuit
V_t	Voltage at time t
z	Ion charge

ACKNOWLEDGEMENTS

To begin, I would like to thank Dr. Heather Andreas for allowing me the opportunity to conduct research in a field in which I am extremely interested. Had Heather not taken a chance on me during my undergraduate degree, I can honestly say I would not have had this amazing research opportunity, and for that, I will be forever grateful. She has been tremendously supportive throughout my years with her group, not only having taught me many things, but her knowledge and patience have been unending, making for an overall enjoyable graduate degree.

I would also like to acknowledge Dr. Russ Boyd, Dr. Jeff Dahn and Dr. Norm Schepp for being members of my graduate supervision committee and for their helpful feedback. Thanks to the Department of Chemistry for the opportunity to continue my scientific education here at Dalhousie University. I would also like to sincerely thank Dr. Keryn Lian from the University of Toronto for taking the time to act as my external examiner.

To the other members of the Andreas research group (Jennifer Black, Michelle Everist, Zachary Cormier, Sarah Goertzen and Justin Tom): you all have been extremely helpful with the discussion of ideas. It is amazing the strong friendships that can grow from spending day in, day out in the same office and lab, and also somehow end up not wanting to kill each other. Special thanks to Anthony Tarasuk for carrying out the open-circuit potential measurements, Katelyn Hopper for assistance with the standardization of the Boehm titration and all the other undergraduate research assistants over the years.

I would like to thank friends and family for their ongoing support over the span of my degree. Putting up with me during the stressful moments isn't always easy. I am also so thankful for my parents for giving me the confidence to even accept the offer to attend graduate school in the first place, and supporting my decisions. You two were always able to keep me level-headed when I began to catastrophize every decision I made along the way. To my fiancé Dave – what more can I say than *Thank You*. You gave me the drive to continue to my goal when I didn't have it inside myself and allowed me to lean on you when research and writing became hard to handle. Your love and support has been unending, and for that I am eternally grateful.

Chapter 1 INTRODUCTION

Electrochemical capacitors, originally patented in the 1950's by Becker,[1] are energy storage devices which have experienced an increase in research interest over the last twenty years.[2, 3] Also known as supercapacitors, ultracapacitors and in certain situations double-layer capacitors, electrochemical capacitors are high power devices with uses in applications such as regenerative braking in hybrid vehicles,[4-6] energy storage from alternative energy sources,[6-8] and uninterruptible power systems for electronics.[9] Compared to other electrochemical energy storage devices,[10] electrochemical capacitors have high power and high cycle lives (> 10^6 cycles) but also lower energy values than fuel cells and batteries.[10] The main difference between these energy storage devices is due to the charge storage method.

Charge can be stored in two ways in electrochemical capacitors: through the formation of an electrochemical double-layer, and through fast reversible redox (Faradaic) reactions called pseudocapacitance.[2, 11] The electrochemical double-layer stores charge through electrostatics at the electrode/electrolyte interface which results in high power due to the fast formation and rearrangement of the double-layer charge (on the order on nanoseconds).[10] Pseudocapacitive reactions are electron transfer reactions which mimic capacitive behavior and result in higher capacitance values than pure double-layer capacitance.[2, 10, 11]

Although electrochemical capacitors have many beneficial characteristics, mentioned above, like all electrochemical energy storage devices, they suffer from a phenomenon called self-discharge – the spontaneous loss of charge at open-circuit configuration.[11] The magnitude of self-discharge is larger for electrochemical capacitors

than for other energy storage devices,[2, 11] and must be investigated to reduce the charge loss. The goal of this research was to undertake a systematic study of the self-discharge mechanisms in carbon-based, aqueous electrolyte systems.

Many materials are examined as electrochemical capacitor electrode materials including carbon, some metal oxides and conductive polymers.[2, 11] Carbon will be described as this was the electrode material used in this work. Carbon is an abundant, versatile element, and is relatively inexpensive compared to other electrode materials.[5, 11] Its low weight and possible high porosity, which can be tailored to the application, are other benefits of carbon electrode materials.[5, 11] The systems studied in this research were carbon electrodes (as both the positive and negative electrode) for use in electrochemical capacitors with acidic aqueous electrolyte. Although carbon electrodes in aqueous electrolyte must be used in a smaller potential window than carbon in organic electrolyte (thereby limiting the energy and power), aqueous electrolyte is advantageous due to its high conductivity and the possible pseudocapacitive reactions with protons.[12]

Five self-discharge mechanisms were proposed and investigated: electrolyte contaminants in the form of Fe (discussed in Chapter 4);[13, 14] the decomposition of the aqueous electrolyte within the potential window resulting in H_2 and/or O_2 evolution (see Chapter 5);[15, 16] O_2 reduction to H_2O_2 or H_2O on the negative electrode (Chapter 5);[15, 16] carbon oxidation to CO or CO_2 (Chapter 7);[17] and heteroatom-containing groups on the carbon surface (so called "carbon surface functionalities") removing charge from the electrodes surface (Chapter 8). By individually validating or disproving the abovementioned self-discharge mechanisms, a better understanding of self-discharge in aqueous electrolyte (primarily H_2SO_4) carbon electrode electrochemical capacitors was

realized. The data shown in Chapter 8 focuses on the effect of carbon surface functionality changes through continued potential cycling on self-discharge; therefore a method to identify these carbon surface groups was needed.

A commonly used chemical method to determine O-containing acidic surface functionalities on carbon samples is the "Boehm titration".[18, 19] Although the Boehm titration procedure is widely used,[20-22] it varies between research groups, making comparison of results between the groups difficult. As a result, the standardization of the Boehm titration was partially undertaken herein (Chapter 6) with a particular focus on the effect of filtering the carbon sample from the reaction base, the optimal agitation method, and the use of dilute titrant (earlier work done by Sarah Goertzen *et. al* related to the optimal method of CO_2 removal and endpoint determination).[23, 24]

Another aspect of this research was the development of an electrochemical identification method for carbon surface functionalities to replace *ex situ* chemical methods such as the Boehm titration. Comparison of Boehm titration results along with cyclic voltammograms and open-circuit measurements were tested on carbon electrodes to attempt to identify a "signature" in open-circuit profiles based on surface functionalities and the oxidation of the carbon surface (Chapter 7).

Background information on the topics and techniques used in this thesis are presented in Chapter 2. Experimental methods are reported in Chapter 3. Chapters 4, 5 and 8 discuss identification of self-discharge mechanisms. Chapter 6 discusses the standardization of the Boehm titration. Chapter 7 examines the effect of continued cycling on the carbon electrodes with regard to redox peak development, and the open-circuit potential data. All conclusions and future work are in Chapter 9.

Chapter 2 BACKGROUND

2.1 Energy Storage Devices

With the recent move towards green-energy technologies,[10, 25, 26, 26-28] such as wind, solar and tidal energy, and the movement away from energy generated from the combustion of fossil fuels, energy storage devices have become of significant interest.[3, 10, 26-30] Since alternative energy sources based on nature cannot be controlled to align with peak usage, the energy must be stored until it is needed. Electrochemical energy storage devices, such as batteries and electrochemical capacitors, are capable of storing the generated energy. Batteries and electrochemical capacitors are similar in many ways: both contain two electrodes, separated by a membrane, in contact with an electrolyte solution.[3, 10, 26] The significant difference between electrochemical capacitors and batteries is in the way each stores charge, however only charge storage in electrochemical capacitors will be discussed as it pertains to the research presented.

2.2 Charge Storage Mechanisms

Charge storage in electrochemical capacitors occurs through two processes: double-layer charging and pseudocapacitance. The mechanisms of these charge storage processes are described in detail below. Generally charge storage is discussed as occurring by either double-layer charging or pseudocapacitance, when in reality, both occur to varying degrees.[11, 31] The magnitude of charge stored per surface atom is five to ten times smaller with double-layer formation than that of a one or two electron pseudocapacitive process,[11] and therefore it is important to understand the charge storage

for both processes. Here, both double-layer charging and pseudocapacitive charging will be discussed separately.

2.2.1 Double-layer Charging

When a material is placed in solution, an inherent surface charge, either positive or negative, develops. Solution ions, of the opposite charge, align at the surface to balance the charge resulting in an electrochemical double-layer.[11, 31] By applying a potential to the material, in this case an electrode, the charge increases resulting in more energy being stored. Representations of a double-layer formed on both a positive and negative electrode can be seen in Figure 2.1. It is important to note that the schematic shown in Figure 2.1 is a very simplified representation of the complex double-layer region. Although there is an excess of one ion at the electrode's surface (anions for the positive electrode, and cations for the negative electrode) there are still oppositely-charged ions near the surface, and the overall solution remains electroneutral.[31]

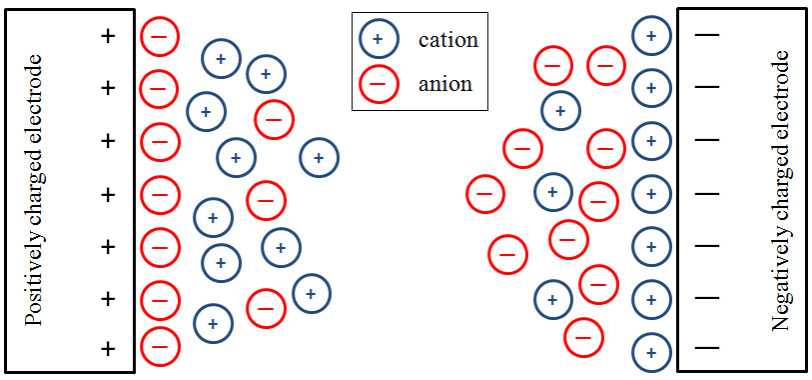

Figure 2.1: Simple schematic of an electrochemical double-layer formed on a planar electrode. Both a positive electrode (left), and negative electrode (right) are shown.

The formation and relaxation of the electrochemical double-layer results in high power values, *ca.* 100 W kg^{-1}.[32] The high power of electrochemical capacitors is due to the double-layer formation/relaxation being a fast process, on the order of nanoseconds.[10] Although double-layer formation is a fast process, it does not store as much charge per surface atom as redox processes, and therefore results in lower energy (1 – 10 Wh kg^{-1})[32] compared to devices based on redox reactions. Since the double-layer electrochemical capacitors do not rely on chemical reaction, they have a long cycle-life (>100 000) before failure.[11, 32]

The cyclic voltammogram of a double-layer electrochemical capacitor is similar to the cyclic voltammogram of a conventional capacitor.[11, 31] In a conventional capacitor, when the applied voltage (or potential) switches direction, the current changes in sign but not magnitude, resulting in a rectangle centered about the zero-current axis.[11] With an electrochemical capacitor based on a high-surface-area electrode there is often a dependence of current on the applied potential, resulting in a cyclic voltammogram that is a mirror-image about the zero-current axis but not ideally rectangular.

2.2.2 Pseudocapacitance

The term "pseudocapacitance" refers to charge passed across the double-layer through highly reversible Faradaic (redox) reactions, electrosorption, or intercalation processes.[11, 31, 33] Although electron transfer reactions occur, the equilibrium established by the fast reversible reactions allows the system to be treated electrochemically like a capacitor; at each potential there is a characteristic ratio of concentrations that satisfies the Nernst equation.[11, 33] The cyclic voltammogram of a pseudocapacitive material is

similar to that of a double-layer material where the current does not vary significantly with voltage (or potential) and is a mirror image about the zero-current axis.

Electrochemical capacitors based on pseudocapacitive materials include transition metal oxides[33-36] and conductive polymers.[28, 37] Transition metal oxide electrochemical capacitors have higher energy values than electrochemical double-layer capacitors, however the energy is still less than most battery technology.[10, 11] Like double-layer capacitors the devices based on pseudocapacitive materials are still higher power than other electrochemical energy storage devices.[10, 11]

2.3 Capacitance, Energy, and Power of Electrochemical Capacitors

When discussing electrochemical capacitors, and energy storage devices in general, there are certain parameters which are important in assessing the devices. Simply put, capacitance (C) is the ability to store charge (Q) at a given potential (V) and can be represented by equation 1[11, 31]

$$C = \frac{Q}{V}. \quad (1)$$

Capacitance can also be calculated from the following equation:

$$C = \frac{\varepsilon_o \varepsilon A}{d}, \quad (2)$$

where ε_o is the permittivity of a vacuum, ε is the dielectric constant of the solvent in the double-layer, A is the electrode area and d is the distance between the electrode and the ions in the double-layer.[31] It can be seen that either increasing the area of the electrode, or decreasing the distance between the electrode and the electrolyte ion in the double-layer will result in an increase in capacitance. To increase capacitance, generally high-surface-area electrode materials are used.

It is difficult to accurately measure the surface area of a porous electrode material that is used in charge storage, as well as to accurately determine the distance between the ions of the double-layer from the electrode. Therefore, it is necessary to calculate capacitance in ways that do not rely on these aforementioned values. Capacitance and differential capacitance (capacitance values at each potential) can be calculated from various electrochemical techniques such as constant current charge/discharge, however since cyclic voltammetry is used extensively in this thesis, it is the focus of capacitance calculations. A practical method for calculating the differential capacitance (C_{diff}) is to divide the response current (I) of a cyclic voltammogram by the sweep rate (ν),

$$C_{diff} = \frac{I}{\nu}. \tag{3}$$

The capacitance value of an electrochemical capacitor is very important since energy (E) is directly related to both capacitance and voltage[5, 11]

$$E = \frac{1}{2}CV^2. \tag{4}$$

From equation 4 it can be seen that an improvement in either the capacitance or voltage window results in an improvement in the energy value. Increasing the voltage also effects the maximum power (P_{max}) of an electrochemical capacitor,[5, 11]

$$P_{max} = \frac{V^2}{4R_s} \tag{5}$$

where R_s is the solution resistance. All the factors mentioned above, such as area, dielectrics of solution, voltage window and solution resistance are dependent on the choices of electrode materials and electrolyte. The work presented later in this thesis focuses on a high-surface-area carbon electrode to increase the capacitance, in aqueous electrolyte which has a high dielectric constant and low solution resistance.

2.4 Electrode Materials

Electrochemical capacitors have been developed using many electrode materials, from multiple forms of carbon, to transition metal oxides, and conductive polymers. Carbon is widely used for a number of reasons including its high conductivity, relatively inexpensive cost, many possible forms and surface areas, and high abundance.[2, 5, 28] Additionally, carbon is air stable and able to be used in a wide variety of electrolytes, including acidic and basic aqueous electrolyte, organic electrolyte and ionic liquids.[38] Before discussing carbon, transition metal oxides and conductive polymers will be briefly discussed.

2.4.1 Transition Metal Oxides

Transition metal oxides electrodes are based on pseudocapacitive reactions (see section 2.2.2), that occur on electrode materials such as ruthenium oxide (RuO_2),[33, 36, 39-42] manganese oxide (MnO_2)[43-46] and iridium oxide (IrO_2).[11, 47-49] These pseudocapacitive materials have been studied since the late 1970's due to their high capacitance (*ca.* 770 F g^{-1} for RuO_2)[50] and highly reversible Faradaic reactions.[4, 11, 28] In the typical aqueous electrolyte window (0 – 1.2 V), $RuO_2 \bullet xH_2O$ has three oxidation states and therefore passes multiple electrons per surface atom, resulting in more charge stored than double-layer charge storage. Although these pseudocapacitive electrochemical capacitors have higher capacitance values than double-layer electrochemical capacitors, the cost of many of the transition metals limits the application, and those with lower costs generally have other issues limiting application, such as poorer reversibility and smaller potential windows. Therefore work has focused on both making composite electrodes where metal

oxides are deposited onto other, less expensive materials such as carbon,[28, 34] and also the use of other pseudocapacitive electrode materials such as conducting polymers.[37]

2.4.2 Electronically Conducting Polymers

Polymers can also be used as electrode materials for electrochemical capacitors. Conductive polymers such as polyanaline (PANI), and polypyrrole (PPy) are commonly studied for use as electrodes in electrochemical capacitors.[37, 51] Electronically conducting polymers are capable of higher capacitance values (*ca*. 150 F g^{-1} for PANI)[52] than purely double-layer electrochemical capacitors due to the diffusion of ions within the polymer allowing the entire polymer to be used for charge storage, unlike activated carbons. Unfortunately, conductive polymers do not have the stability when compared to other electrode materials over long-term cycling.[32, 37, 53] The instability is partly due to volume changes with charging that results in a decrease in capacitance over time, and eventual mechanical failure.[32, 37, 53] Research is also being done on making conductive polymer composites with carbons (similar to composites seen in metal oxide literature) to increase the capacitance values, as well as alleviate the instability due to swelling.[37, 53-56]

2.4.3 Carbon

An ideal material for use in energy storage, carbon can be used as negative electrodes in Li-ion batteries,[57] and in fuel cells as catalyst supports,[58] as well as for electrodes in electrochemical capacitors.[5] Pure carbon stores charge through double-layer charging only.[11] The activation process of carbons increases the surface-area to increase double-layer charge storage and, sometimes, to create surface groups.[59]

Activated carbons are generally high-surface-area (can be up to 2500 m^2 g^{-1}), and high-porosity materials produced via either thermal activation, or chemical activation of a raw material.[59] The raw material varies widely and can be from any carbonaceous material, including, but not limited to, rice hull,[21, 60, 61] coconut shells,[62, 62-64], olive stones,[65-67] bagasse,[61, 68, 69] petroleum pitch[70] and black ash.[59] In addition to a variety of precursor materials, the form of the activated carbon product can vary widely from powder to fibres, fibres woven into cloth, and felts.[71] The various carbon precursors result in activated carbons of different porosities, surface areas and heteroatom content.

Physical (thermal) activation is a treatment where a charred material is heated to high temperatures *ca.* 700 - 1100 °C and then exposed to an oxidizing gas such as oxygen, carbon dioxide or steam.[38, 59, 71-74] Physical activation is considered a two-step process where the precursor material is first heated to high temperatures to remove oxygen or hydrogen content, and then treated with the oxidizing gas.[75] Surface oxides can then be formed by exposure to air at temperatures *ca.* 400 °C.[59] By varying the temperature, the oxidizing agent and the length of exposure to these various conditions, the porosity of the carbon can be modified.[5] During the gasification process pores develop, increasing the surface area.[5, 71]

Chemical activation is considered a one-step activating process where a carbon precursor is exposed to a chemical agent such as strong base (KOH, NaOH),[60, 76] strong acid (H_3PO_4, HNO_3)[77-80] or oxidizing agents (*e.g.* H_2O_2)[78, 81, 82] Since a chemical reagent is used, lower temperatures can be used in comparison to thermal activation, resulting in more controlled pore development.[59, 83] Depending on the activation reagents, the surface areas, porosity and thereby the capacitance values, vary significantly.[69, 80]

Although high-surface-area carbon materials can be made from both activation methods, not all surface area is useable for charge storage.[5, 84] It might be expected that capacitance would increase with increasing surface area, however this trend is not directly seen in the literature, meaning there is likely parts of the electrode not accessed by the electrolyte.[5, 84, 85] Pores adapted to the electrolyte ion size are considered the best for charge storage since ultramicropores (< 0.7 nm)[5, 85] may not be accessible to electrolyte ions and therefore, double-layer charging cannot occur on a portion of the electrode. Another important consideration that may affect the charge stored is surface groups on the carbon surface that may be capable of Faradaic reactions.

2.4.3.1 Oxygen-containing Carbon Surface Functionalities

Carbon materials may contain heteroatoms, in the form of oxygen,[86-92] nitrogen,[22, 93, 94] sulphur,[19, 95] and phosphorus[21, 80, 96] incorporated into the carbon materials along the edge of the graphene sheet. The most common surface groups, also called carbon surface functionalities, are surface oxides in the forms of ethers, phenols, lactones and lactols, carboxylic acids and anhydrides, as well as quinones, pyrones, esters, and ketones.[97, 98] Examples of possible oxygen-containing carbon surface functionalities can be seen in Figure 2.2. Carbon surface functionalities can add to the overall capacitance through pseudocapacitance via highly reversible redox reactions. Quinones are the most well-known surface group to add pseudocapacitance to carbon electrodes.[89-91]

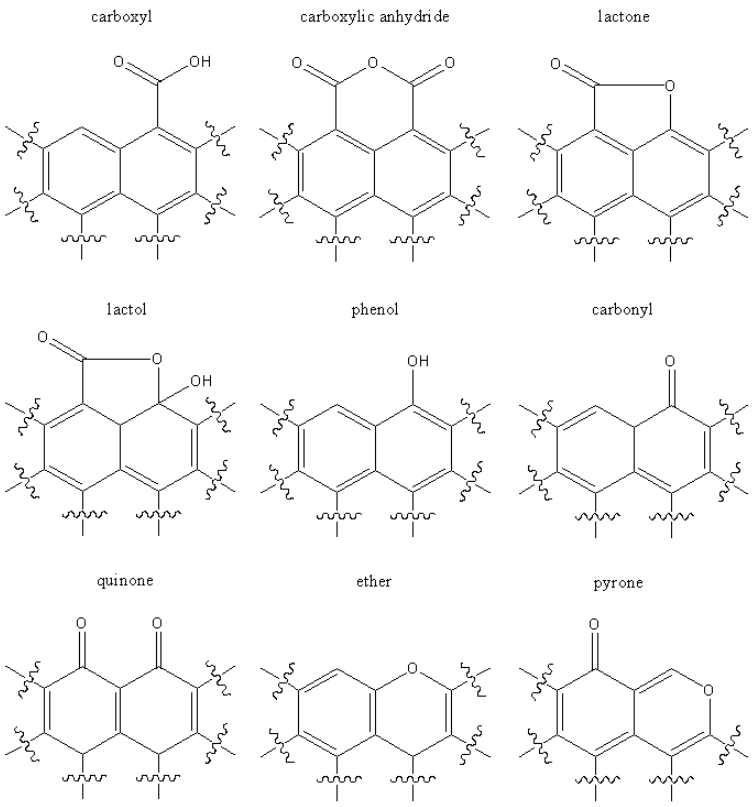

Figure 2.2: Possible oxygen-containing functional groups on the edge of carbon materials. Modelled after references 19 and 98.

Through identification of carbon surface functionalities their role in both pseudocapacitance and self-discharge (described below) can be examined. It is thought that by identifying redox active surface functionalities on the electrode material may increase the overall capacitance through highly reversible Faradaic reactions. However, only electroactive surface groups within the experimental potential window will add to the increase in capacitance through pseudocapacitance. These Faradaic reactions, such as quinones,[89-91] are able to pass electrons (as seen in R1) resulting in increased charge storage compared to double-layer charging. By increasing the electroactive carbon surface functionalities content, more charge can be stored on the carbons surface. It is possible that carbon surface functionalities may also remove charge from the electrode's

surface through Faradaic reactions causing self-discharge (described in section 2.6).[99-101] It has yet to be determined whether surface groups are beneficial to aqueous electrochemical capacitors through an increase in charge storage, or detrimental to electrochemical capacitors by increasing the self-discharge of carbon electrodes.

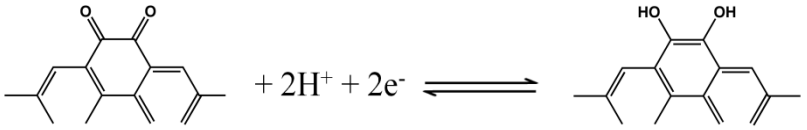

(R1).

2.4.3.2 Boehm Titration

A commonly used method to identify acidic oxygen-containing carbon surface functionalities is the so-called "Boehm titration".[86, 92, 102] The Boehm titration works by placing carbon samples in bases of increasing basicities. Sodium bicarbonate ($NaHCO_3$), the weakest reaction base, neutralizes carboxylic groups, while sodium carbonate (Na_2CO_3) neutralizes both carboxylic groups and lactonic groups, and sodium hydroxide (NaOH) neutralizes carboxylic, lactonic and phenolic groups. The population of each group of carbon surface functionalities is found by difference between the number of carbon surface functionalities determined by each reaction base.[102]

While the Boehm titration is a widely used technique and the 1966 Boehm paper is typically referenced, most research groups do not state their methodology for carrying out the Boehm titration in detail.[66, 79, 96, 103-106] As such, the results obtained from different research groups cannot be compared accurately. The Boehm titration will be partly standardized in this thesis.

2.5 Electrolyte

Another important component of electrochemical capacitors is the choice of electrolyte: aqueous, organic or ionic liquids.[5] When selecting an electrolyte there are multiple criteria that must be met and there is generally a trade-off in one category for another. Parameters of interest include conductivity,[7, 11, 38] viscosity,[107-109] matching the electrolyte ion size to the electrode's pore size of the electrode material,[85, 110, 111] and the electrolyte decomposition potentials which determines, in conjunction with the electrode material, the potential window.[28, 38, 108]

The high conductivity and low viscosity of acidic aqueous electrolytes make them attractive, although the potential limits are lower (1.23 V)[112] compared to other electrolytes.[5] Aqueous electrolytes have lower potential windows due to water decomposition at potentials above 1.23 V vs. SHE to oxygen,[112] and below 0.0 V vs. SHE, to hydrogen.[112] The use of an acidic aqueous electrolyte is desirable as the quinone/hydroquinone redox couple (see reaction 1 in section 2.4.3.1), that may be present on some carbons used as electrodes, is dependent on protons and can add a significant amount of charge storage to carbon electrodes in acidic aqueous electrolytes. With the same carbon electrode material and only changing the acidic aqueous electrolyte to basic aqueous electrolyte results in a change of specific capacitance values from 250 F g^{-1} to 150 F g^{-1}, due largely in part to the proton-based quinone/hydroquinone redox reaction.[84, 93, 113] Examples of common aqueous electrolytes are H_2SO_4 and KOH.

Organic electrolytes are generally the electrolyte of choice for commercially available carbon-based electrochemical capacitors (*i.e.* Maxwell Technologies and Cap-XX), in part due to larger voltage windows (*ca.* 2.5 V).[71, 100] The increase in voltage

directly increases the energy of the system as seen in equation 4, making a larger voltage advantageous. However, the use of an organic electrolyte rather than an aqueous electrolyte results in a smaller dielectric constant,[112, 114] which from equation 2, results in a smaller capacitance. Organic electrolytes are also generally more resistive than aqueous electrolytes[93, 114] resulting in a lower power compared to aqueous systems due to the inverse relationship as seen in equation 5. Since trace amounts of water can significantly decrease the voltage window and thereby the energy, organic electrolytes must be highly pure which increases the cost. Commonly used organic electrolytes are combinations of tetraalkylammonium cations, such as tetramethylammonium (Me_4N^+), and tetraethylammonium (Et_4N^+), with tetrafluoroborate (BF_4^-), or hexafluorophospate (PF_6^-) anions dissolved in acetonitrile or propylene carbonate.[114]

Another class of electrolytes examined for use in electrochemical capacitors are ionic liquids. Ionic liquids are salts composed of a bulky organic cation and a counter anion that are thermally stable as liquids at, or close to, room temperature.[108, 115] Ionic liquids are of interest due to an additional increase in the voltage window, up to 5.0 – 6.0 V for commercially available salts and examples in the literature.[108, 115, 116] Although a larger voltage window is advantageous to increase the energy, ionic liquids are extremely viscous and have a much lower dielectric constant than other electrolytes. Examples of ionic liquids used as electrolytes in electrochemical capacitors are alkyl-substituted imidazolium, pyridinium or tetraalkylammonium cations with halogenated aluminate, or cuprate anions, or bis(trifluoromethanesulfonimide) ($[N(CF_3SO_2)_2]^-$) anions.[117] To increase the conductivity, and therefore reduce the viscosity, organic solvents like acetonitrile or carbonates are generally added.[108, 115, 117]

2.6 Self-discharge

When an electrochemical capacitor is charged and left in open-circuit configuration there is a thermodynamic "driving force" to lose charge over time since the Gibbs' energy, is higher in the charged state compared to the Gibbs' energy in the discharged state.[11] The difference in Gibbs' energy results in a loss of voltage (and therefore loss of energy) over time, which is called self-discharge.[11] Ideally, when the electrode is charged to a final potential it would stay constant, and then remain at that potential over time. However, what is actually seen is a potential decay over time, as illustrated in Figure 2.3.

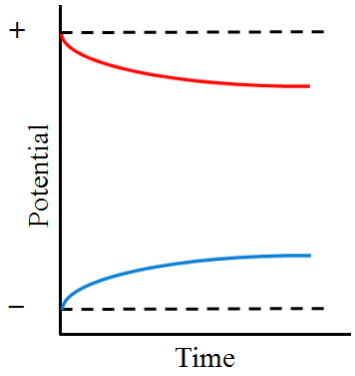

Figure 2.3: Schematic of self-discharge (loss of potential) from both a positive (—) and (—) negative electrode. Ideal potential over time behaviour is represented by (– –).

An electrochemical capacitor in open-circuit configuration does not have an external circuit through which current can flow. As a result, the potential loss must be due to a species or reaction within the electrochemical capacitor. Faradaic reactions causing self-discharge can therefore result from dissolved impurities in the electrolyte, the electrolyte decomposing, or the electrode material itself undergoing Faradaic reaction(s). These Faradaic reactions determine the "shelf-life" of an electrochemical capacitor through the voltage (and therefore energy) available over prolonged time;

Faradaic reactions also therefore limit the performance of an electrochemical capacitor.[11] A positively-charged electrode in H_2SO_4 electrolyte would form a double-layer with the HSO_4^- ions adsorbed to the electrode. If there is a redox-active species in the electrolyte and the positive electrode's potential is above the equilibrium potential, then the redox species (M^{2+}) would oxidize at the electrode's surface, thereby donating an electron to the electrode's surface, decreasing the charge and releasing a HSO_4^- into solution. A generalized form of a carbon electrode in sulphuric acid with a redox reaction discharging the electrode is shown in R2. Note *n* is large (*ca.* 10^{19} electrons calculated from 0.18 e^- per atom,[11] an atom density of 10^{15} atoms cm^{-2},[11] and a surface area of an electrode *ca.* 2.5 x 10^5 cm^2).

$$C^{n+}_{(surface)} + n HSO_{4\,(ads)}^{-} + M^{2+}_{(aq)} \rightarrow$$

$$C^{(n-1)+}_{(surface)} + (n-1) HSO_{4\,(ads)}^{-} + M^{3+}_{(aq)} + HSO_{4\,(aq)}^{-} \qquad \text{(R2)}$$

Conversely, a negatively-charged electrode in H_2SO_4 electrolyte would form a double-layer with the H^+ ions adsorbed to the electrode's surface. If a redox species is present in the electrolyte and the negative electrode's potential is below the equilibrium potential of the redox species, then the oxidized species (M^{3+}) would reduce at the electrode's surface, shown in R3. The reduction reaction would remove an electron from the electrode's surface, again decreasing the charge and releasing a proton into solution.

$$C^{n-}_{(surface)} + n H^{+}_{(ads)} + M^{3+}_{(aq)} \rightarrow C^{(n-1)-}_{(surface)} + (n-1) H^{+}_{(ads)} + M^{2+}_{(aq)} + H^{+}_{(aq)} \qquad \text{(R3)}$$

Self-discharge is one of the major limiting factors impeding the further applications of electrochemical capacitors. By determining the mechanisms of self-discharge, modifications can be made to the devices to increase the performance and make electrochemical capacitors a more viable electrochemical storage device option.

2.6.1 Conway's Kinetic Models of Self-discharge

Since Faradaic processes are the cause of self-discharge, and these Faradaic species are not present in purely double-layer electrochemical capacitors, self-discharge should theoretically not occur. Due to the chemistry of the electrochemical system, such as impurities from electrode material provenance, Faradaic reactions can occur and this results in a decrease in voltage.[11] Conway *et al.* developed three kinetic models to determine the mechanism of self-discharge;[118, 119] note that these equations were derived for a planar electrode surface. The work presented later is on highly porous electrode surfaces, and so it might be expected that these models would not hold for porous systems: however, these equations are still used to determine the method of self-discharge in the following chapters, but caution is used in the analysis based on these models. The three diagnostic kinetic cases are shown below.

I. Self-discharge caused by an activation-controlled Faradaic reaction where the electron transfer is the rate-determining step. For example, high concentrations of impurities such as Fe^{2+}/Fe^{3+} undergoing oxidation/reduction, reactions for the decomposition of electrolyte, or the redox reaction of a carbon surface group all would be expected to result in a linear voltage (V) versus log t:

$$V_i - V_t = \frac{-RT}{\alpha F} \ln\left(\frac{\alpha F i_o t}{RTC} + \alpha F C \tau\right) \qquad (6)$$

where V_t is the voltage at a specific time (t), V_i is the initial voltage, R is the universal gas constant, F is Faraday's constant, i_o is the exchange current density, α is a symmetry factor, T is temperature, C is capacitance and τ is the integration constant.[118, 119]

II. Self-discharge caused by a diffusion-controlled Faradaic reaction where the electron transfer is fast and the movement of the species to the electrode is the rate-determining step. Low concentrations of redox species such as $Fe^{2+}/Fe^{3+,}$ or dissolved O_2 are examples of diffusion-controlled self-discharge. Self-discharge plots would be linear when plotting voltage versus $t^{½}$:

$$V_i - V_t = \frac{2zFAD^{½}\pi^{½}c_o}{C} t^{½} \quad (7)$$

where z is the charge of the ion, A is the electrode area, D is the diffusion coefficient, and c_o is the initial concentration.

III. Self-discharge arising from an "ohmic leakage", or short-circuit leakage from one electrode to another would give a linear plot with ln V versus t:

$$\ln V_t = \ln V_i - \frac{t}{RC} \quad (8)$$

where R is the ohmic load resistance.[118, 119]

Of the three diagnostic cases derived by Conway *et al.*,[118, 119] only I and II are possible in the laboratory conditions used for the work in this thesis. Since three-compartment cells (individual compartments for the reference electrode, counter electrode and working electrode) do not allow contact between the electrodes to create a short-circuit, mechanism III cannot occur. The prevention of mechanism III is an engineering issue rather than a chemical one and therefore, mechanism III will not be used in subsequent data analysis.

2.6.2 Charge Redistribution

When a porous electrode is charged the potential at the electrode's external surface (the pore mouth) responds more quickly than the potential at the pore base deeper within the electrode material.[120-122] As the cell is switched to open-circuit configuration, there is a distribution of potentials along the electrode's surface down the pores. The electrode's potential gradient must equalize through the movement of charge along the pore's surface until the surface charge is equal at all positions (see Figure 2.4). As a result of this potential equalization, the charge at the pore mouth moves deeper into the electrode material. Since the potential is measured at the external electrode surface (the pore mouth), this also results as a loss of potential on switching to open-circuit configuration. This phenomenon is called charge redistribution.

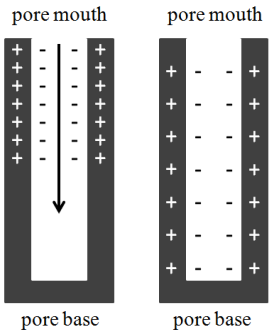

Figure 2.4: Schematic of the charge placed on a pore during charging (left) and charge movement (arrow) on open-circuit as charge equilibrates (right).

It has previously been determined that charge redistribution in porous systems results in a profile similar to the activation-control Conway mechanism (a linear plot of potential versus log time, after an initial plateau).[118, 123] This means that when data are analyzed, and found to be linear versus log time it could be either an activation-controlled self-discharge mechanism (mechanism I) or charge redistribution.[123]

Charge redistribution results in an apparent loss of potential, although it is truly a

rearrangement of charge throughout the electrode. In porous systems it is difficult to separate the amount of charge loss due to charge redistribution from that lost from a Faradaic self-discharge reaction. Charge redistribution can be minimized by a potential holding step to ensure a smaller potential loss when switching to open-circuit configuration. A balance must be found when studying the self-discharge processes of a porous system, because any redox species causing self-discharge processes may also be depleted during the charge redistribution minimization step (*i.e.* a potential hold step).

2.6.3 Self-discharge Measurements

Significant research from many research groups has been undertaken on carbon electrochemical capacitors in regards to increasing capacitance,[73, 93, 124-131] energy,[111, 132-135] and power values.[4, 50, 135-137] However, research to specifically understand the causes of potential loss are much less common in the literature.[13, 118, 119, 138-144]

The research presented in this thesis focused on a systematic approach to determining causes of self-discharge. This approach involved predicting the possible outcomes if a given mechanism was causing self-discharge and then determining if the experimental data matched the predicted effect. In the proposed self-discharge reactions (see Reactions 2 and 3), there is an uptake/release of ions along with the transfer of electrons. In an electrochemical capacitor (or two-electrode system) the requirement of charge neutrality in the electrolyte ensures that the kinetics of the overall self-discharge for the system is limited by the slower of the self-discharge reactions.[11] The research began with external contamination in the form of Fe-contamination in the electrolyte causing self-discharge (section 2.6.3.1), then moved to the electrolyte possibly causing

self-discharge in the form of water decomposition (section 2.6.3.2), and oxygen reduction (section 2.6.3.3), and finally to the electrode itself undergoing Faradaic reactions as a possible self-discharge mechanism (section 2.6.3.4 and 2.6.3.5).

2.6.3.1 Fe-contamination

A possible self-discharge mechanism discussed in the literature by the Kazaryan group has focused on external contaminants such as Fe,[13, 139] Ti and Mn,[141] discharging an asymmetric electrochemical capacitor system. An asymmetric system means the positive and negative electrodes are made from different materials. In Kazaryan's system only the negative electrode examined was carbon-based as the positive electrode was a PbO_2 battery-type electrode.[13] A schematic representation of external contamination causing loss of charge is shown in Figure 2.5.

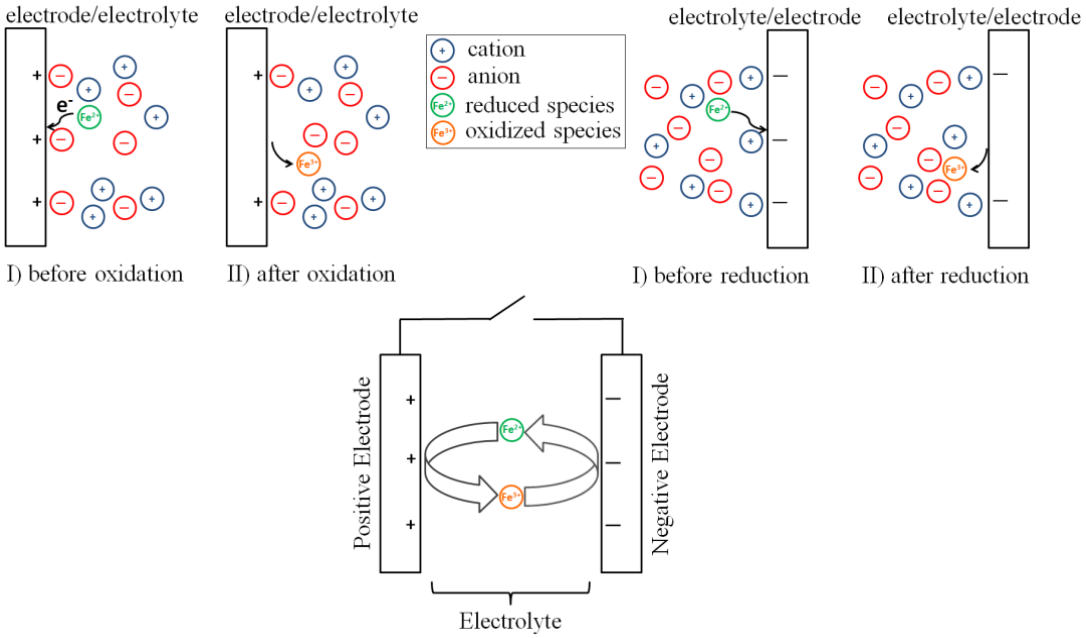

Figure 2.5: Schematic of Fe electrolyte electrochemical capacitor. The left two panels show the oxidation process including double-layer charging, and the right two panels show reduction. The bottom shows the Fe-shuttle mechanism without the solution ions.

Similar to the reaction shown in Reaction 2, a more specific oxidation reaction can be written for Fe-contamination as the redox-active species, and is shown in Reaction 4. With a positively-charged carbon electrode, the anions (HSO_4^-) are adsorbed to the surface resulting in an electrochemical double-layer. When the Fe^{2+} comes into contact with the electrode's surface, the Fe^{2+} is oxidized to Fe^{3+} and an electron is transferred to the carbon surface. The transfer of the electron results in a decrease in both the positive charge and potential and a HSO_4^- desorbing from the electrode's surface.

$$C^{n+}_{(surface)} + nHSO^-_{4\,(ads)} + Fe^{2+}_{(aq)} \rightarrow$$

$$C^{(n-1)+}_{(surface)} + (n-1)HSO^-_{4\,(ads)} + Fe^{3+}_{(aq)} + HSO^-_{4\,(aq)} \qquad \text{(R4)}$$

A similar reduction reaction can be written for the negative electrode, as seen in Reaction 5. When the carbon electrode is negatively-charged, the H^+ cations adsorb to the electrode's surface and create an electrochemical double-layer. When the Fe^{3+} comes into contact with the negative surface, the surface donates an electron to the Fe^{3+}, thereby reducing it to Fe^{2+}. The donation of the electron from the surface results in an H^+ desorbing from the surface and there is an overall loss of negative charge.

$$C^{n-}_{(surface)} + nH^+_{(ads)} + Fe^{3+}_{(aq)} \rightarrow C^{(n-1)-}_{(surface)} + (n-1)H^+_{(ads)} + Fe^{2+}_{(aq)} + H^+_{(aq)} \qquad \text{(R5)}$$

After the Fe^{2+} diffuses to the electrode's surface and undergoes oxidation (see Reaction 4), the oxidized contaminant (Fe^{3+}) can no longer undergo a reaction at this electrode as the Fe^{3+} is fully oxidized. However, it is possible that the Fe^{3+} can diffuse to the negative electrode where it can undergo reduction, and thereby discharge the negative electrode (Reaction 5). This process of continually discharging both electrodes is called a "redox shuttle" reaction.

Kazarayn *et al.* have shown that at relatively high Fe concentrations (10^{-2} to 10^{-1} M), Fe can enhance self-discharge on the negative electrode.[13] They have also shown that Fe has a much greater effect on the rate of self-discharge than other common metal impurities, such as Ti or Mn.[141] It is of interest to note that Ti and Mn-based Faradaic reactions are not possible within the potential window under study in this thesis and therefore the focus was on Fe-contamination.[112] Additionally, Fe-contamination has not yet been studied on a positive carbon electrode and since the reactions on the positive and negative electrode can vary, it is important to study both independently.

2.6.3.2 Electrolyte Decomposition

Electrolyte decomposition at potentials outside the region of electrolyte stability is a common problem in electrochemical systems using organic electrolytes, including organic-based electrochemical capacitors.[100, 145-147] Water decomposition has not been specifically studied as a possible self-discharge mechanism for electrochemical capacitors using aqueous-based electrolytes. The possibility of electrolyte decomposition occurring as a side reaction when aqueous-based electrochemical capacitors are charged near the maximum voltage has been previously mathematically modelled by Pillay and Newman to predict the diminished performance based on these side reactions.[15] Pillay and Newman suggested, with reservations, that although the potentials of the electrochemical capacitor electrodes stay within the thermodynamically stable potential window for water (0.00 – 1.23 V based on standard conditions at 298 K), water may still decompose to evolve oxygen or hydrogen due to low concentrations of oxygen and hydrogen in the electrolyte, leading to a loss in electrode charge.[15]

Although Pillay and Newman[15] were referring to water electrolysis as a side-reaction occurring concurrently with electrochemical capacitor charging, the suggested water electrolysis could also be a cause of self-discharge. If the necessary potentials for water electrolysis are reached, as would be expected for a charged electrochemical capacitor, water electrolysis on the electrodes would cause the electrochemical capacitor to spontaneously discharge (self-discharge). On the positive electrode, the evolution of O_2 from H_2O (Reaction 6) would provide electrons to the electrode which would discharge the positive electrode.[112]

$$C^{n+}_{(surface)} + nHSO^-_{4\,(ads)} + 2H_2O_{(aq)} \rightarrow$$

$$C^{(n-4)+}_{(surface)} + (n-4)HSO^-_{4\,(ads)} + 4HSO^-_{4\,(aq)} + O_{2(aq)} + 4H^+_{(aq)} \quad \text{(R6)}$$

On the negative electrode, the evolution of H_2 from the protons in the acidic electrolyte (Reaction 7) will cause the negative electrode to be discharged. [112]

$$C^{n-}_{(surface)} + nH^+_{(ads)} + 2H^+_{(aq)} \rightarrow C^{(n-2)-}_{(surface)} + (n-2)H^+_{(ads)} + 2H^+_{(aq)} + H_{2(aq)} \quad \text{(R7)}$$

Thus, the modeling by Pillay and Newman supports the possibility that water decomposition may be a cause of self-discharge in aqueous electrochemical capacitors.[112]

2.6.3.3 Oxygen Reduction

Oxygen reduction using catalysts has been extensively studied for fuel cell research because O_2 reduction occurs at the cathode of fuel cells.[17, 148, 149] Pure carbon electrodes along with carbon electrodes with Pt have been used for O_2 reduction to H_2O_2 (Reaction 8),[148] with decreased performance over time.[17, 148]

$$O_2 + 2H^+ + 2e^- \rightarrow H_2O_2 \qquad E^\circ = 0.69\ V \qquad \text{(R8)}$$

Since oxygen reduction is possible on carbon electrodes at the potentials reached in electrochemical capacitors, this reaction is also a possible self-discharge reaction. If O_2 reduction was occurring in the electrochemical set-up employed in the work presented in this thesis, oxygen would be removing electrons from the negatively-charged electrode which would thereby discharge the electrode (Reaction 9)

$$C^{n-}_{(surface)} + nH^{+}_{(ads)} + O_{2(aq)} + 2H^{+}_{(aq)} \rightarrow$$

$$C^{(n-2)-}_{(surface)} + (n-2)H^{+}_{(ads)} + 2H^{+}_{(aq)} + H_2O_{2(aq)} \qquad \text{(R9).}$$

Therefore, the O_2-reduction reaction must be studied to determine if there is any effect on the negative electrode of carbon electrochemical capacitor systems.[112]

2.6.3.4 Carbon Electrode Oxidation

Carbon oxidation (or "carbon corrosion") is a common problem in fuel cell catalysts, when, in the presence of a Pt catalyst and a high applied potential the carbon support oxidizes to CO or CO_2.[17, 150] However, carbon oxidation has yet to be significantly studied in electrochemical capacitors, nor has it been examined as a cause of self-discharge. Carbon corrosion is thermodynamically viable in the potential window used in aqueous electrochemical capacitors, as seen by the standard reduction potential of the following reaction:[59, 151, 152]

$$C + 2H_2O \rightarrow CO_2 + 4H^+ + 4e^- \qquad E^\circ = 0.207\ V \qquad \text{(R10).}$$

Since the reaction kinetics are slow,[152] carbons are commonly exposed to potentials above 0.207 V, however, it is possible that at higher potentials the carbon is oxidized to CO_2 resulting in a decrease in charge, as shown in Reaction 11:

$$C^{n+}_{(surface)} + nHSO^-_{4\,(ads)} + 2H_2O_{(aq)} \rightarrow$$

$$C^{(n-4)+}_{(surface)} + (n-4)HSO^-_{4\,(ads)} + 4HSO^-_{4\,(aq)} + CO_{2(aq)} + 4H^+_{(aq)} \quad \text{(R11)}.$$

For a positively-charged electrode, the carbon electrode forms a double-layer with the HSO_4^- anions in the electrolyte. Water can then come to the surface and the electrode itself can be oxidized to CO_2. As a result, the positive electrode has now decreased in charge, and this would be self-discharge caused by carbon oxidation. It has been reported that the oxygen surface groups (see section 2.4.3.1) greatly reduce carbon corrosion,[153, 154] and are therefore an important parameter to investigate (see sections 2.4.3.1 and 2.6.3.5).

The cyclic voltammograms of many carbon electrodes in acidic aqueous electrolyte exhibit a significant oxidation wave at potentials above *ca.* 0.7 V during the first cycle which diminishes with increased cycle numbers.[59, 153, 155-158] The oxidation wave is generally attributed to carbon oxidation to carbon dioxide, which then, having left the surface, is unable to be reduced again and therefore is not seen in the cathodic sweep of the cyclic voltammogram.[153, 155] Since the potentials applied in the cyclic voltammogram are similar to the potential of the positive electrode, the processes occurring at the higher potentials of the cyclic voltammogram would also occur in the self-discharge profile.

The development of electrochemically active surface groups such as the quinone/hydroquinone redox couple (see section 2.4.3.1) may be concurrent with the diminishing oxidation wave, suggesting the oxidation wave may also be partly an oxidation process to surface oxides before the surface oxides are further oxidized off the surface to CO_2.[159, 160] Determining the potential at which CO_2 begins to leave the surface,

and the connection between the oxidation wave and electroactive redox peaks in the cyclic voltammogram (and also the self-discharge behaviour) is necessary to understand the role of surface groups on self-discharge.

2.6.3.5 Carbon Surface Group Development

Carbon surface functionalities, specifically acidic oxides,[99, 100] have been linked to increased self-discharge in organic electrolyte electrochemical capacitors.[99-101] Surface oxides do not increase the capacitance in aprotic electrolytes as they do in aqueous electrolyte due to the absence of protons necessary for the electron transfer reactions.[93] Therefore, carbon surface groups are undesirable in organic-based electrochemical capacitors. However, surface groups are considered advantageous to acidic aqueous electrochemical capacitors due to the increase in specific capacitance for carbon electrodes in acidic electrolyte.[113, 157, 158] Generally, the capacitance values for the same active material are significantly higher in acidic aqueous media than those obtained in alkaline aqueous electrolyte.[113, 157, 158] Again, this is due to the lack of protons in the alkaline electrolyte compared to the acidic electrolyte, though the increased capacitance has also been linked to adsorption of protons.[157, 158] The role of carbon surface groups on self-discharge in aqueous electrolyte electrochemical capacitor systems has yet to be determined.

Chapter 3 EXPERIMENTAL METHODS

3.1 Electrochemical Set-up

All electrochemical experiments were conducted in an all-glass three-compartment cell with the exception of section 3.4.3 where experiments were run in a one-compartment cell. A three-electrode half-cell set-up was used since the processes of the negative and positive electrodes can be very different from one another and cannot be determined with a two electrode system; the addition of a third electrode allows the examination of each electrode separately, without a dependence on the other electrode.

A standard hydrogen electrode (SHE) was used as the reference electrode, unless otherwise stated in the experimental methods. A large piece of Spectracarb 2225 carbon cloth (Engineered Fibers Technology) connected to either a Pt or Au wire sealed in glass was the counter electrode. The Pt or Au wire was used as electrical connection to the instrument. The counter electrode was at least 150 mg (> 300 m^2) to ensure the kinetics of the counter electrode did not influence the data collected on the working electrode. EC-Lab software was used for data collection from a Bio-Logic VMP3 multi-potentiostat. All experiments were run at 22 ± 3 °C in electrolyte degassed with N_2 (Praxair), unless otherwise stated, and all potentials are referenced to the SHE.

3.2 Working Electrode Preparation

Working electrodes were prepared in a polytetrafluoroethylene (PTFE) Swagelok pipe fitting (5/8" outer diameter, 1/4" inner diameter) sealed to a glass tube. Spectracarb 2225 carbon cloth was used as the working electrode material. Spectracarb 2225 carbon

cloth was chosen as an electrode material due to its ease of use and high surface area (BET *ca.* 2500 m^2 g^{-1}). The mechanical stability of a woven carbon cloth allowed the electrodes to be purely active material without the addition of a binder. The addition of a binder would result in loss of a portion of the surface area and therefore less double-layer formation. Carbon cloth electrodes (*ca.* 10 mg weighed to 0.01 mg) were removed from the carbon sample using a 3/8" diameter leather punch (Tandy Leather Factory), and placed in the Swagelok fitting (see Figure 3.1) with a current collector (an electronically conducting, ionically insulating material). The current collectors used were a Parafin-based carbon gasket (Axion Power International, Ltd.), a Pt mesh and silicone gasket combination, or a sticky carbon mixture (described below). The Axion current collector was connected to a Pt wire sealed in glass tubing attached to Ni wire (see Figure 3.1 I). Axion Power discontinued the production of the parafin-based gasket and therefore another current collector was needed. With the Pt mesh current collectors a silicone gasket was used to apply even pressure to the Pt mesh and the carbon (see Figure 3.1 II), as well as to stop leaking (the carbon-parafin current collector was self-sealing and needed no gasket to prevent leaking).

It was deemed necessary to remove Pt from the current collector as it has been shown to be a catalyst in carbon corrosion.[17] Working electrodes were then prepared with a "sticky carbon" mixture for the current collector (see Figure 3.1 III). Beeswax was melted and graphite powder (Aldrich, <150 μm) was added in a carbon to beeswax ratio of *ca.* 2:1 by volume. The sticky carbon paste was then quickly placed into the Swagelok PTFE ferrule with connection to a Ni wire.

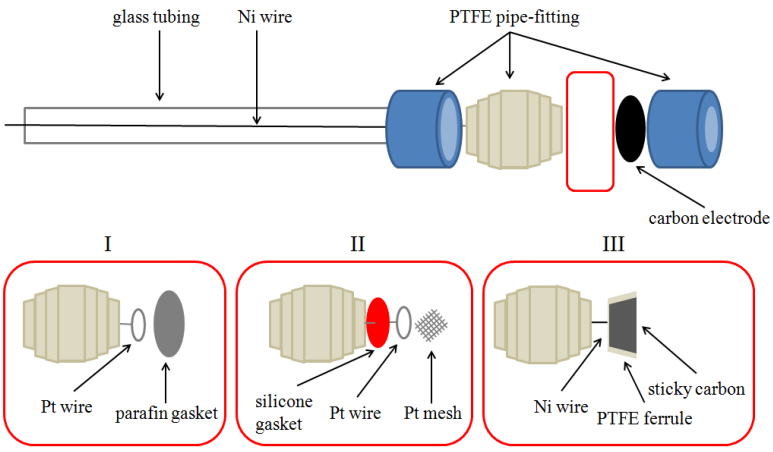

Figure 3.1: Schematic representations of the three current collectors used in the working electrodes for electrochemical research.

3.3 Cyclic Voltammetry

Cyclic voltammetry is an electrochemical technique where the potential is scanned at a certain sweep rate between two potentials and the response current is measured, and then plotted versus the potential.[161, 162] Cyclic voltammetry is commonly used to identify redox reactions since oxidation and reduction peaks and/or waves appear in the cyclic voltammogram. Additionally, cyclic voltammetry is used to identify the reversibility of an electrochemical system.

3.3.1 Continuous Cycling to Steady-state

Working electrodes were cycled between 0.0 and 1.0 V at a sweep rate of 1 mV s^{-1} for one week (*ca.* 300 cycles) in 1.0 M H_2SO_4 (Aldrich, 99.999% pure, trace metal basis). The potential window of 0.0 – 1.0 V was chosen as outside this potential window irreversible damage occurs to the carbon electrode,[38, 112] resulting in a lowered capacitance and increased electrode resistance.[28, 163] Steady-state means there were no

changes in the shape or size of the cyclic voltammogram over consecutive cycles. The continuous cycling procedure ensured any changes in the self-discharge experiments were due to the applied experimental conditions and not changes in the electrochemical cyclic voltammogram since the electrodes had already reached a steady-state.

3.3.2 Incremental Potential Cyclic Voltammograms

Spectracarb 2225 carbon cloth working electrodes were cycled from 0 – 0.6 – 0 V at 1 mV s^{-1} to steady-state in 1.0 M H_2SO_4. The upper potential limit was then increased by an increment of 25 mV until a steady-state was reached with the new potential limit. The upper potential was increased in these 25 mV increments to 1.0 V. Incremental potential cyclic voltammograms were also run where the lower potential limit was 0.4 V. The first cyclic voltammogram was run from 0.4 – 0.5 – 0.4 V, and once a steady-state was reached the upper potential limit was increased in 25 mV steps, to a final upper potential limit of 1.0 V.

Similar experiments were conducted on working electrodes which were cycled from 0.5 – X – 0.0 – 0.5 V at 1 mV s^{-1}, where X is the upper potential limit of the cyclic voltammogram and the first cyclic voltammogram was 0.5 – 0.55 – 0.0 – 0.5 V. In this case only two cyclic voltammograms were collected in each potential window before the upper potential window was increased by 10 mV, up to 1.05 V. Open-circuit potential measurements were collected for 2 hours between each potential window change to determine whether the changes evident in the cyclic voltammogram result in a change in open-circuit potential.

3.3.3 Cyclic Voltammetry in the Presence of Caffeine

Benzoquinone has previously been shown as an electrochemical method of detection for caffeine;[164] therefore it was thought caffeine might detect, or influence, the quinone/hydroquinone surface groups on the carbon electrode. Cyclic voltammograms were collected from electrodes previously cycled to steady-state in 1.0 M H_2SO_4 (see section 3.3.1). After initial steady-state cyclic voltammograms were collected in "0 M caffeine" electrolyte, the electrolyte was exchanged for a 0.01 M caffeine-containing electrolyte in 1.0 M H_2SO_4. The electrolyte was prepared using 0.48 g of caffeine anhydrous (Sigma-Aldrich, ReagentPlus) in 250 mL 1.0 M H_2SO_4.

3.4 Self-discharge Measurements

Self-discharge experiments (see section 2.6) were performed on positive electrodes with ramps from 0.5 – 1.0 V, and negative electrodes with ramps from 0.5 – 0.0 V with a 1 mV s^{-1} ramp rate in both cases, in 1.0 M H_2SO_4. The ramps were initiated at 0.5 V as this is roughly the open-circuit potential (OCP) of Spectracarb 2225 carbon cloth. Once the electrode was charged to the final potential (either 0.0 or 1.0 V) the potential was held at this value for varying times (from 0 min to 10 hours). The potential hold was employed to remove some portion of the potential loss due to charge redistribution (see section 2.6.2).[123] After the hold step, the system was switched to open-circuit configuration and the potential was measured for varying lengths of time (between 2 – 16 hours).

Another electrochemical measurement that gives information on the electrode's self-discharge processes is a potentiostatic float current measurements. Float current data

were analyzed to determine the charge passed, by integrating the area under the current versus time plot, and the also the current necessary to keep the electrode at a given potential. Potentiostatic float current experimental methods will be discussed in section 3.4.4.

3.4.1 Self-discharge in the Presence of Fe2+/Fe3+

It was of interest to determine the iron concentration limits of carbon-based electrochemical capacitors without an increase in self-discharge. Working electrodes which were previously cycled to steady-state (see section 3.3.1) were used in these experiments. The iron "contaminant" was pipetted from stock solutions into the electrochemical cell to provide increasing concentrations ranging from 10^{-8} to 10^{-1} M Fe^{2+}/Fe^{3+} in 1.0 M H_2SO_4. The iron stock solutions were prepared with both ferrous sulfate ($FeSO_4 \bullet 7H_2O$, Fisher Scientific, ACS grade) and ferric sulfate ($Fe_2(SO_4)_3 \bullet xH_2O$, Mallinckrodt Baker, AR grade) in 1.0 M H_2SO_4. Although the system is highly reversible and the electrochemical system should automatically respond to the applied potential, an approximately equimolar concentration of ferric and ferrous sulfate was used to ensure that the Nernstian potential did not shift from its standard reduction potential.

3.4.2 Self-discharge with Dissolved Gases in the Electrolyte

Electrolyte decomposition and oxygen reduction as possible self-discharge mechanisms in carbon-based electrochemical capacitors were examined by varying dissolved gases in the electrolyte. Working electrodes that had been cycled to steady-

state (see section 3.3.1) were placed in 1.0 M H_2SO_4 electrolyte. Self-discharge profiles, as per section 3.4, were collected for both 1.0 V and 0.0 V. Oxygen or hydrogen was bubbled through the electrolyte for 24 hours prior to self-discharge measurements for solution saturation of the dissolved gas and bubbled continuously throughout the self-discharge measurements. Oxygen was quantified using a dissolved oxygen probe and meter (VWR International). Self-discharge profiles collected from electrolytes with various dissolved gases were compared to profiles collected with either an electrolyte that had not been degassed, or a N_2-degassed electrolyte.

3.4.3 Self-discharge in pH 0 – 7 Electrolyte

The Faradaic reactions presented as possible self-discharge mechanisms in section 3.4.2 depend on protons, as do carbon surface functionalities, and therefore self-discharge profiles were collected in multiple pH electrolytes. Spectracarb 2225 carbon cloth working electrodes, previously cycled to steady-state, were used in this work. Electrodes were placed in a one compartment cell containing 100 mL of 1.0 M HCl which was diluted from concentrated hydrochloric acid (Aldrich, 99.999% pure, trace metal basis) with 18.2 MΩ·cm. The electrolyte also contained 1.0 M NaCl (5.84 g, Fluka Analytical, >99.5% pure) supporting electrolyte because with increasing pH the electrolyte conductivity decreases. The addition of the supporting electrolyte caused a change in charge carrier (from H^+ to Na^+), resulting in a change of the electrochemistry from acid-base chemistry, and therefore decreased the extent of conductivity change over the pH range. Self-discharge profiles from 1.0 V (see section 3.4) were collected at each pH as well as cyclic voltammograms between 0.0 and 1.0 V vs. RHE before and after the self-

discharge profiles. The cyclic voltammograms were collected to ensure the pH did not vary over the self-discharge data collection, since if the cyclic voltammograms overlapped there was no change in pH. The electrolyte was then titrated with the addition of NaOH in either solid form, or 5.0 M, 1.0 M, 0.1 M or 0.01 M solutions (made from serial dilutions) to reach the next desired pH. The NaOH concentration added to the cell was chosen to ensure there was no substantial volume change over the pH range.

A one-compartment cell was used to allow for thorough mixing of the solution, and also ease of pH measurement collection. pH readings were taken using a sympHony posi-pHIo electrode (VWR International) and meter. An Accumet sodium saturated calomel electrode (Fisher Scientific) was used with a 1.0 M NaCl filling solution, with an experimentally measured potential of 0.27 V vs. SHE.

3.4.4 Potentiostatic Float Current Measurements

Potentiostatic float current measurements were collected to determine the effect cycling to steady-state had on the current needed to hold the electrode at a given potential. Float currents were recorded for 30 or 60 minutes at various polarization potentials beginning at 0.0 V, and increasing in 50 mV increment potential steps up to 1.0 V on Spectracarb 2225 carbon cloth working electrodes in 1.0 M H_2SO_4. Float current measurements were collected on both as-received (uncycled) electrodes as well as electrodes that had already reached a steady-state through potential cycling (see section 3.3.1).

3.5 Open-circuit Potential Measurements

Open-circuit potential (OCP) measurements occur when external current does not flow through an electrochemical cell.[161] These potential measurements give an indication of the natural state of an electrode in a certain electrolyte and are also able to identify adsorption processes,[165] or the overall oxidation of a carbon electrode.[166, 167] It is important to differentiate between the terminology of open-circuit potential, the first meaning the natural (uncharged) state of an electrode without applied electrochemistry compared to the open-circuit potential profile measured after being charged, such as in a self-discharge profile. Open-circuit potential measurements of Spectracarb 2225 carbon cloth electrodes were collected between 2 – 144 hours in 1.0 M H_2SO_4.

3.6 Boehm Titration Standardization

3.6.1 Preparation and Standardization of Solutions

Solutions of the reaction bases, $NaHCO_3$ (Sigma-Aldrich, 99.5%), Na_2CO_3 (Anachemia, ACS Reagent) and NaOH (Sigma-Aldrich, 99.998%) were prepared by dissolving an exactly weighed mass (to 0.01 mg) of the appropriate base in 18.2 MΩ·cm water. The solution was then quantitatively transferred to a 1.00 L volumetric flask and topped up with 18.2 MΩ·cm. 0.05 M solutions of HCl were prepared from pure HCl (Sigma-Aldrich, 99.999%) and 18.2 MΩ·cm water.

The standardization of the NaOH solutions was carried out using potassium hydrogen phthalate (KHP) (Sigma-Aldrich) as the primary standard, and phenolphthalein as the indicator. A mass of *ca.* 0.2 g dried KHP, weighed to 0.01 mg, was diluted in

20.00 mL of 18.2 MΩ·cm water using a volumetric pipette, and then 2 drops of phenolphthalein were added as an indicator. The KHP solution (*ca.* 0.05 M) was then titrated with NaOH from a 25-mL burette, with at least triplicate measurements. The HCl solutions were standardized by titrating with the previously standardized NaOH and phenolphthalein to determine the endpoint.

3.6.2 Titration Procedure

The titration method suggested by Boehm was followed for these experiments.[18, 92, 102] A mixture of *ca.* 1.5 g (weighed to 0.01 mg) Black Pearls 2000 (Cabot Corporation) and 50.00 mL of one of the three 0.05 M reaction bases, $NaHCO_3$, Na_2CO_3 and NaOH was agitated using the various methods described below.[12, 18, 19, 86, 92, 102, 168] The mixtures were then filtered and three 10.00 mL aliquots were removed from the mixture. The $NaHCO_3$ and NaOH samples were acidified with the addition of 20.00 mL of standardized 0.05 M HCl, whereas for Na_2CO_3, 30.00 mL of 0.05 M HCl was added to completely neutralize the diprotic base and allow a strong acid-strong base titration. Although NaOH is a strong base it was also treated in this back-titration manner rather than a direct titration with HCl since it was previously found to give better values with a back-titration.[23] The acidified solutions where then bubbled with N_2 for 2 hours to expel dissolved CO_2 from solution.[23] All samples were titrated with standardized 0.05 M NaOH while being continually saturated with N_2, and the endpoints were determined potentiometrically using a SympHony pH meter and posiIo electrode (VWR International). All titrations were carried out at room temperature (22 ± 3 ºC). All solutions were made up with 18.2 MΩ·cm water. Additionally, all volumes are based on

calibrated pipettes. For ease, the $NaHCO_3$, Na_2CO_3 and NaOH bases used to react with the acidic surface functionalities are denoted as reaction bases, and the base used for titration is denoted as the titrator base.

The carbon used for these experiments was chosen to be Black Pearls 2000. The Black Pearls carbon was chosen for the standardization of the Boehm titration since it produced reproducible results in multiple Boehm titrations and because it has a high surface area (*ca.* 1400 m^2 g^{-1}) with the majority (*ca.* 68%) of its surface area in micropores (diameter < 2 nm), but also 18% in mesopores (2 to 50 nm diameter) and the remainder in macropores (> 50 nm diameter).[169] The Black Pearls 2000 carbon have a regular and well defined macroscopic structure, that of spherical particles of approximately 1 mm in diameter. This spherical shape allowed for easy determination of any visible changes to the particle surface from agitation, which might not otherwise be seen with other carbon types with less regular surfaces (*e.g.* graphite or activated carbon).

3.6.3 Carbon Removal and Filtering Experiments

Blank solutions (no carbon present) were used in the filtering experiments to ensure there was no variation in results due to heterogeneity of the carbon samples. By removing carbon from the titration to determine the effect of filtering, it allows any bias to be easily seen since the moles of carbon surface functionality (n_{CSF}) would be expected to be zero. 50.00 mL of a 0.05 M reaction base ($NaHCO_3$, Na_2CO_3 and NaOH) were passed through either qualitative Grade 1 filter paper (Whatman) or Pall glass-fibre filter papers (Sigma-Aldrich). Aliquots were then prepared and titrated as per section 3.6.2.

Carbon may also be removed from the carbon/reaction base mixture by allowing

the carbon to settle to the bottom of the vessel, followed by supernatant removal using a pipette (during removal of the aliquot). With this method, the carbon was allowed to settle from solution for 24 hours before the aliquots were removed from the supernatant.

3.6.4 Dilute Titrant

To determine whether more precise endpoints could be reached using a lower concentration of titrant, titrations using standardized 0.025 M NaOH as the titrator base were carried out on blank solutions. These results were then compared to similar titrations using a 0.05 M NaOH titrator base. Blank solutions were used to prevent differences which might arise as a result of carbon surface heterogeneity (see section 3.6.3). At least three "one-point" endpoint determination titrations were conducted (to a pH of 7 rather than an entire titration curve), and the average of these values and standard deviations were reported.

3.6.5 Effect of Exposure to Air on the Standardization of NaOH

In order to determine whether the concentration of NaOH determined by standardization was valid for a NaOH solution which had been transferred repeatedly between vessels or stored for extended periods or whether exposure to air changed the concentration of the NaOH during transferring and storage (necessitating standardization immediately prior to the Boehm titration), a solution of NaOH was initially standardized. Then half of the NaOH stock solution was transferred into a beaker and stirred manually with a stir rod to introduce air into the solution while the other part of solution was stored in a polyethylene bottle for one week and then standardized. Standardization of the

NaOH was carried out with at least triplicate measurements as per section 3.6.1.

3.6.6 Method and Duration of Agitation

To determine which method of agitation (stirring, shaking or sonicating) was optimal, carbon and reaction base mixtures were either: shaken for 24 hours using a MS 3 Shaker (Fisher Scientific); stirred for 24 hours using a stir plate; or sonicated for 10 minutes and then let stand for 6 hours before filtering. Carbon samples from the various agitation methods (in 0.05 M Na_2CO_3) were washed in 18.2 MΩ·cm water for 24 hours and then dried in an oven at 80 ºC. These samples were then observed under an Olympus-1MT-2 inverted microscope (Dalhousie University, Department of Biochemistry, Ridgway laboratory) at 4x magnification connected to a digital camera. The images were used to determine the effect of each agitation method on the macroscopic structure of the carbon sample.

Chapter 4 EXAMINATION OF ELECTROLYTE FE-CONTAMINATION AS A POSSIBLE SELF-DISCHARGE MECHANISM

All of this work was published in *"Effect of Fe-contamination on rate of self-discharge in carbon-based aqueous electrochemical capacitors", Heather A. Andreas, Kate Lussier, Alicia M. Oickle, Journal of Power Sources, 187, 2009, 275 – 283.* I was responsible for the data collection and analysis, and was heavily involved in the writing and editing process for this paper. The chapter is different from the paper as the cause of the potential loss for the 0.0 V has been identified (see Chapter 5).

4.1 Introduction

One possible self-discharge mechanism for electrochemical capacitors using sulphuric acid electrolytes discussed in the literature is self-discharge due to an iron shuttle redox reaction,[13, 141] wherein Fe from contamination of the carbon or the aqueous electrolyte, may undergo a $Fe^{3+} + e^{-} \leftrightharpoons Fe^{2+}$ reaction (see reactions 4 and 5 in Chapter 2 for fully balanced reaction) where it is reduced on one electrode (discharging the negative electrode in the process) and diffusing to the other electrode where it is oxidized (discharging the positive electrode), as shown pictorially in Figure 2.5.

The Fe-contamination mechanism has been studied by Kazaryan *et al.*[13] for asymmetric sulfuric acid electrolyte electrochemical capacitors, where the Fe-induced self-discharge was studied on only the negative carbon electrochemical capacitor

electrode, as the positive electrode was a PbO_2 battery-type electrode. They have shown that at relatively high Fe concentrations (10^{-2} to 10^{-1} M),[13] Fe can enhance self-discharge on the negative electrode. It was also shown that Fe has a much greater effect on the rate of self-discharge than other common metal impurities, such as W or Mn.[141]

The results presented in this chapter show the effect of Fe-contaminant concentration on the rate of self-discharge and also the maximum Fe-contamination which does not result in an increase in the self-discharge rate for a carbon-based aqueous electrochemical capacitor. Additionally, results are presented for a symmetric electrochemical capacitor system. As a result, this was the first time Fe-induced self-discharge of the positive carbon electrochemical capacitor electrode was studied. Also, the research presented here was for relatively short self-discharge times (*ca.* 16 hours), where Kazaryan *et al.*[13] showed a significantly different self-discharge profile, compared with the profiles at longer times. It is possible that differences in self-discharge profiles at short versus long times were due to the effect of pores on the charging of the electrode, and as a result potential holds were employed in the following experiments.

4.2 Continuous Cycling to Steady-state

As evidenced by the mirror-image, reversible and almost rectangular cyclic voltammograms seen in all but the first cycle of Figure 4.1 (discussed more extensively in Chapter 7), the Spectracarb 2225 carbon cloth is a capacitive material and would be suitable for carbon aqueous electrochemical capacitors. The working electrodes were cycled to steady-state prior to self-discharge measurements and as seen in Figure 4.1, this required approximately 300 cycles. During this process quinone groups on the edges of

the graphene sheets in the carbon develop, as evidenced by the increasing size of the peaks centered at *ca.* 0.5 V.[89-91] Thus, the working electrodes were cycled to steady-state to ensure that any changes seen in the subsequent self-discharge curves were due to changes in iron-contamination, rather than changes due to quinone group development.

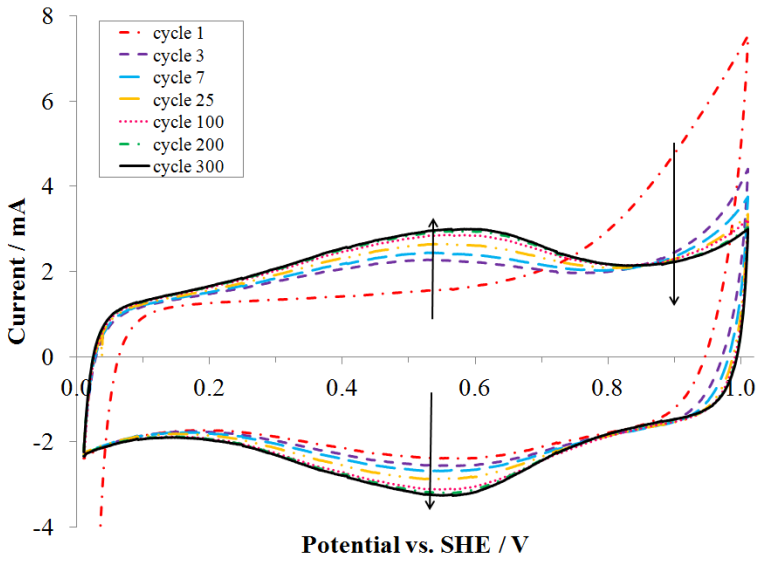

Figure 4.1: Cyclic voltammograms of Spectracarb 2225 carbon cloth (*ca.* 10 mg) in 1.0 M H_2SO_4 at 1 mV s^{-1}.

As an important benefit for this research, this week-long cycling procedure also allowed for any minute amount of Fe-contamination which may come from the carbon itself to be minimized. This is due to the fact that during this cycling procedure any Fe-contaminants will dissolve into the electrolyte and after cycling to steady-state the electrodes are moved to an electrochemical cell containing clean 1.0 M H_2SO_4 electrolyte. As a result, any Fe-contaminants are left behind in the cell in which the electrode was cycled to steady-state.

4.3 Effect of a Hold Step on Charge Redistribution and Fe Concentration

The carbon used in this work and in carbon-electrode electrochemical capacitors often has a very high electroactive surface area as a result of the highly porous nature of these materials. However, because of these small pores, the surface at the mouth of the pore charges more quickly during charging than the surfaces deep within the pore (see section 2.6.2).[120, 121] Charge redistribution can be mitigated by adding a holding step after electrode charging, allowing more of the surface to reach the desired potential. Longer holding steps lead to much less drastic initial potential drops. Thus, various holding times were introduced to all self-discharge measurements to ensure changes in self-discharge profiles during the Fe-contamination studies were actually due to changes in Fe concentration rather than these charge redistribution effects.

The addition of the holding step may change the Fe concentration in the pores of the electrode, as the Fe will be oxidized or reduced during the holding step. If the Fe is oxidized (as it would be at the positive electrode), then the concentration of Fe^{2+} would decrease (become depleted). Since Fe^{2+} to Fe^{3+} is the reaction which would be expected to discharge the electrode at the 1.0 V potential, by depleting the Fe^{2+}, less self-discharge may be expected. So, various holding steps were examined during the concentration studies (0 s, 0.5 h, 1 h and 10 h) to determine if the holding time had any effect on the Fe concentration and any subsequent influence on the Faradaic portion of the self-discharge. It should be noted that Fe-contamination results (charging, holding and Fe-induced trends in the self-discharge profiles) were consistent between these different hold time experiments suggesting that the holding step does not affect the Fe in the pores. In fact, as will be shown, it is the charging ramp which depletes the reactive Fe in the pore (*i.e.*

when charging to 1.0 V, the Fe^{2+} will be oxidized to Fe^{3+} when the ramp potential is above 0.68 V,[170] and when charging to 0.0 V the Fe^{3+} will be reduced to Fe^{2+}).

As seen in Figure 4.2 the current recorded during the holding step was the same for each "bulk" concentration from 0 M to 10^{-3} M, suggesting that, for these bulk electrolyte concentrations the Fe^{2+} concentration in the pores is 0 M. The shape of the holding current (also a float current measurement) drops until the steady-state current is reached. The current becomes smaller due to charge moving farther down the pores, resulting in an even distribution of charge on the electrode`s surface.[119, 163] The full depletion of Fe from the pores is completed during the charging ramp (which is the same for all experiments) and the holding step has no effect on this depletion. It is expected that a similar depletion would occur during the charging of a commercial electrochemical capacitor. Note, though, that the holding step will affect the amount of charge redistribution due to the pore effect, as the same amount of current which passes during holding (see Figure 4.2a inset) is the double-layer charging current as the distributed potential reaches further into the pores.[119, 163]

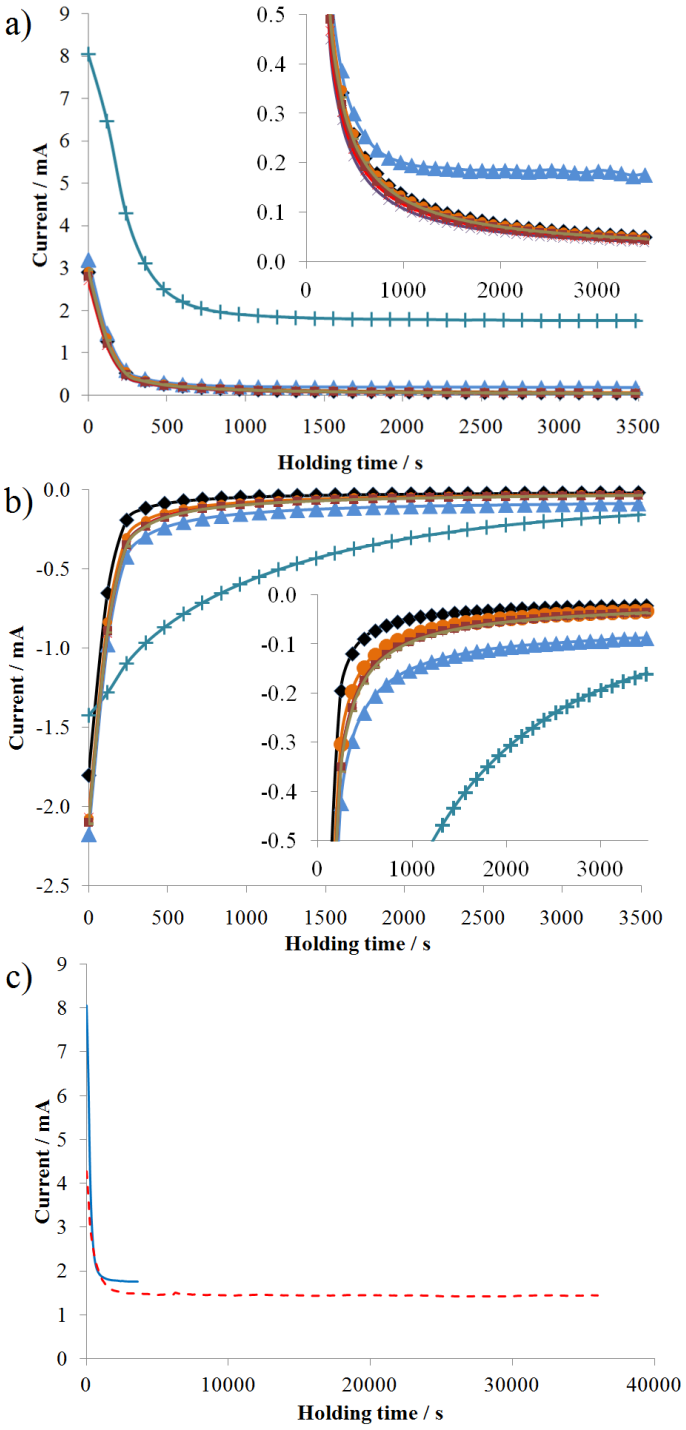

Figure 4.2: Current during 1 hour holding (a – 1.0 V, b – 0.0 V) for Spectracarb 2225 carbon cloth in 1.0 M H_2SO_4 contaminated with different concentrations of Fe^{2+} and Fe^{3+} sulphate: 0.0 M (♦); 10^{-8} M (–); 10^{-6} M (■); 10^{-5} M (●); 10^{-4} M (*); 10^{-3} M (×); 10^{-2} M (▲); 10^{-1} M (+), insets are magnifications at low current; c) Comparison between current profile for 10^{-1} M electrolytes during hold times of 1 hour (——) and 10 hour (— —).

At concentrations greater than 10^{-3} M, the pore Fe may not be completely depleted during charging, as the current is higher than that for 0 M, indicating that there are some species in the pores to be oxidized. For the 10^{-2} M concentration this current increase is marginal (see inset Figure 4.2a) but is considerable at 10^{-1} M. A similar result is seen for the negative electrode (Figure 4.2b), where the Fe^{3+} is essentially depleted at concentrations less than 10^{-2} M, but the residual Fe^{3+} remains at higher concentrations.

For 10^{-1} M, the current decays initially and then reaches a steady-state (Figure 4.2a) where the Fe^{3+} is likely diffusing into the pores as fast as it is being reacted. This is confirmed by Figure 4.2c where it is shown that this current is constant, even over 10 hours of holding. Integration of the current with time indicates that *ca.* 55 C of charge is passed during this 10 h holding step, which would require *ca.* 5.5 x 10^{-4} mol of Fe for reaction (using Faraday's constant and a one electron oxidation of Fe^{2+} to Fe^{3+}). The amount of Fe in the pores of this carbon can be estimated based on the "bulk" concentration (10^{-1} M, the pore volume of the carbon (1.2 mL g^{-1}) and the electrode mass (10 mg), and it can be shown that there is *ca.* 1 x 10^{-6} mol of Fe available in the pores of the carbon, assuming no diffusion. Since the moles of Fe reacted is greater than that available in the pores, Fe must be diffusing into the pores to react. The constant current seen in Figure 4.2c, suggests that diffusion is not the rate-limiting step, which would be expected to exhibit a decreasing current with time and the constant current suggests that the system is under convective diffusion-control, caused by the N_2 bubbling. The difference in current between the 1 h and 10 h hold in Figure 4.2c is likely due to small differences in the N_2 bubbling rate. This steady-state current is reached in both profiles for a 1 and 10 hour holding step (Figure 4.2c) showing a 1 hour hold is sufficient to

achieve steady-state, and thus longer hold times do not change the Fe concentrations in the pores.

There was no apparent difference between the results obtained with the different holding times. Also, the pore Fe depletion is dependent only on the charging ramp and not the hold times. Only 1 hour of hold time is required to reach the steady state current exhibited in the 10^{-1} M Fe electrolytes. Due to all of these factors, only the 1 hour hold data are presented here.

4.4 Self-discharge Profiles in the Absence of Fe

The carbon cloth self-discharge profiles were examined when the electrodes were charged from 0.5 V to either 1.0 or 0.0 V. Figure 4.3a shows that even with a 1 hour holding time in the charging procedure, there is still significant self-discharge during the 16 hour experiments. Part of this self-discharge is likely to be a residual potential drop due to charge redistribution as a 1 hour hold may be insufficient to remove all the pore effects (*i.e.* 1 hour is not long enough to allow the full surface to charge to the desired potential).[123] The remainder of the self-discharge must be due to at least one, possibly several, unidentified self-discharge mechanism(s). These data show that even in an Fe-free system, both electrodes of a symmetric carbon-electrode, aqueous sulfuric acid-electrolyte electrochemical capacitor may undergo significant self-discharge. Thus, even with full scrubbing of the Fe from the electrolyte, self-discharge will continue to occur via the other mechanism(s). And, the other mechanism(s) must be identified and minimized to prevent self-discharge (see Chapters 5 and 8) in symmetric carbon-electrode, aqueous-electrolyte electrochemical capacitors.

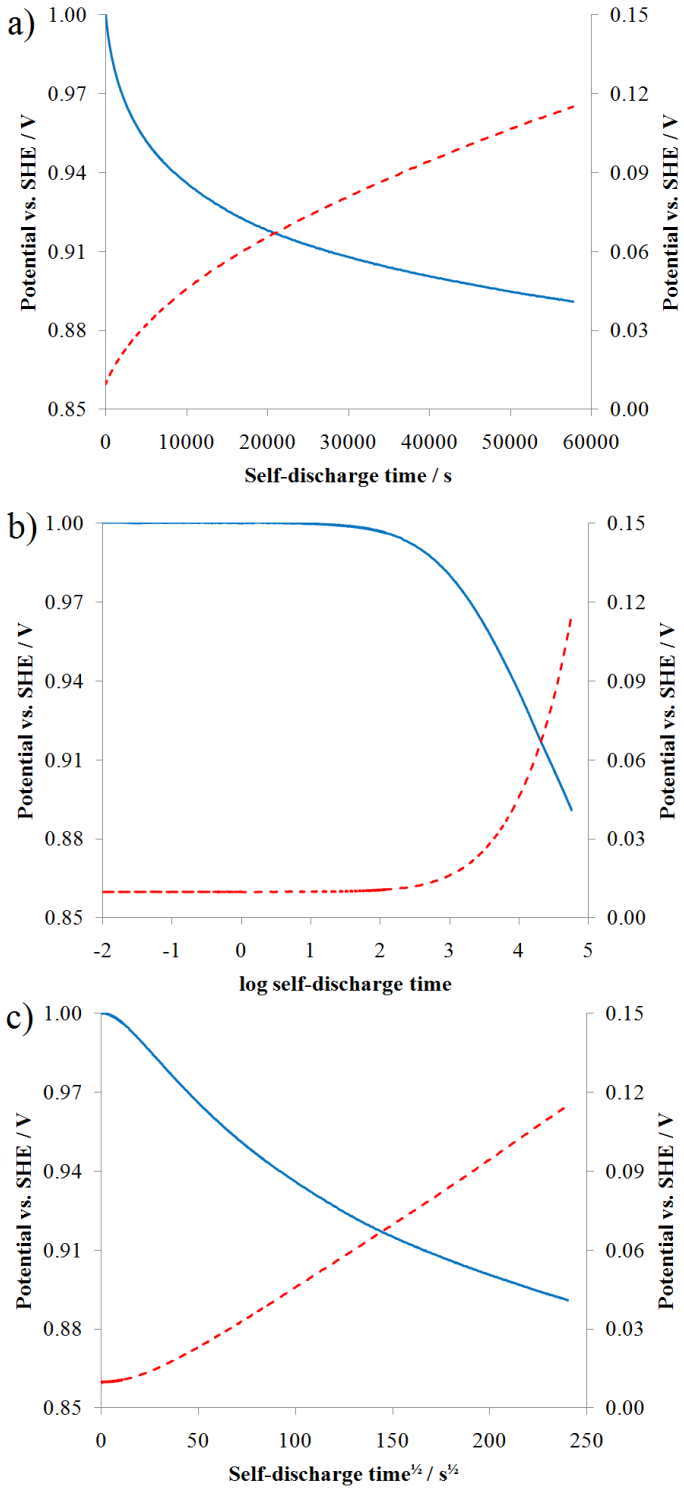

Figure 4.3: Self-discharge profiles of Spectracarb 2225 carbon cloth in 0 M Fe from 0.5 V at 1 mV s^{-1} in 1.0 M H_2SO_4 for the electrode charged to 1.0 V (——, left axis) and 0.0 V (— —, right axis), with a 1 hour holding time, plotted as voltage as a function of (a) time; (b) log time; and (c) $t^{½}$.

The self-discharge profiles were fit using the Conway models[118, 163] (see section 2.6.1) in order to learn about their possible self-discharge mechanisms (see Figure 4.3b and c). When the self-discharge profile of the electrode charged to 1.0 V was plotted as a function of log time (Figure 4.3b), a linear plot resulted, after an initial plateau. This fitting suggests the self-discharge mechanism on the positive electrode is not a diffusion-controlled mechanisms (as might be expected if Fe-contamination was the cause), but may be either an activation-controlled mechanism, or charge redistribution, as both result in a linear region when plotted as a function of log time. The non-linearity of the self-discharge profile when plotted as a function of $t^{1/2}$ (Figure 4.3c) was also consistent with the mechanism of self-discharge for this electrode, under Fe-free conditions, is not diffusion-controlled. The self-discharge could also be due to charge redistribution in the carbon electrode material, or an unidentified activation-controlled (assuming the Conway models hold for porous electrodes), and therefore, the reactant species causing self-discharge is either at high concentrations in the cell or is confined to the electrode surface. Activation-controlled self-discharge mechanisms of either electrolyte decomposition (Chapter 5) or carbon surface functionality oxidation/reduction (Chapter 8) are possible explanations for this relationship.

The opposite situation is seen for the electrode when it is charged down to 0.0 V. Figure 4.3b and c show that the self-discharge profile is not linear when plotted as a function of log time, but is linear when plotted versus $t^{1/2}$, suggesting that when the electrode is charged to 0.0 V the self-discharge mechanism for the negative electrode relies on the diffusion of a reactive species to the electrode surface (it cannot be Fe, as this is an Fe-free system). The negative electrode self-discharge mechanism has been

identified as oxygen reduction and will be discussed Chapter 5. Although N_2 is bubbled through the electrochemical cell during these measurements, the cell is not sealed and the small amount of O_2 present in the electrolyte results in increased self-discharge, though the potential loss is likely due to charge redistribution, in some part.

It should be pointed out, that as expected these data have shown that the same electrode material has two different self-discharge mechanisms when used as a positive, or negative, electrode in a symmetric electrochemical capacitor. The difference in self-discharge mechanisms highlights the necessity of performing three-electrode experiments when determining self-discharge mechanisms, as doing a full-cell experiment may obscure what is truly happening at each electrode. A full understanding of the cause of mechanism(s) of self-discharge at each electrode is required to truly be able to minimize or prevent self-discharge in a cell.

It is surprising to note that the self-discharge profile can be fitted as predicted by the Conway models, as these models were developed for planar electrodes, and the electrodes examined here are highly porous. Even more surprising is that the diffusion-control model fits, as one may expect that in a porous system, one would not have the semi-infinite diffusion to the electrode surface (as covered by the model), but also diffusion and migration effects down the pores, as well as radial diffusion in the pores. This will be addressed again below, but the agreement between the porous electrode self-discharge profile and the planar self-discharge model may suggest that the electrode is acting as a planar electrode, and that it is only the surface of the electrode which participates in the self-discharge, and the pores (especially deep in the pores) do not contribute to self-discharge.

4.5 Effect of Fe-contamination on Self-discharge Profiles

4.5.1 Electrodes Charged to 1.0 V

The effect of Fe-contamination on self-discharge profiles of the Spectracarb 2225 carbon cloth in 1.0 M H_2SO_4 was examined by incrementally adding $FeSO_4$ and $Fe_2(SO_4)_3$ in equimolar concentrations to the electrochemical cell. The carbon and H_2SO_4 used in this work is essentially Fe-free; however, the carbons and electrolytes used in commercial electrochemical capacitors may have significant Fe-contaminations, leading to the suggestion that Fe may be causing self-discharge. As can be seen in Figure 4.4a, there is no significant difference in the self-discharge profile until the electrolyte concentration of Fe reached 10^{-4} M. Significant difference between the self-discharge profiles is determined using ± 3 standard deviations for potentials from the 0 M Fe self-discharge profile. This suggests that for systems with Fe concentrations lower than 10^{-4} M, the self-discharge mechanism is not Fe-induced on the carbon electrode charged to 1.0 V. This agrees with the predicted mechanism using the Conway model[118, 163] which suggested an activation-controlled self-discharge mechanism, or, charge redistribution.[123] Diffusion-controlled self-discharge might be expected for a Fe-shuttle, and therefore, a linear profile with log time suggests at low concentration is not Fe discharging the 1.0 V electrode. This is confirmed for all the low Fe concentrations when the Fe data is plotted as a function of log t and $t^{1/2}$ (Figure 4.4b and c). Thus, for all the concentrations up to 10^{-5} M the self-discharge profile is consistent with an activation-controlled, or charge redistribution mechanism.

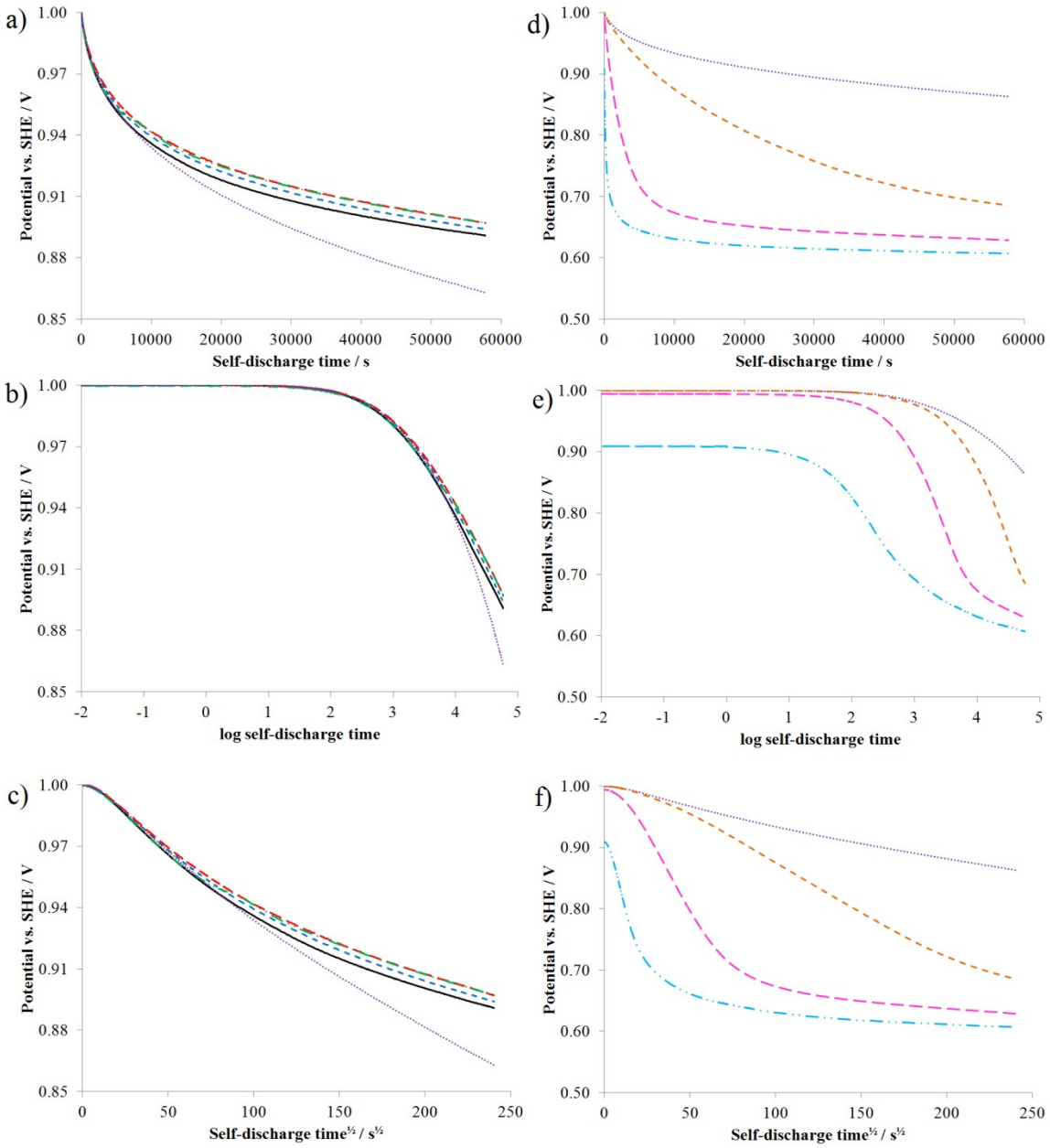

Figure 4.4: Self-discharge profiles for Spectracarb 2225 carbon cloth (*ca.* 10 mg) charged from 0.5 – 1.0 V at 1 mV s^{-1} in 1.0 M H_2SO_4, with a 1 hour hold time, contaminated with various concentrations of Fe^{2+}/Fe^{3+} sulfate: (a-c) 0 M (——); 10^{-8} M (— —); 10^{-6} M (— —); 10^{-5} M (— • •); 10^{-4} M (•••); and (d-f) 10^{-4} M (•••); 10^{-3} M (— —); 10^{-2} M (— —); 10^{-1} M (— • •).

It is not surprising that at low Fe-concentrations the self-discharge mechanism is not due to Fe for two reasons. All the Fe in the pores has been reacted before self-

discharge begins. During charging to 1.0 V all the Fe^{2+} in the pores is reacted to Fe^{3+}, leaving little to no Fe^{2+} in the pores to be oxidized when the cell is placed on open-circuit configuration. The depletion of Fe^{2+} in the pores would result in there being no source of electrons which are necessary to discharge the positive electrode. Secondly, even if the Fe in the pores was not completely reacted, there is still insufficient Fe in the pores to cause the degree of self-discharge exhibited in Figure 4.3. From this figure it is seen that during the 16 hours of self-discharge the electrode has lost 0.1 V. If it is assumed that a full half of that potential loss is due to charge redistribution, then the potential loss due to the Faradaic reaction is 0.05 V. The current of the electrode near a potential of 1.0 V can be found from Figure 4.1 (cycle 300) and is seen to be *ca.* 2.5 mA. The gravimetric capacitance (250 F g^{-1}) can be found by dividing the current by the sweep rate (1 mV s^{-1}) and the mass of the electrode (*ca.* 10 mg). The charge density (q, in C g^{-1}) required for a 0.05 V potential loss (V_{loss}) at this capacitance (C) can be calculated from

$$q = CV_{loss}, \tag{9}$$

resulting in a required charge density of 12.5 C g^{-1}. The mass of the electrode is *ca.* 10 mg, meaning 0.125 C of charge (Q) is needed to cause this self-discharge. Assuming no diffusion down the pores, the Fe concentration required for this degree of self-discharge can be calculated from

$$[Fe] = \frac{Q}{FVm}, \tag{10}$$

where F is Faraday's constant, V is the pore volume (1.2 mL g^{-1})[171] for Spectracarb 2225 carbon cloth and m is the mass of carbon. Using this calculation *ca.* 10^{-1} mol L^{-1} of Fe is required in the pores for this degree of self-discharge. Obviously there is insufficient Fe in the pores to cause this self-discharge at these low Fe concentrations.

Figure 4.4b shows that at concentrations above 10^{-4} M, the self-discharge profile deviates away from linearity on the log t scale, suggesting it is no longer activation-controlled, or charge redistribution. When the data is plotted as a function of $t^{½}$ (Figure 4.4c) the linearity of the plot at 10^{-4} M is consistent with a diffusion-controlled mechanism. Additionally, Figure 4.4d shows at concentrations above 10^{-4} M, an increase in Fe concentrations leads to an increase in self-discharge. This confirms that the mechanism of self-discharge has changed and at concentrations greater than 10^{-4} M the Fe in the cell will discharge the cell.

As expected, the self-discharge profile for Fe concentrations of 10^{-4} – 10^{-2} M are all consistent with a diffusion-controlled mechanism (Figure 4.4e and f), exhibiting linear potential versus $t^{½}$ profiles, at least in part. It is important to note the initial potentials shown in the self-discharge profiles of Figure 4.4d-f are due to an instrumentation lag between the ramp/hold file and the open-circuit potential file, and not due to the system being unable to charge to the desired potential (1.0 V). The loss of the first few data points would unlikely effect the self-discharge profile analysis as the beginning of the profile generally does not fit the Conway models. For the 10^{-2} M concentration, the profile deviated from a linear $t^{½}$ plot at a potential of *ca.* 0.7 V. It is suggested that at this potential the electrode is nearing its open-circuit potential (0.68 V)[170] for the system and therefore the rate of self-discharge is diminished. For even higher concentrations the self-discharge profile no longer can be fit with the Conway models. Interestingly, this concentration corresponds to that calculated above to be the point at which the Fe in the pores may be sufficient to discharge the electrode without requiring diffusion, although diffusion of course still occurs. However, since the amount

of potential loss due to charge redistribution is not known, and was estimated at 50% of the total potential lost, it is possible the concentration values matching are a coincidence. It is suggested that the profile of the 10^{-2} M Fe concentration is likely a combination of Fe-induced self-discharge which is activation-controlled and diffusion-controlled.

It is also interesting to note that for 10^{-4} M and 10^{-3} M, the self-discharge mechanism is not consistent with a diffusion-controlled mechanism at high potentials. In fact, the profile for the 10^{-4} M shows that at potentials above *ca.* 0.9 V, the self-discharge mechanism is the same as that previously seen at lower Fe concentrations. This suggests either charge redistribution is still the main contributor to self-discharge in this time domain (despite the 1 h holding step), some other activation-controlled self-discharge mechanism is responsible for self-discharge above this potential or the Fe concentration in the pores is sufficient to not be diffusion limited. There are two arguments against the latter possibility. First, the agreement between the data for 10^{-3} M and that for lower concentrations suggests Fe is not the main self-discharge mechanism here, as it was shown earlier that at low concentrations Fe does not contribute to the self-discharge. Secondly, based on the calculation above, and the results in Figure 4.4 which showed complete depletion of the Fe in the pores during charging, it is unlikely that the Fe concentration in the pores is sufficiently high enough to cause this degree of self-discharge. Indeed, it can be seen in Figure 4.4 that at higher concentrations (*e.g.* 10^{-3} M in Figure 4.4f) this region of the self-discharge profile changes, suggesting that 10^{-4} M is not a high enough concentration to account for this activation-control region. Thus the two other possibilities are more likely.

In order to examine whether the pore effect (leading to charge redistribution) was

the main self-discharge process at these high potentials and short self-discharge times, different hold times were introduced into the electrode charging regime. Presumably, longer holding times would result in a more even potential being reached in the pores, leading to less charge redistribution and a shorter initial period before Fe-induced self-discharge takes over. Conversely, if the self-discharge at short self-discharge times (high potentials) is due to a different Faradaic reaction (the oxidation of an unknown species), then the holding time would be irrelevant and the potential where Fe-induced self-discharge takes over would be constant. Thus, the time and potential required for the self-discharge profile at 10^{-4} M Fe to deviate more than 10 mV from the self-discharge profile at 0 M was determined. The data in Table 4.1 show the results for a hold time of 0, 30 and 60 min. As can be seen from this table, there is no trend in the self-discharge time required for deviation to occur, with time for individual electrodes varying significantly. However, the potential of deviation is reasonably constant, with deviation occurring at *ca.* 0.90 ± 0.02 V. These results suggest that at high potentials self-discharge is not dominated by charge redistribution, but rather is due to the oxidation of an unknown species. The self-discharge mechanism must be an oxidation, as it is the loss of electrons of the Faradaic process which discharges the positive electrode. There are two possibilities as to why this new oxidation has become the main mechanism of self-discharge at potentials above 0.9 V. First, it may be kinetically faster than the $Fe^{2+} \rightarrow Fe^{3+}$ oxidation at these potentials. Second, the concentration of Fe at the surface of the electrodes has fallen to zero (limiting current conditions) and the kinetics of the unidentified reaction is faster than the diffusion of Fe. This is supported by the fact that at higher concentrations of Fe, which would result in faster diffusion (due to the steeper

concentration gradient), the Fe-induced self-discharge becomes the dominant self-discharge mechanism at higher potentials (Figure 4.4), hence at these high concentrations diffusion is faster than the kinetics of the unidentified reactions.

Table 4.1: Time and potential of deviation of self-discharge data collected at 10^{-4} M Fe vs. 0 M Fe self-discharge for different hold times.

Holding time / min	Time at deviation / h	Potential at deviation / V
0	4 ± 2	0.88 ± 0.01
30	3 ± 1	0.92 ± 0.01
60	7 ± 3	0.91 ± 0.01

The error represents one standard deviation.

Conveniently, the addition of a hold time also tests the argument that Fe is at sufficiently high concentrations to not be diffusion-controlled, as longer hold times will result in more thorough conversion of Fe^{2+} to Fe^{3+} and less Fe^{2+} remaining in the pores. Thus, at longer hold times, diffusion-control should dominate at earlier self-discharge times since the Fe^{2+} would be used up in the pores and would need to diffuse in from the bulk electrolyte. Again, this is not supported by the data in Table 4.1, confirming that Fe is not the main self-discharge mechanism at these potentials.

Interestingly, for all of the different hold times examined, the Fe concentration at which the self-discharge profile began to be dependent on the Fe reaction was 10^{-4} M. This was surprising since long hold times may be expected to deplete the Fe inside the pores to a greater extent than shorter hold times, and thus with longer hold times there would be insufficient Fe to allow for Fe-induced self-discharge; whereas short hold times may leave sufficient Fe to induce self-discharge. Therefore, for longer hold times, it would be expected that a higher Fe concentration would be required before Fe-induced

self-discharge was evident. The fact that all systems begin to demonstrate Fe-induced self-discharge at 10^{-4} M suggests it is not the pore Fe concentration which is the limiting factor, but rather the bulk concentration. This implies the self-discharge does not occur in the pores, but is, rather, primarily occurring on the electrode surface (at the pore mouth). This is easily rationalized in that the Fe^{2+} in the pores has been depleted during charging, and thus the Fe^{2+} must diffuse in from the bulk to allow self-discharge to occur. As the Fe^{2+} diffuses in, it will react as soon as it encounters the electrode, which is likely to be on the surface of the electrode, or, at most, only a very short distance down the pores. Thus, this result gives the first real indication about where on the electrode surface the self-discharge processes are actually occurring. As well, this likely is the explanation for the fact that the Conway diffusion model is able to fit the self-discharge profiles for porous electrodes, even though the model was derived for semi-infinite diffusion to a planar electrode. Since the pores are essentially depleted of Fe and therefore cannot participate in the self-discharge process, the pores essentially become "invisible" to self-discharge and the electrode appears simply as a nearly planar surface, such as would be appropriate for the Conway model.

Based on the above discussion, it should theoretically be possible to increase the Fe concentration such that the Fe concentration in the pores is sufficient to discharge the electrode without reliance on diffusion (based on the above calculations, this concentration is likely at or above 10^{-1} mol L^{-1}) and this may be the cause of the fact that the Conway models cannot fit the self-discharge profile at 10^{-1} M Fe concentrations.

4.5.2 Electrodes Charged to 0.0 V

The Fe-induced self-discharge of the negative carbon electrode in an asymmetric Pb/C electrochemical capacitors has been studied at high Fe concentrations (10^{-2} – 10^{-1} M) by Kazaryan *et al*.[13] The effect of Fe concentration on the self-discharge of the negative carbon electrode in a three-electrode configuration at low Fe concentrations was examined here. As discussed earlier, the self-discharge profile for the carbon electrode when it is charged negatively fits with the Conway diffusion model when a Fe-free electrolyte is used. It should be noted that although the Fe-free self-discharge profile begins at a higher potential (due to an instrumentation lag between the ramp/hold file and the open-circuit potential file), it is unlikely to affect the data analysis as the Conway models do not fit the early potential versus time data collected. As shown in Figure 4.5, within the error of the experiment, the Fe concentration does not affect the self-discharge profile up to concentrations of 10^{-3} M, consistent with Kazaryan,[13] although with all the electrodes examined, the self-discharge profile of the electrolyte containing 10^{-1} M Fe shows a more rapid self-discharge, suggesting that at this high concentration, the Fe is participating in the self-discharge. This is unlike the results on the positive electrode, where the Fe-induced self-discharge begins at 10^{-4} M. Thus the negative electrode is less susceptible to Fe-induced self-discharge and can withstand greater Fe contamination concentrations without enhanced self-discharge. At the lower concentrations it appears that O_2 reduction (Chapter 5) is the cause of self-discharge, however at 10^{-3} M the Fe^{3+} reduction begins to become the more dominant discharging species. This is a benefit for asymmetric electrochemical capacitors where carbon is often used for the negative electrode.

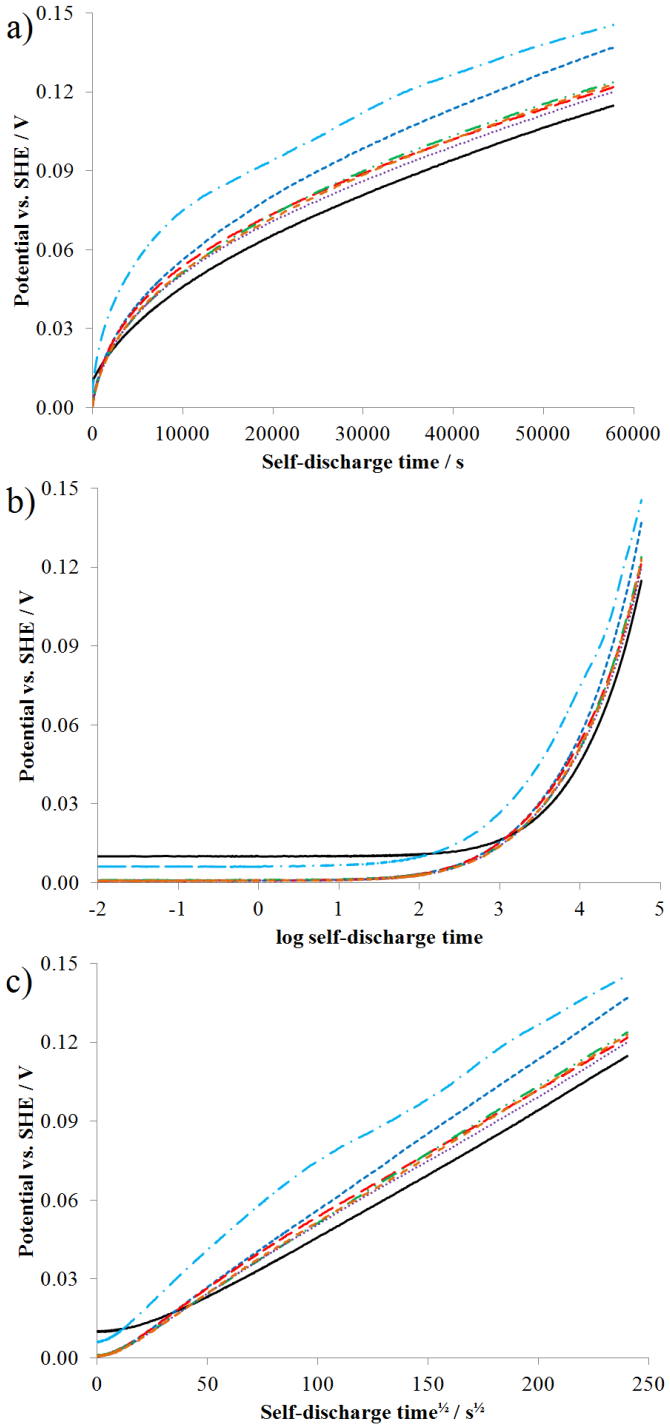

Figure 4.5: Self-discharge profiles of Spectracarb 2225 carbon cloth (*ca.* 10 mg) charged to from 0.5 – 0.0 V at 1 mV s^{-1} in 1.0 M H_2SO_4, with a 1 hour hold time, contaminated with various concentrations of Fe^{2+}/Fe^{3+} sulfate: (a-c) 0 M (——); 10^{-8} M (– –); 10^{-6} M (— —); 10^{-5} M (— • •); 10^{-4} M (•••); 10^{-3} M (- -); 10^{-1} M (— •).

4.6 Conclusions

It was shown that for a symmetric carbon-based, aqueous-electrolyte electrochemical capacitor, the self-discharge mechanism on the positive and negative electrodes are different and should be studied with a three-electrode set-up. In an H_2SO_4 electrolyte, which is free of Fe-contamination the positive electrode has a self-discharge profile which is predicted to be activation-controlled as per the Conway models, or charge redistribution. Conversely the self-discharge mechanism for the negative electrode in the same situation is predicted to be diffusion-controlled.

No Fe-induced self-discharge is seen at concentrations up to 10^{-5} and 10^{-3} M for the positive and negative electrodes, respectively. At intermediate Fe-concentrations, the Fe mechanism does become the major self-discharge mechanism, and it is consistent with diffusion-control. Importantly, it was shown the Fe-induced self-discharge occurs primarily on the exterior surface of the porous electrodes and the pores do not take part in the Fe-induced self-discharge mechanism. This is due to the depletion of the Fe in the pores during charging. This can be used to explain the fact that the Conway diffusion-control self-discharge model, which was derived for semi-infinite diffusion to a planar electrode, is able to fit the self-discharge profile of a porous electrode.

At high Fe concentrations (*e.g.* 10^{-1} M) Fe-induced self-discharge is still the main self-discharge mechanism; however, at these concentrations, the system is no longer diffusion-controlled and the rate-limiting step is the reaction of Fe on the carbon surface.

Chapter 5 ELECTROLYTE DECOMPOSITION AND OXYGEN REDUCTION AS POSSIBLE SELF-DISCHARGE MECHANISMS

The majority of this work was published as *"Examination of water electrolysis and oxygen reduction as self-discharge mechanisms for carbon-based, aqueous electrolyte electrochemical capacitors", Alicia M. Oickle, and Heather A. Andreas, Journal of Physical Chemistry C.*, 115*, 2011,* 4283 – 4288. I collected and analyzed all the data presented in the paper, and was also responsible for the first draft and editing of the paper. The pH self-discharge data was not previously published.

5.1 Introduction

In Chapter 4, the effect of a common external contaminant (Fe) was examined as a cause of self-discharge. With an electrochemical capacitor system that is under the maximum Fe-concentration necessary to increase self-discharge, or completely void of Fe, there is still a significant loss of potential over time. As previously discussed in section 2.6.3.2, Pillay and Newman[15] proposed side reactions of oxygen and hydrogen evolution via the electrolysis of water as possible causes of Coulombic efficiency losses in electrochemical capacitors. Additionally, oxygen within the electrolyte may also increase the self-discharge through oxygen reduction.

In this work, electrolyte decomposition and oxygen reduction have been experimentally studied as self-discharge mechanisms in aqueous electrolyte, carbon electrode electrochemical capacitors using the Nernst equation, along with le Châtelier's

Principle, to predict the effect of varying the dissolved oxygen and hydrogen content on self-discharge from both the positive and negative electrodes. The proposed Faradaic self-discharge processes (O_2-evolution, H_2-evolution, and O_2-reduction) have written redox reactions associated with them (see section 2.6.3). As such, it is possible to make predictions using both le Chatelier's Principle and the Nernst equation, on the effect of changing certain parameters such as partial pressures and proton concentrations. The Nernst equation applies when there is no current flowing through the cell, similar to the open-circuit measurements in self-discharge profiles (see section 2.6) and is defined as

$$E = E^o + \frac{RT}{nF}\log\frac{a_{ox}}{a_{red}}. \quad (11)$$

where E is the potential of the reaction, E^o is the potential of the reaction at standard conditions and 298 K (1 atm, 1 M), R is the universal gas constant, T is the temperature of the cell, n is the number of electrons in the half reaction, F is Faraday's constant, a_{ox} is the activity of the oxidized species and a_{red} is the activity of the reduced species in the half reaction (at low concentrations, concentration can be substituted for activity).[161]

Both possible self-discharge mechanisms studied have a dependence on proton concentration at the 1.0 V electrode (summarized in Table 5.1): with an increase in proton concentration, electrolyte decomposition and oxygen reduction predict a decrease in self-discharge. If electrolyte decomposition is the predicted self-discharge mechanism and the electrode is positively charged to 1.0 V, there is no initial hydrogen available. The addition of H_2 now introduces a new species and also a new reaction. As a result, with the addition of hydrogen no self-discharge information can be found and is denoted as "no information". With the addition of O_2 to the electrolyte, a decrease in self-discharge would be predicted since R6 would be shifted positively, farther outside the

potential window. Increasing the O_2 electrolyte content predicts a positive potential shift of oxygen reduction and therefore a decrease in self-discharge.

Table 5.1: Predicted effect of changing electrolyte components on the 1.0 V self-discharge mechanism. SD is an abbreviation for "self-discharge".

	Increase $[H^+]$	Increase p_{H_2}	Increase p_{O_2}
Electrolyte Decomposition	Decrease SD	No information	Decrease SD
Oxygen Reduction	Decrease SD	No effect	Decrease SD

If the concentration of protons was increased on the 0.0 V electrode, as shown in Table 5.2, and the self-discharge mechanism was electrolyte decomposition, the potential of R7 would shift more positively according to the Nernst equation and le Châtelier's Principle; the shift to a more positive potential (into the potential window) would increase self-discharge. If the partial pressure of H_2 increased and the self-discharge mechanism was electrolyte decomposition, R7 would shift negatively away from the E^o and the reaction would not proceed, resulting in a decrease in self-discharge. O_2 is not readily available in a deaerated solution so oxygen reduction cannot occur even with the addition of protons (another component necessary for the reaction is missing and therefore the reaction cannot occur) and this is indicated by "no reaction". Changes in p_{O_2} add a new species (O_2) which can be reduced to hydrogen peroxide or water.

Table 5.2: Predicted effect of changing electrolyte components on the 0.0 V self-discharge mechanism. SD is an abbreviation for "Self-discharge".

	Increase $[H^+]$	Increase p_{H_2}	Increase p_{O_2}
Electrolyte Decomposition	Increase SD	Decrease SD	No information
Oxygen Reduction	No reaction	No effect	Increase SD

By identifying the mechanism of self-discharge through the Nernstian predictions and the Conway self-discharge mathematical models[11, 118, 163] a better understanding of, and possible decrease in, self-discharge may be realized.

5.2 Testing O_2-evolution as Self-discharge Mechanism on 1.0 V Electrode

Predictions using le Châtelier's Principle and the Nernst equation suggest that if electrolyte decomposition (reaction 6) on the 1.0 V electrode, was the self-discharge reaction the addition of oxygen content to the electrolyte would have a positive shift in the reaction potential. The positive shift would move the reaction potential farther out of the potential window, resulting in a decrease in self-discharge from 1.0 V (less potential change during the self-discharge measurement). Similarly, the removal of O_2 from the electrolyte (by sparging with N_2) should result in a negative shift in reaction potential and a concomitant increase in self-discharge on an electrode held at 1.0 V.

As seen in Figure 5.1a, with the addition of oxygen by bubbling O_2 through the cell, there is no effect on self-discharge within experimental error. In addition, the removal of oxygen from the electrolyte, by bubbling N_2 through the cell, results in no significant change in self-discharge. Self-discharge profiles are considered the same if the profiles are within ± 10 mV of the self-discharge profile collected in N_2-bubbled electrolyte. Since the self-discharge profiles do not follow the trend predicted based on the amount of dissolved oxygen in the electrolyte, this suggests that electrolyte decomposition is not the self-discharge mechanism on the carbon electrode charged to 1.0 V in aqueous electrolyte electrochemical capacitors.

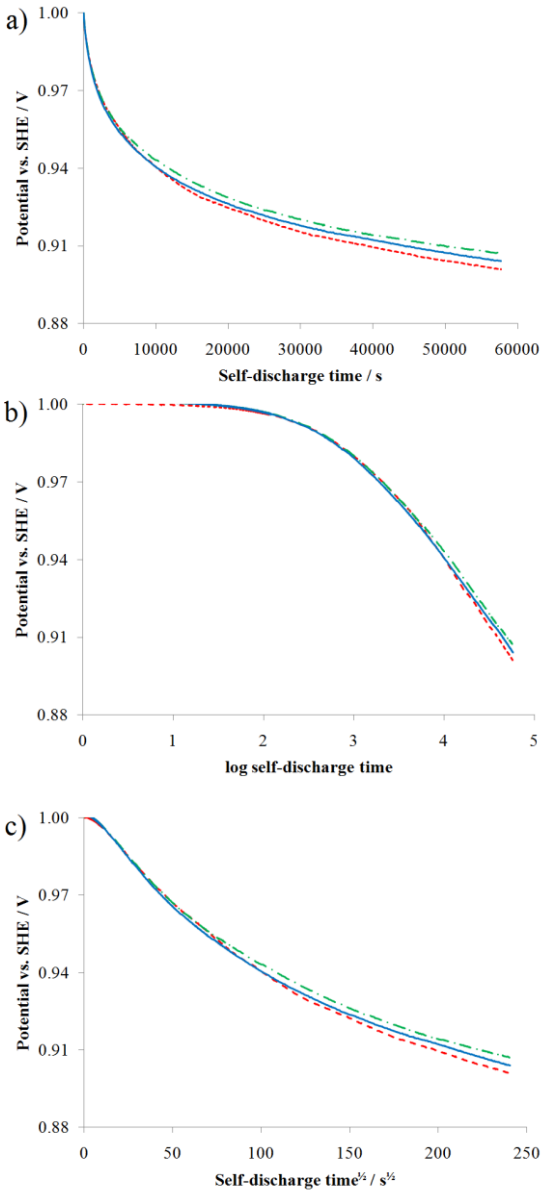

Figure 5.1: Self-discharge profiles of Spectracarb 2225 carbon cloth (*ca.* 10 mg), in 1.0 M H_2SO_4, ramped from 0.5 – 1.0 V at 1 mV s^{-1} with a 30 minute holding step. Solution not bubbled (— —); saturated with N_2 (— •); saturated with O_2 (——).

The evidence against oxygen evolution on the 1.0 V electrode can be strongly supported by calculations of the O_2 content required to shift the reaction potential into the electrode's potential window. Assuming the electrolyte is not deaerated, the dissolved oxygen content can be calculated using Henry's Law and a typical atmospheric oxygen content of 0.2 atm. Combining this dissolved oxygen concentration with 1.0 M H_2SO_4

into the Nernst equation would result in only a -50 mV shift in the potential to 1.18 V. The quantity of oxygen necessary to shift the equilibrium potential even to 1.0 V (the very upper limits of the potential window) would be 2.8 x 10^{-16} mol L^{-1}, a trace amount unlikely to be reached under normal conditions. Dissolved oxygen probe measurements showed the quantity of O_2 in a N_2-saturated solution to be 0.1 atm O_2 (1.3 x 10^{-4} mol L^{-1}), which is significantly more than the trace value calculated to be necessary to move the water oxidation reaction into the potential window used in this work.

To further elucidate the kinetics of the self-discharge reaction occurring on the positive electrode, the self-discharge profiles were plotted versus log t as well as $t^{1/2}$ (from section 2.6.1). An electrolyte decomposition mechanism is expected to be activation-controlled, rather than diffusion-controlled. With O_2, N_2 and no bubbling, there is a linear region, after an initial plateau, in the self-discharge profile when plotted versus log t (Figure 5.1b), which is consistent with an activation-controlled self-discharge mechanism. However, it is also consistent with charge redistribution which may not have been completely removed in the 30 minute hold.[14, 123] That the self-discharge mechanism is not diffusion-controlled is further confirmed by the lack of a linear region in the self-discharge profile when plotted versus $t^{1/2}$ (Figure 5.1c). From this data, it is shown that while the self-discharge mechanism may be activation-controlled, the lack of trend with varying dissolved O_2 concentration argues against self-discharge at the positive electrode being caused by electrolyte decomposition, in the form of O_2 evolution. Additionally, the slope in the linear region of Figure 5.1b was found to be 45 ± 2 mV dec^{-1}, rather than the expected 120 mV dec^{-1} Tafel slope for oxygen evolution (assuming the first or second electron transfer is the rate-determining step).[172] Therefore, oxygen evolution is not the

cause of self-discharge on the 1.0 V electrode. Rather, self-discharge from the 1.0 V electrode is due to either another, as yet unidentified, activation-controlled Faradaic reaction or is governed chiefly by charge redistribution.

5.3 Testing H_2-evolution as Self-discharge Mechanism on 0.0 V Electrode

When the working electrode is charged to 0.0 V in 1.0 M H_2SO_4 the electrolyte decomposition reaction would be in the form of protons being reduced to H_2 (see reaction 7). Under typical conditions (no bubbling of any gas) the dissolved H_2 concentration in the electrolyte solutions is 6.2×10^{-7} mol L^{-1}, using Henry's Law and atmospheric H_2 content. Using the Nernst equation this H_2 concentration in 1.0 M acid results in a positive potential shift of 0.18 V, which is a shift into the voltage window, suggesting that electrolyte decomposition is a reasonable self-discharge reaction.

The addition of H_2 would be predicted, using the Nernst equation, to cause the reaction potential to shift negatively, causing a decrease in self-discharge, and the removal of H_2, through N_2 sparging, should cause an increase in self-discharge (see Table 5.2). As can be seen in Figure 5.2a, the self-discharge profile of the negative electrode with the addition of H_2 was not significantly changed (within experimental error) from profiles where the electrolyte was N_2 saturated to remove dissolved H_2. The small variation seen is inconsistent with the predictions of increased self-discharge due to H_2 in solution causing electrolyte decomposition. The self-discharge profile for the non-bubbled system is surprisingly large, and is out-of-line with the prediction of electrolyte decomposition. Since the non-bubbled solution is not sparged with any gas, very little H_2 would be present; therefore it is unlikely that electrolyte decomposition to H_2 is causing

the increased self-discharge. The results for this non-bubbled system will be discussed again in section 5.4, but, in general these results argue against electrolyte decomposition as the self-discharge mechanism on the negative electrode.

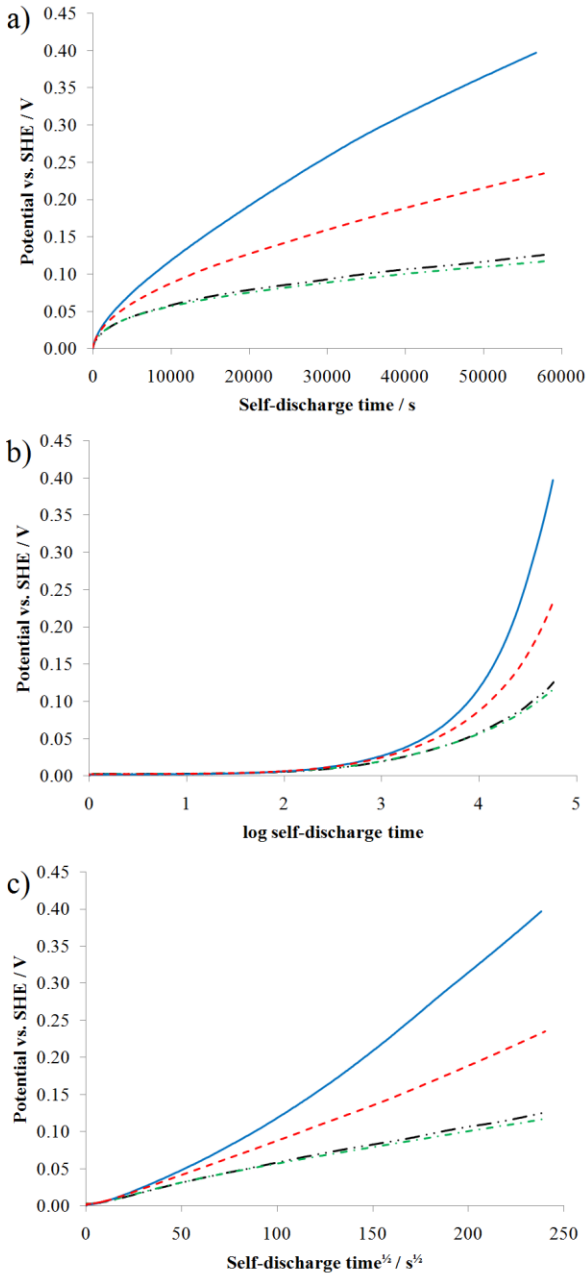

Figure 5.2: Self-discharge profiles of Spectracarb 2225 carbon cloth (*ca.* 10 mg), in 1.0 M H_2SO_4, charged from 0.05 – 0.0V at 1 mV s^{-1} with a 30 min hold step. Solutions not bubbled (— —); saturated with N_2 (— •); saturated with H_2 (— • •); saturated with O_2 (——).

The kinetic relationships of the self-discharge profiles, when compared to the Conway models, also provide strong evidence that electrolyte decomposition is not the dominant self-discharge mechanism on electrodes charged to 0.0 V. The non-linear relationship when plotted versus log t (Figure 5.2b) suggests that the self-discharge mechanism is not activation-control or charge redistribution. The self-discharge profiles are, rather, consistent with a diffusion-controlled self-discharge mechanism, as can be seen with a linear region when potential is plotted versus $t^{½}$ (Figure 5.2c). Electrolyte decomposition should not provide a diffusion-controlled profile, as the electrolyte is at a sufficiently high concentration such that it does not need to diffuse to the surface to react, and should, instead result in an activation-controlled mechanism. Therefore, the presence of a diffusion-controlled profile also strongly negates the possibility of electrolyte decomposition being the self-discharge mechanism on the negative electrode in carbon electrode, aqueous electrolyte electrochemical capacitors.

5.4 Testing O_2-reduction as Self-discharge Mechanism on 0.0 V Electrode

The presence of oxygen in the electrochemical capacitor electrolyte provides another possible self-discharge reaction in the form of oxygen reduction to water or hydrogen peroxide.[139] Hydrogen peroxide is the expected product for the system under study, as is typical with carbon electrodes.[148] Self-discharge profiles were collected from 0.0 V with varying concentrations of dissolved oxygen in the electrolyte to provide insight into a possible oxygen reduction self-discharge mechanism. Oxygen reduction as the self-discharge reaction would be consistent with the larger degree of self-discharge exhibited by the non-bubbled system (*cf.* the N_2-saturated and H_2-saturated systems) in

Figure 5.2. Bubbling either N_2 or H_2 through the electrolyte would be expected to remove O_2, preventing O_2 reduction and therefore resulting in less of a potential change if oxygen is the self-discharge mechanism. Additionally, the low concentration of O_2 present in either the non-bubbled or N_2/H_2 bubbled cases would be expected to result in a diffusion-controlled self-discharge reaction, as indeed is seen in the linear V vs. $t^{½}$ profile in Figure 5.2c at times greater than 25 $s^{½}$.

Near the beginning of the N_2- and H_2-saturated self-discharge profiles at times less than 25 $s^{½}$, the system is likely under mixed-control, where the oxygen reduction reaction rate may depend on activation-control (with an exchange current density similar to the 10^{-4} A cm^{-2} rate for graphite or carbon nanotubes)[173] charge redistribution and/or transport-control. At longer times, the self-discharge current, *I*, (calculated by

$$I = -C\frac{dV}{dt} \tag{12}$$

where *C* is the capacitance[11, 118, 163]) falls below that of the exchange current density suggesting that diffusion is limiting self-discharge. Thus, the results seen for the situation where N_2 and H_2 is bubbled in the cell in Figure 5.2 are consistent with oxygen reduction as the self-discharge mechanism on the negative electrode, with diffusion as the rate determining step at longer self-discharge times.

Further support for oxygen reduction being the self-discharge mechanism was seen when O_2 was bubbled through the electrolyte for 24 hours prior to and during self-discharge. The increase in dissolved oxygen content resulted in a significant increase in the self-discharge (a much larger potential change over time), as seen in Figure 5.2, and suggests that minimization of the O_2 content in the electrolyte is necessary when the electrode is charged negatively.

Assuming the loss of potential is solely due to O_2 reduction, an O_2 electrolyte concentration can be calculated. The concentration of O_2 near the electrode or in the pores which is required to cause the degree of self-discharge seen in the non-bubbled system in Figure 5.2, can be estimated. Using the loss in potential (*ca.* 0.24 V), the capacitance of the carbon in 1.0 M H_2SO_4 at 0.0 V (155 F g^{-1}, Figure 4.1), Faraday's constant (96485 C per mole of electrons), the pore volume of the carbon (1.2 mL g^{-1}) and the ratio of two electrons being used for the reduction of one O_2 molecule to hydrogen peroxide. This estimation suggests that a dissolved oxygen concentration of 0.16 mol L^{-1} in the pores is required to cause the degree of self-discharge evident in these systems. The oxygen content of a non-bubbled electrolyte is *ca.* 1.6 x 10^{-4} mol L^{-1} (as measured by the dissolved oxygen probe). Thus, the amount of oxygen in the pores is insufficient to fully account for the degree of self-discharge seen in Figure 5.2 and the discharge would require O_2 from the bulk electrolyte to diffuse to the electrode surface, and may account for the $t^{½}$ profile evident in this system.

The linearity of the self-discharge profile when plotted versus $t^{½}$ (as seen in Figure 5.2c) argues for the electrolyte in the pores having been depleted of dissolved oxygen, as this $t^{½}$ model was developed for semi-infinite diffusion to a planar electrode.[11, 118, 163] In contrast, if the limiting reaction was diffusion in the pores of the electrode a much more complex relationship between the flux to the surface and time is expected. Since the flux of material is directly related to the current, and the current discharges the electrode, thereby changing the electrode potential, the self-discharge potentials would also be expected to have a similar relationship with time if there is diffusion in a cylindrical pore. Pore narrowing and pore size poly-dispersity are also expected in the carbon used in this

work and will also cause a more complex relationship between voltage and time. Thus, the clear linearity in self-discharge potential with square-root time argues that the diffusion-control Faradaic reaction controlling self-discharge does not occur inside the pores to any great extent. This suggests the O_2 reactant is depleted in the pores during the electrode charging process or early on in the self-discharge. The electrodes in this work likely result in this planar-type of diffusion because of the small pores in this carbon, resulting in a high surface area to volume ratio in the pores. This allows for the pores to be depleted of oxygen rapidly, and may minimize the active surface area for Faradaic self-discharge based on diffusion.

As the charge on the external surface of the electrode is removed through the Faradaic self-discharge process, the charge deeper in the pores is likely fed up to the surface through charge redistribution.[123, 174] Thus, while the Faradaic self-discharge reaction may only be occurring on the face of the electrode, with a charge redistribution process, the whole electrode surface may eventually be discharged.

To examine if the pores may be depleted during the ramp and subsequent hold step in charging of the electrode, the current recorded during the holding step is shown in Figure 5.3. It can be seen that the current was higher for the non-bubbled situation versus the system when bubbled with either H_2 or N_2, as is consistent with a higher concentration of O_2 in the electrolyte. The curve for the non-bubbled system is, however, approaching the curves for the system where O_2 has been removed, suggesting that the O_2 in the pores may be in the process of being depleted during the holding step. The equilibrium current never reaches the level of the H_2 and N_2 currents, always remaining slightly higher. This slightly higher current is likely due to O_2 diffusing from the bulk

and reacting on the face of the electrode. Again, having O_2 reacting on the face (or outer surface) of the electrode is consistent with the linear potential drop with $t^{½}$ (seen in Figure 5.2c), which the Conway model suggests is due to a diffusion-controlled process. Therefore, the external surface is where the majority of the self-discharge reaction occurs.

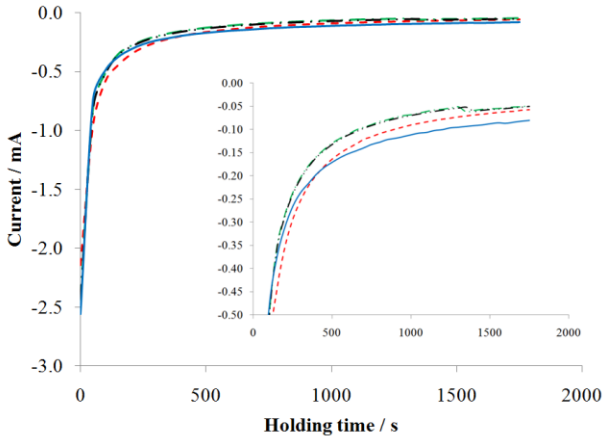

Figure 5.3: Comparison of current profiles of Spectracarb 2225 carbon cloth, in 1.0 M H_2SO_4, charged 0.5 – 0.0 V at 1 mV s^{-1} during a 30 minute holding step. Inset is a magnification at low current. Solutions not bubbled (— —); saturated with N_2 (— •); saturated with H_2 (— • •); saturated with O_2 (——).

From the current profiles seen in Figure 5.3 it can be seen that the current of the O_2-bubbled electrolyte has a larger cathodic current during the holding step which is consistent with some residual O_2 content in the pores not reacting during the 30 minute holding step. Had the entire O_2 content been used up during the holding step the current profile would have been similar to those for N_2-bubbled or H_2-bubbled systems. The higher current seen in Figure 5.3 suggests more O_2 reacting on the electrode, arising from a higher oxygen content of the electrolyte, and therefore the higher concentration of the O_2 in the pores. This higher concentration, at least initially, may be sufficient to lead to a mixed activation- and diffusion-control situation, explaining why the curve in Figure 5.2c

for the O_2-bubbled system is not linear with $t^{1/2}$ (diffusion-controlled) at short times. As the O_2 in the pores is used up during self-discharge, the system may become more diffusion-controlled as the reaction becomes limited by transport of the O_2 from the bulk electrolyte to the surface of the electrode, and therefore resulting in the diffusion-controlled profile at longer times (greater than 150 $s^{1/2}$), as is seen in Figure 5.2c.

The N_2-bubbled and H_2-bubbled systems exhibit considerably less self-discharge than the non-bubbled and O_2-bubbled systems, but their self-discharge is not insignificant. It is possible that enough oxygen remains in the electrolyte that it is responsible for this self-discharge. Nevertheless, O_2 reduction has been identified as a main cause of self-discharge, suggesting that removal of O_2 from an electrolyte will minimize self-discharge in electrochemical capacitors.

5.5 Examining Effect of pH on Self-discharge

Self-discharge profiles in aqueous electrolyte have a predicted dependence on proton concentration; on the electrode charged to 1.0 V, self-discharge is predicted to decrease when the pH is decreased (increase in $[H^+]$). The oxygen-evolution, hydrogen-evolution and oxygen-reduction are all dependent on protons and therefore the potential would shift more positively, resulting in a predicted decrease in self-discharge. The dependence on proton concentration can be seen in Figure 5.4, where the slope of the oxygen evolution reaction (reaction 6) is shown. At pHs higher than 4, the potential of oxygen production is within the potential window of 0.0 – 1.0 V vs. SHE and can therefore result in an increase in self-discharge for the 1.0 V electrode.

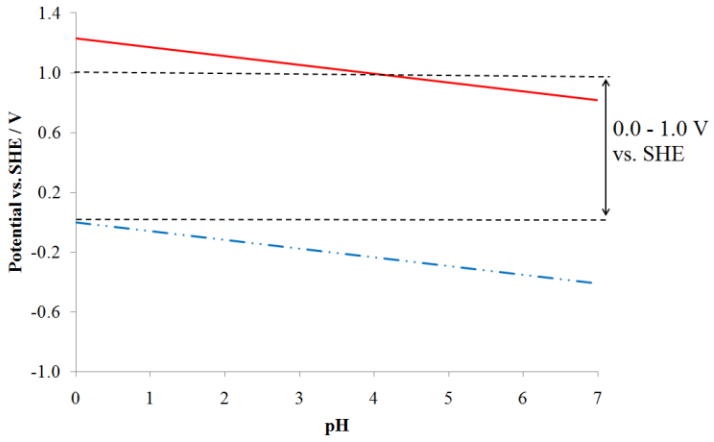

Figure 5.4: Schematic of oxygen and hydrogen evolutions' dependence on pH. Potential limits (— —), with the O_2 evolution potential (——) and H_2 evolution potential (— • •). The slope of oxygen and hydrogen evolution is equal to -59 mV per pH unit assuming 1 atm of O_2 and H_2.

Experimentally, the self-discharge profiles were run versus a constant SHE potential window (the potential window did not change with the H^+ concentration through the use of an SSCE reference electrode). As seen in Figure 5.5, there are differences between profiles over the acidic pH range in regards to the amount of self-discharge and also the shape of the initial drop in potential. The overall predicted trend of increased H^+ concentration resulting in a decreased self-discharge was observed in Figure 5.5. The self-discharge profile for pH 7 electrolyte has a more gradual drop in potential suggesting protons are likely involved in the self-discharge mechanism, though not directly related to the predicted mechanism of oxygen evolution. It is possible that the protons are involved in a reaction with carbon surface functionalities, and therefore in higher pH electrolyte the reaction is essentially "starved" of protons, resulting in a change in self-discharge profile shape.

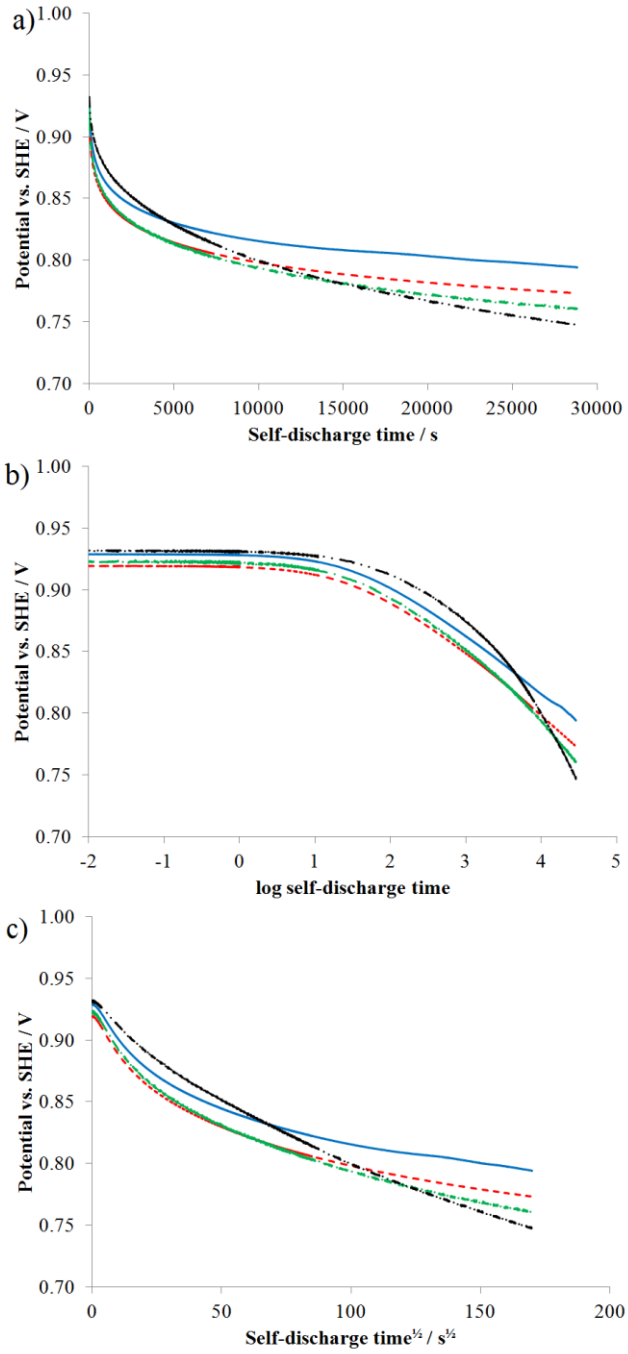

Figure 5.5: Self-discharge profiles of Spectracarb 2225 carbon cloth (*ca.* 10 mg) ramped from 0.5 – 1.0 V versus SHE at 1 mV s^{-1} in various concentrations of HCl with 1.0 M NaCl supporting electrolyte. pH 0.5 (——); pH 1 (— —); pH 2 (— •); pH 7 (— ••).

The addition of NaCl to the electrolyte as a supporting electrolyte may be influencing the self-discharge profiles obtained. It is difficult to ascertain whether the

differences seen in the self-discharge profile at higher pH values are in fact due to the depletion of protons, or if Na^+ is now becoming an important part of the self-discharge process. Unfortunately, a supporting electrolyte is necessary to ensure close to constant ionic strength in the electrolyte to eliminate ionic strength changes from having a part in the electrochemistry. As a result, self-discharge profiles in various pH values were not continued.

5.6 Conclusions

Predictions of partial pressure effects on self-discharge were made using the Nernst equation, and le Châtelier's Principle. The experiments were carried out by varying the dissolved oxygen and hydrogen content, individually. Comparisons of self-discharge profiles showed that self-discharge is not caused by electrolyte decomposition in the form of water electrolysis.

It was predicted that the addition of O_2 would result in a positive shift in the reaction potential, moving the reaction farther outside the potential window in this work, and thereby a decrease in self-discharge would be expected. The 1.0 V (positive) electrode did not show the expected decrease in self-discharge upon the addition of O_2, indicating electrolyte decomposition was not the mechanism of self-discharge.

In regard to the negative electrode, the self-discharge profile indicated a diffusion-controlled mechanism, which when coupled with the absence of any relationship between H_2 content and degree of self-discharge suggests that the electrolyte decomposition reaction of protons being reduced to water is not the mechanism of self-discharge.

In varying the dissolved oxygen content of the electrolyte, the self-discharge profile of the negative electrode was shown to exhibit significantly larger self-discharge with increasing O_2 concentration. This result is consistent with oxygen reduction to hydrogen peroxide as a main cause of self-discharge on the negative electrode. Additionally, although sparging of the electrolyte with N_2 removes O_2 and lessens the amount of self-discharge experienced, enough oxygen remains to allow for some degree of self-discharge. The kinetics of the oxygen reduction, while slow, are sufficient to account for the degree of self-discharge seen in these systems. A self-discharge profile which is linear with $t^{1/2}$ suggests that the electrolyte in the pores of the carbon has been depleted of dissolved oxygen, and that the self-discharge is limited by diffusion of oxygen to the external face of the electrode, and that the pores do not directly play a role in the Faradaic self-discharge process. It is likely, however, that the pores may feed their charge up to the surface through charge redistribution, allowing the whole electrode to eventually be discharged through the external electrode surface area.

Chapter 6 STANDARDIZATION OF THE BOEHM TITRATION

All of this work was published as *"Standardization of the Boehm titration: Part II – Method of agitation, effect of filtering and dilute titrant", Alicia M. Oickle, Sarah. L. Goertzen, Katelyn R. Hopper, Yasmin O. Abdalla, and Heather A. Andreas, Carbon, 48, 2010, 3313 – 3322.* I was responsible for collecting all the data presented herein except for the "dilute" titrant experiments that were run by Katelyn Hopper. I wrote the first draft of the paper and was heavily involved in the editing process. The error calculation equations presented in the paper were not included in this chapter as they were done by Heather Andreas.

6.1 Introduction

Carbon surfaces, like the surfaces of the electrodes used in this work, contain heteroatoms.[86, 168, 175, 176] These heteroatoms may be electrochemically active and store charge through pseudocapacitive reactions (like the quinone/hydroquinone redox couple), though it is also possible that heteroatoms may remove charge from the electrode through Faradaic reactions. As a result, it is important to understand the carbon surface functionalities on the electrodes surface. To identify oxygen-containing functional groups on the surface, many research groups use the Boehm titration.[18, 92, 102] Carbon is placed in bases of different strengths to quantify carboxyl, lactonic and phenolic carbon surface functionalities (see section 2.4.3.2); however, the method followed is rarely clearly described and a standardized method is not used. For results between research groups to be comparable, a standardized methodology must be determined and followed.

Previous work on standardizing the method of CO_2 removal and endpoint determination has been done by this group[23, 177] and was continued with the research described in this chapter. The specific focus of the Boehm titration standardization was on the method of agitation, the effect of filtering the carbon from the reaction base solution, and the use of dilute titrant.

In the most frequently referenced Boehm paper where the titration is described, the carbon and reaction base solution (the reaction mixture) was shaken for 12 hours in 0.05 N NaOH to complete neutralization.[102] After neutralization the base is acidified and then back-titrated. Since the original Boehm paper, research groups have modified the method of agitation to include shaking,[22, 178-180] stirring,[149, 181, 182] and, occasionally, sonicating.[105, 183] Other groups use no agitation at all.[60, 70, 106, 184-186] The duration of agitation time also varies between research groups, from one hour to five days. A discussion of the agitation method will be undertaken. After agitation, most groups filter the carbon from the reaction base before making aliquots to titrate.[22, 106, 179, 187] The effect of the filter paper on the reaction base was tested to see if this influences the moles of carbon surface functionality (n_{CSF}) results. Some groups, however, allow the carbon to settle to the bottom of the reaction vessel and then remove the aliquots from the solution above the settled carbon and this was also addressed here. The effect of using a dilute titrant on precisely obtaining the endpoint was also dealt with in this study, along with the need to standardize the base directly before titrations.

6.2 Carbon Removal and Filtering Experiments

Since carbon surfaces often have both acidic and basic surface functionalities, it is important to remove all of the carbon from the reaction mixture in the Boehm titration. The basic carbon surface functionalities of any carbon remaining in the sample would react with the HCl used in the acidification step of the titration, resulting in a higher pH. The increase in pH would lead to a negative bias for the amount of acidic carbon surface functionalities determined through this method.

Literature methodologies suggest allowing the carbon to settle out of solution for between 6 and 24 hours before removal of the aliquots.[21, 80, 96, 187] Two issues arise from this method. The first is that allowing the carbon to settle from the mixture adds substantial experimentation time to the Boehm titration. Of greater concern, however, is the likelihood of carbon being transferred into the aliquots for the titration. Even with 24 hours of settling time, a very small amount of carbon may remain at the solution/air interface, and this may allow for carbon to adhere to or enter the pipette when the aliquots are removed, leading to contamination of the aliquot. Additional problems with possible contamination arise with the last aliquot to be removed from the mixture, since when the volume of the solution is low (as with the last of the three aliquots, where a 10 mL aliquot is being removed from a 30 mL mixture containing the significant amounts of carbon), it is more likely that placing the pipette in the remaining solution and withdrawing the aliquot will cause agitation of the mixture, causing carbon to enter the pipette and be included in the aliquot.

Carbon sample removal from the reaction mixture is generally undertaken with filtering. Unfiltered blank samples (*i.e.* no carbon present) were compared to blank

samples passed through filter paper to examine whether the process of filtering the sample was significantly changing the amount of moles of carbon surface functionalities (n_{CSF}) determined in the Boehm titration. This is a concern since the typical filter paper found in laboratories is cellulose-based and has many hydroxyl functional groups on the surface. Therefore, the filter paper's functional groups could actually take up some of the reaction base when being filtered. Because the glucose units which comprise cellulose are stabilized with both intra- and inter-molecular hydrogen bonding,[188] it is unlikely that even NaOH may undergo a reaction with the filter paper hydroxyl groups, but this must be examined. As a corollary, the weaker basicity of the other reaction bases ($NaHCO_3$, Na_2CO_3) ensures that these bases are not strong enough to react with the filter paper and therefore, no filtering error is expected with these reaction bases. Given the large size of the holes/pores in the filter paper (*ca.* 11 μm) compared to the predicted size of the solvated ions of interest in the Boehm titration (< 1 nm), it is unlikely that there would be any loss of base through size-exclusion, and rather, any loss of base must therefore be due to a reaction between the NaOH and the filter paper. Titration curves of blank NaOH bases, seen in Figure 6.1, were collected on a blank unfiltered sample and blank samples filtered with a cellulose-based filter paper or a glass-based filter paper to determine any differences between methods. Glass-based filter paper was tested to remove surface functionalities, which may undergo neutralization, from the experimental set-up.

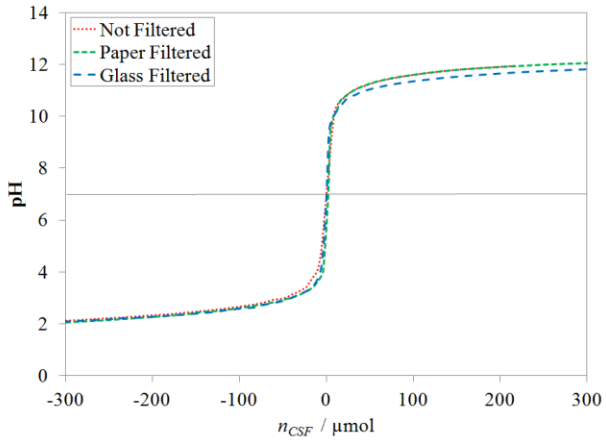

Figure 6.1: Comparison of titration curves of unfiltered NaOH aliquots of blanks to NaOH aliquots of blanks filtered through cellulose-based and glass-based filter paper.

From Figure 6.1, it can be seen there is no significant difference between the aliquots, whether filtered or unfiltered as all methods are within ± 2 µmol of zero (a value of 0 for n_{CSF} would be expected for a blank titration without carbon). This suggests the NaOH base is not reacting with the cellulose or glass filter papers and therefore filtering the sample with cellulose-based filter paper (the most commonly used method) is an appropriate method to remove carbon from the carbon/reaction base mixture and can be used in the Boehm titration procedure without having to take into account base losses.

Centrifugation has also been suggested as a method to separate the carbon from the reaction base mixture,[66, 189] and would require significantly less time than allowing the carbon to naturally settle. Also, centrifugation heats the sample slightly, and would require covers on the sample tube to avoid evaporation. If the solution was heated enough to result in evaporation of water, the 10-mL aliquot taken after centrifugation would be a slightly concentrated, resulting in an error in the future calculation. Since the filtering experiments did not show any signs of reaction base uptake, then the use of a centrifugation is unnecessary.

Because of the potential of a negative bias in the results caused by any carbon that is not removed from the carbon/reaction base mixture, it is vital that all of the carbon be removed from the carbon/reaction base mixture before the acidification step. The removal of carbon by allowing it to settle from solution is not recommended because of the extra time this introduces into the titration, as well as the possibility of contamination of the aliquots due to incomplete carbon removal. Since filtering the carbon from the mixture does not lead to any loss in reaction base, and provides a simple, quick and efficient method for removal of carbon, it is suggested that filtering (using either a cellulose- or glass-based filter paper) is an appropriate method for removal of carbon in the standardized Boehm titration.

6.3 Effect of Dilute Titrant

Blank titrations of $NaHCO_3$, Na_2CO_3 and NaOH were done with both standardized 0.05 M NaOH and 0.025 M NaOH titrant to determine whether more precise endpoints could be achieved with a more dilute titrant.[149, 190, 191] Since the smallest possible droplet size typically deliverable by a burette (with a human user) is 0.01 mL (a quarter drop), it is possible that using a more dilute titrant might allow for a smaller addition of moles of titrator base, and therefore a more precise determination of the endpoint. The average results (based on at least three measurements) and standard deviation (σ) of titrations using the different titrator base concentration are shown in Table 6.1. It would be expected that the n_{CSF} calculated in Table 6.1 would be zero as there is no carbon present. The lack of carbon would mean no base uptake and therefore, zero would be calculated. Because the quantity of n_{CSF} is on the μmol scale, and the

titration is using a burette with 0.01 mL precision, then the volume will always be slightly off on the endpoint and the calculated n_{CSF} will reflect these minor differences. It should be highlighted that the standard deviation is used in this table to show the variance in the replicate measurements, and does not imply the uncertainty in the measurements.

Table 6.1: Comparison of n_{CSF} determined using dilute 0.025 M titrant and 0.050 M regular titrant for blank samples.

Reaction Base	n_{CSF} ± 1σ / μmol	
	0.05 M NaOH	0.025 M NaOH
$NaHCO_3$	1 ± 1	1 ± 2
Na_2CO_3	11 ± 1	11 ± 2
NaOH	-4 ± 2	-9 ± 5

σ denotes standard deviation.

In Table 6.1, it can be seen for all three reaction bases there is no significant difference in the averages, and this is confirmed statistically as the values found from the dilute and regular titrant are the same for all the reaction bases (using a t-test with 95% confidence). These standard deviations fall within the typical error of this experimental set-up. Since there is no significant difference between the results in Table 6.1, either concentration can be used for the Boehm titration.

6.4 Effect of Exposure to Air on the Standardization of NaOH

Introduction of air, either during storage, mixing, or during solution preparation and titration may lead to changes in the proton concentration. Therefore, changes would be seen in the calculated n_{CSF} value. A standardized titration base solution (NaOH) is typically stored in a polyethylene container, which can make the standardized solution susceptible to concentration decreases. If the standardized concentration changes over

time due to dissolved CO_2, this effect must be taken into account to accurately determine the total n_{CSF}. CO_2 is introduced to the solution and the well-known effect of dissolved CO_2 in aqueous solutions, which can be seen in reactions 12 and 13, results in the formation of carbonic acid (H_2CO_3) which is then in equilibrium with the bicarbonate ion and a proton.[112]

$$CO_{2(aq)} + H_2O \leftrightharpoons H_2CO_{3(aq)} \qquad pK_a = 2.699 \qquad \text{(R12)}$$

$$H_2CO_{3(aq)} \leftrightharpoons HCO^-_{3(aq)} + H^+_{(aq)} \qquad pK_a = 6.352 \qquad \text{(R13)}$$

To determine how the introduction of air (through transfer between vessels and storage), and therefore CO_2, affects the concentration of the NaOH titrator base, several "standardization" titrations were carried out after the introduction of air. When the NaOH solution (*ca.* 0.05 M) was standardized immediately after preparation the concentration was found to be 0.055 ± 0.001 M NaOH. With subsequent stirring (and introduction of CO_2), the concentration changed and a *ca.* -1% concentration change was seen by the fourth standardization (with a concentration of 0.054 ± 0.002 M NaOH). The decline in NaOH concentration is expected since as CO_2 dissolves into the NaOH solution, protons would be produced, decreasing the NaOH concentration. Changes in NaOH concentration (if used in the calculation of n_{CSF}) would result in an experimental standard error of *ca.* 1 µmol at the equivalence point. Although 1 µmol may seem like an acceptable deviation, the error associated with the concentration decrease would be compounded since the HCl solution is standardized from the initially standardized NaOH. At the equivalence point, the difference from the two NaOH concentrations results in an experimental difference of 18 µmol. With the other error in repeated measurements seen previously in Table 6.1, the accuracy of the Boehm titration becomes an issue for carbons

with lower populations of surface functionalities (n_{CSF}). It is then advisable that the NaOH titrator base should be standardized immediately prior to being used.

It has been suggested that storage of solutions in polyethylene containers over extended time periods results in an increase of dissolved CO_2 in solution since CO_2 is able to penetrate the polyethylene. Note that the storage of NaOH in glass vessels is not recommended as the NaOH can cause the slow dissolution of the glass.[192] To determine how storage in polyethylene containers may affect the NaOH concentration samples of the standardized NaOH solution described above were stored in a polyethylene bottle for one week and was subsequently titrated. Its concentration was found to be 0.055 ± 0.001 M NaOH, which is the same as the initially standardized NaOH. This result suggests standardization is not needed immediately prior to each use since the concentration does not change over time; however, from the earlier experiments, the transfer of NaOH does effect the concentration. Therefore, standardization immediately prior should be use should be undertaken.

6.5 Method and Duration of Agitation

All methods of agitation (shaking, stirring and sonicating) were originally investigated to determine the optimal method for agitation. Although Spectracarb 2225 carbon cloth was previously used in Chapter 4 and 5, the high surface area and low weight, as well as the woven fabric makes the Boehm titration difficult to undertake. As a result, another carbon was used to investigate the effects of agitation method. The Black Pearls 2000 carbon used in this study have a spherical macroscopic structure (approximate diameter 1 mm). Therefore, with these Black Pearls it is possible to easily

observe if the agitation method is damaging or changing the carbon surface as this will result in a clearly visible change to the spherical nature of the particles. It is likely that any damage done to the Black Pearls surface will also be mirrored in other types of carbon, where the damage is not so easily seen (*i.e.* with graphite or activated carbon where the surface is already jagged and damage caused by agitation is difficult to recognize). It is important to identify if the method of agitation changes the surface since damage to the surface exposes new surface area (and possibly new carbon surface functionalities) which would otherwise not be exposed to the Boehm titration solution. If the carbon surface has changed it is possible the surface area and groups have also been affected by the agitation method and this may lead to an erroneous calculation of the carbon surface functionalities on the carbon surface.

Upon comparison of the carbon samples after agitation in reaction base, it was observed that after stirring the Black Pearls spheres had been broken apart, resulting in a carbon filtrand which was very much like a thick clay and was difficult to filter from the solution. This is in contrast to the sample reacted with the reaction base using no agitation and the shaken samples, which retained their spherical shape and were easily filtered from solution. To understand why there was such a significant difference in the physical properties of the Black Pearls 2000 after stirring, samples of Black Pearls 2000 carbon were observed using an optical light microscope to view any macroscopic changes to the carbon itself and the results can be seen in Figure 6.2. As can be seen in Figure 6.2, there is essentially no difference in the macroscopic surface structure between the as-received sample (Figure 6.2a), and the sample which had reacted with Na_2CO_3 without agitation (Figure 6.2b) and the sample which was shaken for 24 hours during Na_2CO_3

reaction (Figure 6.2c). Conversely, there is a significant macroscopic change in the structure of the carbon which was stirred (Figure 6.2d), as well as in the structure of the sonicated carbon (Figure 6.2e). The carbon which was stirred is much less smooth than the as-received sample and there is evidence that pieces of the carbon have been fractured off of the Pearls. This suggests that agitation may in fact be modifying carbons in ways which are not visible with the naked eye; though other types of carbons (*e.g.* graphite, carbon cloth) do not visibly show this change through stirring it is very possible these changes do occur.

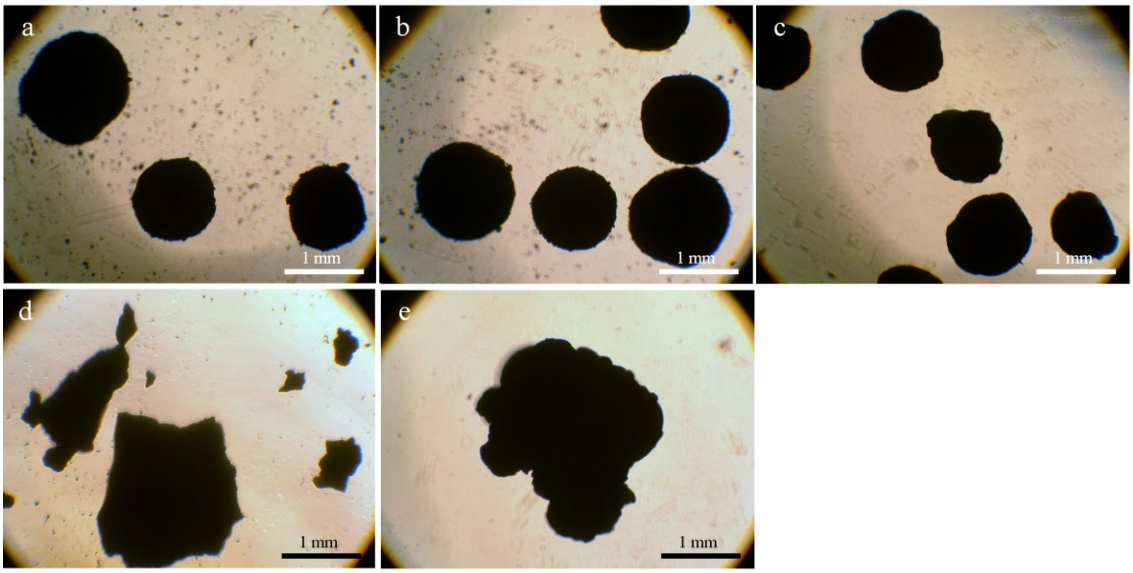

Figure 6.2: Optical microscopy images of Black Pearls 2000 carbon agitated in Na_2CO_3 (except a) at 4X magnification. a) as received from supplier (no contact with solution); b) no agitation; c) shaken for 24 h; d) stirred for 24 h; and e) sonicated for 10 mins.

The carbon sample which was sonicated also shows changes to its surface structure (similar to the stirred carbon sample), as these particles have lost their spherical shape and are, generally, larger in size suggesting that the sonication allowed for some agglomeration of the particles. The carbon was only sonicated for 10 minutes; longer times are expected to result in a more drastic change in the surface area. Along with the

obvious physical changes seen in Figure 6.2, sonication may produce chemical changes in the carbon surface. Ultrasound produces bubbles which collapse and results in high localized temperatures and pressures;[193] this process, called cavitation, can produce radicals and other products which can then interact with the mixture being sonicated, and could give inflated populations of surface groups in regards to the Boehm titration results.[193] In fact, the micro-jets which can be produced by ultrasound have a high kinetic energy which have been shown to displace electrode surface species, resulting in new surfaces. Recently published work by Guittonneau *et al.* has shown the degradation effect of ultrasound on graphite suspensions in degassed deionized water using transmission electron spectroscopy, laser diffraction particle sizing and Fourier transform mass spectrometry.[194] Results from the mass spectrometry experiments show mainly the generation of phenyl and phenol fragments from the graphene layers which have implications for use in the Boehm titration.[194] Increases in the number of phenol groups would have a direct and significant effect on the NaOH reaction base uptake. The degradation of the carbon through sonication would also change the exposed surface area and no longer have the same surface functional groups as carbon that was not sonicated; this would result in inaccurate and non-comparable results. Because of this, the use of ultrasound as a method of agitation is not recommended for use in the Boehm titration.

Since it can be seen in Figure 6.2c, that shaking does not significantly change the spherical shape of the Black Pearls 2000 carbon, shaking was deemed the best method of agitation, as Boehm originally suggested. While it is clear that shaking causes the least damage to the particle itself, each type of carbon under study must be examined to ensure the agitation method is not significantly damaging/altering the surface.

In order to ensure that the reaction bases have fully reacted with the carbon surface functionalities, agitation duration studies must be conducted for each type of carbon examined by the Boehm titration. The reaction base must flood all of the pores to fully react with all of the carbon surface functionalities on the carbon surface. The speed at which the reaction base will diffuse into pores is largely controlled by the size, shape and length of the pores, which is different for each type of carbon. For large pores, the speed of pore penetration by the reaction base may be increased somewhat by agitation of the solution outside of the pores; however, for small pores there is no effect from bulk solution agitation. In the case of small pores (such as the ones usually required in carbons in order to provide high surface area), diffusion will be the main method of transport of the reaction base into the pore, and, the speed of this diffusion will depend on the length of the pores and the tortuosity of the pores. These factors are different for each type of carbon (carbon cloth, graphite, activated carbon, etc.). Thus, because of the differences in pore structure, surface area and structure/particle stability, no standardized method for agitation time can be proposed, although it is anticipated that longer agitation times may be required for high surface area carbons. In order to ensure that the reaction base has had sufficient time to react with the surface, but is not too long as to allow the agitation to damage the carbon surface, the length of agitation time must be examined for each carbon under study.

6.6 Conclusions

The Boehm titration, commonly used for the identification and quantification of carbon surface functionalities, is undertaken in a variety of ways in the literature and

requires a standardized method for the comparison of results between literature groups. Carbon removal, the use of dilute titrant, the effect of air on standardization, and the method of agitation were examined. It was found filtering the carbon and reaction base mixture does not affect the n_{CSF} results and is an acceptable, easy method for separation of the carbon from the reaction base. Allowing the carbon to settle to the bottom of the vessel did not allow sufficient separation as the last aliquot typically had carbon transferred with the reaction base.

It was found that stock solutions (HCl and NaOH) should be standardized immediately prior to titrations as over time, the introduction of air (through transferring to the titration containers) results in changes in concentration which can have significant effects on the n_{CSF}. There is no significant difference between titrations when the regular (0.05 M) and more dilute (0.025 M) NaOH titrant is used. Thus, either concentration is acceptable for the titrant. The solutions must be degassed throughout the titration to avoid a bias.

The best method of agitation was found to be shaking, as originally suggested by Boehm. Stirring and sonication resulted in a change in the macroscopic surface of the carbon particles, and should be avoided in terms of sample agitation. Duration of shaking is dependent of the surface area of the carbon, and high surface area carbons (*i.e.* many small pores) would require a longer agitation time as diffusion into the pores is important in the Boehm titration.

Chapter 7 ELECTROCHEMICAL EXAMINATION OF CARBON SURFACE FUNCTIONALITIES ON CARBON ELECTRODES

7.1 Introduction

It is interesting to study carbon surface functionalities as some surface groups can store charge through pseudocapacitive reactions (see sections 2.2.2 and 2.4.3.1) allowing for higher charge storage compared to purely double-layer charge storage. It has yet to be determined the effect carbon surface groups have on self-discharge in aqueous electrochemical capacitors, and therefore it is of interest to examine their behaviour more closely. Electrochemically active carbon surface functionalities can also be examined using cyclic voltammetry.

Although the Boehm titration (see sections 2.4.3.2 and Chapter 6) is very commonly used for analysis of carbon surfaces, it is difficult to correlate the data collected from this method with the electrochemical data due to a variety of factors, described below. Results from the Boehm titration are not reproducible, possibly due to surface heterogeneity between carbon samples. If the populations of various surface groups are not evenly dispersed on the carbon surface, then results vary depending on the sampling region. The Boehm titration technique is not specific to only electroactive surface groups and therefore the results obtained from the Boehm titration cannot be used to calculate the pseudocapacitive contributions on an electrode. Additionally, if the carbon sample used in the Boehm titration was previously used as an electrode in an electrochemical experiment using an acidic electrolyte, it is necessary to fully remove the

electrolyte before using the electrode as the carbon sample in the Boehm titration, which can prove difficult.[177] Any acid left in the pores of the carbon would then neutralize the Boehm reaction base, resulting in an inflated acidic surface group population.

Since electrochemically active carbon surface functionalities are the ones that store charge and may also cause self-discharge, the best way to examine the appropriate carbon surface groups is through electrochemical means. The data discussed within this chapter focuses on classification of regions within the cyclic voltammogram of Spectracarb 2225 carbon cloth and how the application of given potentials change the cyclic voltammogram. A better understanding of the carbon cyclic voltammogram electrochemical signature is necessary, and therefore, the Faradaic processes occurring at the electrode are studied herein.

7.2 Continuous Potential Cycling to Steady-state

Identifying the redox reactions on carbon electrodes within the aqueous potential window is necessary to understand charge storage since these Faradaic reactions may be pseudocapacitive in nature and therefore enhance charge storage, or may be non-pseudocapacitive and lower columbic- and energy-efficiencies. Using cyclic voltammetry the redox processes are easily visible, making cyclic voltammograms a good electrochemical method for the identification of the multiple Faradaic reactions present on carbon electrodes. It is also important to understand the changes occurring in the cyclic voltammogram data prior to self-discharge data (presented in Chapter 8).

As can be seen in Figure 7.1, there are significant changes in the current with continued potential cycling between 0.0 – 1.0 V. An increase in current (*ca.* 1.5 mA) is

seen with the development of a pseudocapacitive redox peak at *ca.* 0.55 V, which is commonly attributed to quinone/hydroquinone reduction/oxidation.[89-91] The peak is classified as pseudocapacitive as it is highly reversible as evidenced by the symmetry of the current about the zero current axis. Another region with significant change in the cyclic voltammogram of Spectracarb 2225 carbon cloth with continued cycling between 0.0 – 1.0 V is the decrease in the current of an oxidation wave, above 0.7 V. The current decreased by *ca.* 4.5 mA at 1.0 V from the first cycle to cycle 300. Kinoshita and Bett[153] discussed carbon corrosion, visible as an anodic wave, as two separate processes, that of surface oxide formation and CO_2 evolution. They determined the two processes were independent of one another, and also that the corrosion rates were independent of CO_2 pressure.[153] However, Kinoshita and Bett's work used a different carbon system (Vulcan XC-72) and the potential applied was higher, up to 1.2 V, resulting in a larger oxidation wave and likely, more oxidation of the carbon. Generally, carbons in acidic aqueous electrolyte are not exposed to potentials past 1.0 V, and therefore the magnitude of the oxidation seen in the Kinoshita and Bett work would not be seen in typical experimental conditions.[153] It is also important to note that their research did not focus on the effects of continued cycling, or on the potential at which the quinone/hydroquinone peak begins to develop, and therefore this work will focus on these research areas.

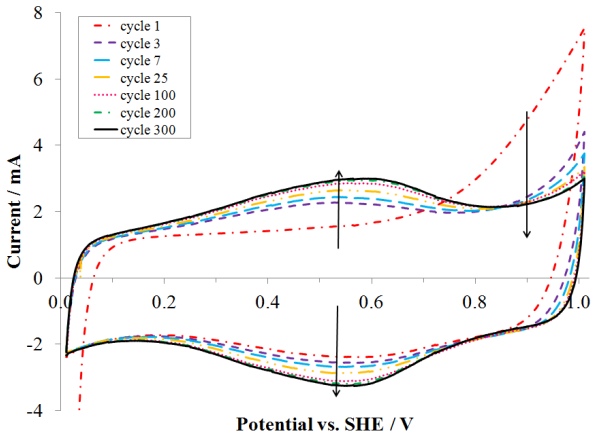

Figure 7.1: Cyclic voltammograms of a continuously cycled Spectracarb 2225 carbon cloth electrode (*ca.* 10 mg) in 1.0 M H_2SO_4 at 1 mV s^{-1}.

With continued potential cycling, the anodic and cathodic charge change significantly. The charge is calculated by the area under the curve, divided by the sweep rate, and is calculated for the anodic and cathodic sweeps of the cyclic voltammogram, down to the zero current line. The charge data are shown in Table 7.1 for both the first cycle and the 300th cycle (steady-state). For the first cycle, it is evident the charge in the anodic and cathodic sweeps are different. Since the anodic charge is significantly larger than the cathodic charge, this suggests that in the anodic sweep there is an irreversible reaction, the product of which cannot be reduced. However, over continued cycling the charge between the anodic and cathodic sweeps become the same. The anodic and cathodic sweep charge becoming the same means the system becomes reversible, as no charge is oxidized that is not reduced.

Examining the oxidation wave and the development of the hydroquinone peak in the cyclic voltammogram is necessary to determine whether the oxidation wave contains the current associated with a conversion to, or production of, quinone groups. The charge was therefore calculated for the oxidation wave from 0.6 – 1.0 V and above 1.5 mA, and

for the reduction peak below -1.5 mA to determine if there was a correlation between these two regions of the cyclic voltammogram. From these data it can be seen that more oxidation occurs in the oxidation wave (1060 ± 60 mC) than the corresponding reduction peak (350 ± 70 mC) in the first cycle. The data suggests that there is an irreversible oxidation in the oxidation wave. Over time, the oxidation wave charge becomes significantly smaller (450 ± 30 mC), and more similar to the charge of the reduction peak (800 ± 150 mC). Although the oxidation wave and the reduction peak (focused on the hydroquinone peak) are not the same, the magnitudes are closer than in the first cycle. With the oxidation wave being smaller than the reduction peak at the 300th cycle, but the overall anodic and cathodic sweep charges being the same suggests that the oxidation wave is not being converted to the quinone groups at steady-state.

Table 7.1: Summary of average charge of nine Spectracarb 2225 carbon cloth electrodes continuously cycled to steady-state from 0.0 – 1.0 V in 1.0 M H_2SO_4.

	Charge ± 1σ / mC			
Cycle number	Anodic sweep*	Cathodic sweep*	Oxidation wave†	Reduction peak‡
1	2370 ± 110	1850 ± 70	1060 ±60	350 ± 70
300	2290 ± 70	2300 ± 150	450 ±30	800 ±150

Results from the Boehm titration for Spectracarb 2225 carbon cloth electrodes were previously analyzed in Sarah Goertzen's MSc thesis (former graduate student in the Andreas laboratory). The most important conclusion from the previous work is the inability to quantify populations of surface groups accurately as the uncertainty encompasses many of the values.[177] The significant uncertainty associated with the

* Integrated from 0.0 – 1.0 V, to the zero current axis.
† Integrated from 0.6 – 1.0 V with a 1.5 mA current baseline
‡ Integrated from 0.0 – 1.0 V, with a -1.5 mA current baseline.

Boehm titration technique, along with such small populations on the surface (μmol g^{-1}) makes it difficult to determine the technique's overall exactness to the correct value. For these reasons, use of the Boehm titration was discontinued for this research.

Since it was not possible to quantify carbon surface functionalities on this particular carbon using the Boehm titration, another method to determine surface functionalities was proposed. Electrochemistry on the electrodes was chosen as it only identifies carbon surface functionalities that are electroactive in charge storage and possibly as a Faradaic cause of self-discharge, rather than all possible surface functionalities.

7.3 Issues with Electrode Mass

In cyclic voltammetry the measured current response is proportional to the capacitance (the ability to store charge at a given voltage). Cyclic voltammograms can also as be plotted as current density where the current is divided by the mass or surface area of the electrode. A problem arose where the masses of electrodes of the same geometric area were not similar (variation of *ca.* 30 %), however when the carbon cloth was placed in the electrolyte, the measured current was the same as the previous electrodes (see Figure 7.2a). Multiple analytical balances were tested and there was no change in the mass reading between balances, thereby eliminating a bias due to the scale.

One possibility of the variation in mass is due to a section of the electrode not connected to the rest of the electrode resulting in inactive electrode material. An electrically unconnected portion of the electrode is not expected with the carbon cloth used in this work as it is woven, and the pressure applied through the current collector

would make contact with a stray piece of carbon. Another possibility is the additional mass is due to an electrochemically inactive contaminant. If it were a contaminant that was not electrochemically active then it would not affect the electrochemistry, and can be ignored, however the mass cannot then be used to calculate the current density.

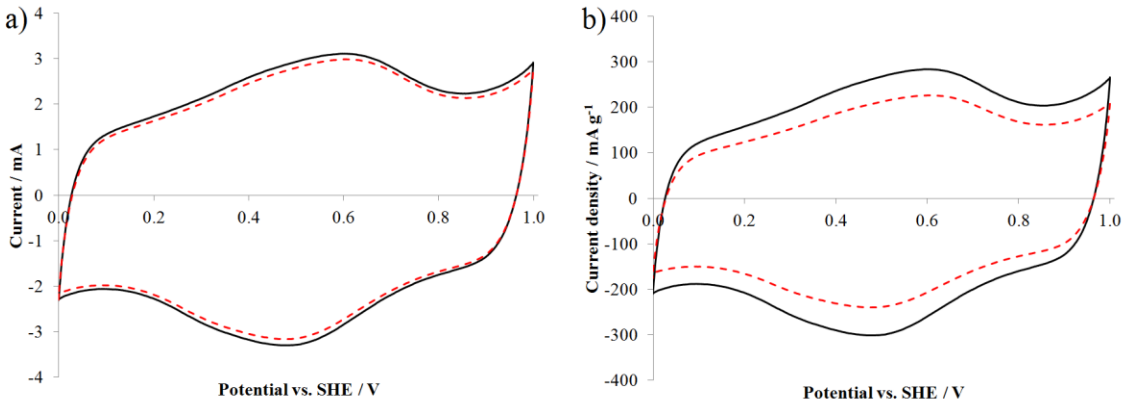

Figure 7.2: Cyclic voltammograms of two Spectracarb 2225 carbon cloth electrodes in 1.0 M H_2SO_4 at 1 mV s^{-1}. a) shows the absolute current value while b) shows the current density. The black line (—) is a 10.96 mg electrode, and the dashed red line (– –) is a 13.19 mg electrode.

Due to the inaccurate masses, when the current was then normalized by dividing by mass there is a significant difference in the current density (see Figure 7.2b). It should be noted that this mass variation was only seen over a short time period, and many years of work with Spectracarb 2225 carbon cloth has shown very similar currents for all electrodes. Since all these electrodes were made using the same diameter punch the electroactive surface areas are very similar and therefore the current density should also be similar. To witness a 60 mA g^{-1} difference between electrodes of the same geometric area, as seen in Figure 7.2b, is not expected. As a result of these mass readings and to be able to compare data between electrodes, the absolute current and charge values will be presented in this chapter.

7.4 Limiting the Lower Potential of the Cyclic Voltammograms

The use of H_2O_2 as a reagent in chemical activation to oxidize the carbon surface is commonly seen in the literature.[78, 81, 82] It was previously suggested (see section 5.4) that at lower potentials (close to 0.0 V) in the cyclic voltammograms of Spectracarb 2225 carbon cloth electrode material, oxygen is reduced to H_2O_2. Since peroxides are known to be strong oxidizing agents for carbon surfaces,[78, 81, 82] it was of interest to truncate the potential window, never exposing the electrode to potentials below 0.4 V, therefore limiting the formation of H_2O_2. If H_2O_2 is not produced in the electrolyte then the quinone/hydroquinone redox peak would not increase due to the presence of the oxidant.

Cyclic voltammograms with a lower potential limit of 0.4 V are shown in Figure 7.3. The cyclic voltammograms have an increased upper potential window in 25 mV increments and are therefore referred to as "incremental cyclic voltammograms". Incremental cyclic voltammograms are used since it is then possible to determine where certain redox processes begin. The cyclic voltammograms in Figure 7.3a clearly show the development of the quinone/hydroquinone redox couple centered *ca.* 0.55 V. The development of the redox couple begins minimally at 0.65 V, and becomes larger with increasing upper potential limits (as seen in Figure 7.3b and c). Since the cyclic voltammograms show evidence of the development of the quinone/hydroquinone redox couple without exposure to potentials below 0.4 V, this suggests that any possible reactions at lower potentials, like H_2O_2, are not responsible for the development of the pseudocapacitive quinone reaction.

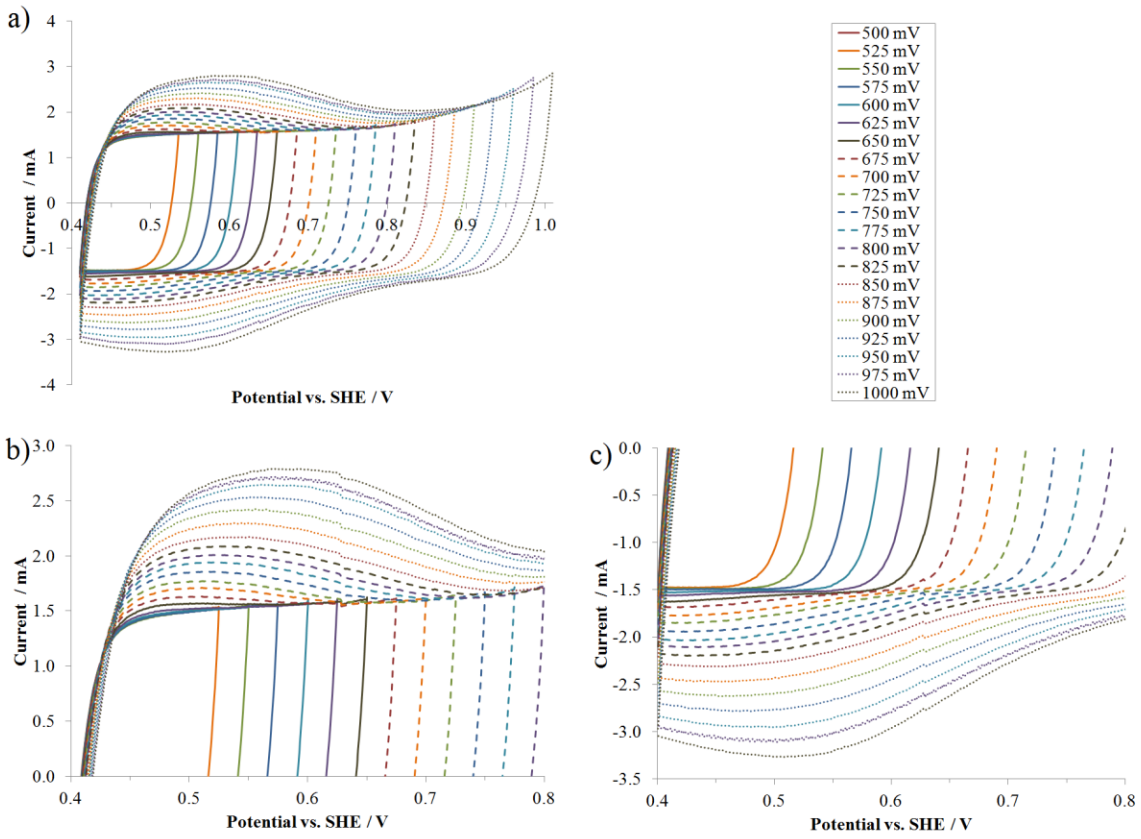

Figure 7.3: Cycle 90 (steady-state) of cyclic voltammograms for a Spectracarb 2225 carbon cloth electrode (15.25 mg) with various upper potentials in 1.0 M H_2SO_4 at 1 mV s^{-1}. b) magnified anodic region from a), and c) magnified cathodic region from a).

A direct comparison of the 0.4 – 1.0 V steady-state cyclic voltammogram to the 0.0 – 1.0 V steady-state cyclic voltammogram is shown in Figure 7.4. The current values are similar within experimental error between two different carbon electrodes, for all regions of the cyclic voltammogram except for in the oxidation of the hydroquinone to quinone (anodic sweep), where the 0.4 – 1.0 V cyclic voltammogram has a lower current value than the 0.0 – 1.0 V cyclic voltammogram. If exposure to lower potentials resulted in an oxidant being produced, it would be expected that the 0.0 – 1.0 V cyclic voltammogram would have a larger current, which is seen in Figure 7.4; however, the current in the reduction peak is the same between the two cyclic voltammograms

suggesting there is not an increase in overall oxidation through the possible production of H_2O_2. Taking into account the experimental conditions that would affect the current in the hydroquinone oxidation in the anodic sweep of the cyclic voltammogram suggests that the exposure to potentials below 0.4 V does not result in a more oxidized carbon electrode through the production of H_2O_2 or some other oxidant.

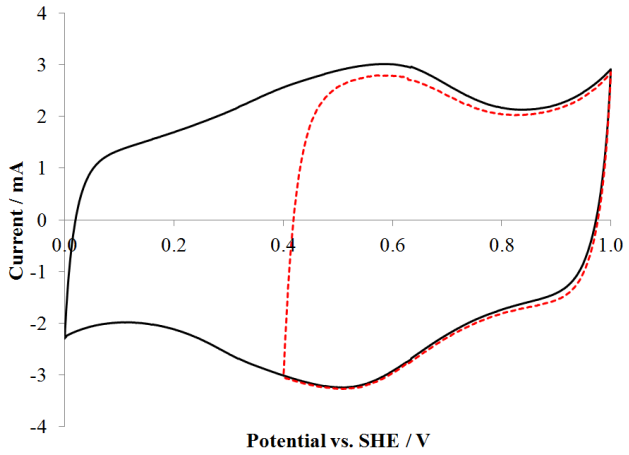

Figure 7.4: Cycle 90 for cyclic voltammograms of two Spectracarb 2225 carbon cloth electrodes (*ca.* 10 mg) cycled to steady-state in 1.0 M H_2SO_4 at 1 mV s^{-1}. The black line (—) is a steady-state cyclic voltammogram from 0.0 – 1.0 V, and the dashed red line (— —) is a steady-state cyclic voltammogram from 0.4 – 1.0 V.

7.5 Faradaic Processes Studied by Incremental Cyclic Voltammetry

Further investigation into the possible relationship between the development of the quinone/hydroquinone peak and the oxidation wave (see section 7.2) is necessary. Since it was previously shown that exposure of the electrode to potentials below 0.4 V does not affect the development of redox peaks on the carbon cyclic voltammograms (see section 7.4), all cyclic voltammograms shown in this section begin at the lower potential of 0.0 V. Cyclic voltammograms collected with truncated upper potential windows above 0.5 V (the redox potential of the quinone/hydroquinone couple), but below the onset of the oxidation wave at *ca.* 0.7 V, do not show redox peaks (see Figure 7.5). The

steady-state cyclic voltammogram between 0.0 – 0.6 V does not show any evidence of a pseudocapacitive redox peak which might be expected since 0.6 V is above the potential where the quinone/hydroquinone redox potential is visible in the 0.0 – 1.0 V cyclic voltammogram (see Figure 7.1 or Figure 7.5). Cyclic voltammograms from 0.0 – 0.6 V show a nearly rectangular shape centered about the zero current axis, indicative of double-layer charging. The lack of peak development suggests that higher potentials must be applied to the carbon electrode before the quinone/hydroquinone species are redox active in the cyclic voltammogram. Since the peaks are not visible in the 0 – 0.6 V cyclic voltammogram, it is possible the surface groups are a conversion from another surface species at higher potentials. Therefore, if the potential has not been reached, the conversion to redox active quinone groups are not seen as peaks in the cyclic voltammogram.

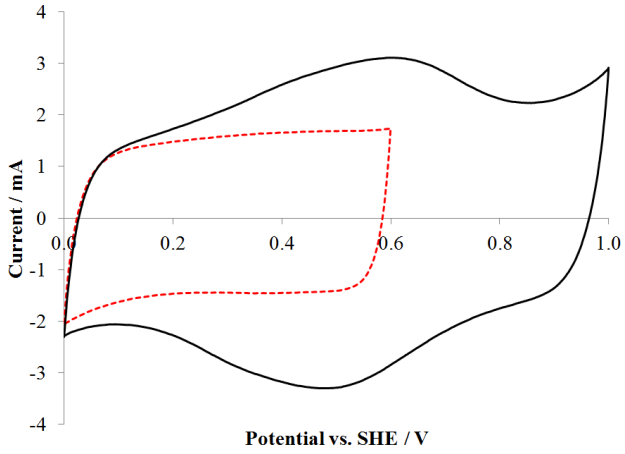

Figure 7.5: Cycle 300 for cyclic voltammograms of a single Spectracarb 2225 carbon cloth electrode (*ca.* 10 mg) cycled to steady-state in 1.0 M H_2SO_4 at 1 mV s^{-1}. The black line (—) is the steady-state cyclic voltammogram run from 0.0 – 1.0 V after a steady-state was reached for cyclic voltammograms from 0.0 – 0.6 V (— —).

After the carbon electrode was continuously cycled to steady-state between 0.0 – 0.6 V with no significant differences in the cyclic voltammogram, the upper potential limit of the cyclic voltammogram was increased by 25 mV to 0.625 V. A steady-state was reached in each potential window before the upper potential limit was increased in 25 mV increments, up to 1.0 V. The potential increment of 25 mV was chosen as it was a large enough change to identify if there was a growth in the current values due to Faradaic charging contributions, yet small enough to localize the potential region in which those Faradaic processes occur. Figure 7.6a shows the cyclic voltammograms for the last cycle (cycle 90) for each given potential window. From the cyclic voltammograms it can be seen that at upper potential limits between 0.6 – 0.7 V the cyclic voltammogram is quite rectangular about the zero current axis, again indicative of double-layer charging. Although the cyclic voltammograms are rectangular up to 0.7 V, there is a slight increase in the current above 0.65 V (see Figure 7.6b and c) suggesting that there is a growth in the quinone/hydroquinone redox peak, and potentials past 0.65 V are necessary to fully develop the redox peak *ca.* 0.55 V. The potential of 0.65 V is consistent with the potential of increased current in the cyclic voltammograms presented in Figure 7.3, again suggesting there is no difference in the cyclic voltammograms when potentials lower than 0.4 V are applied.

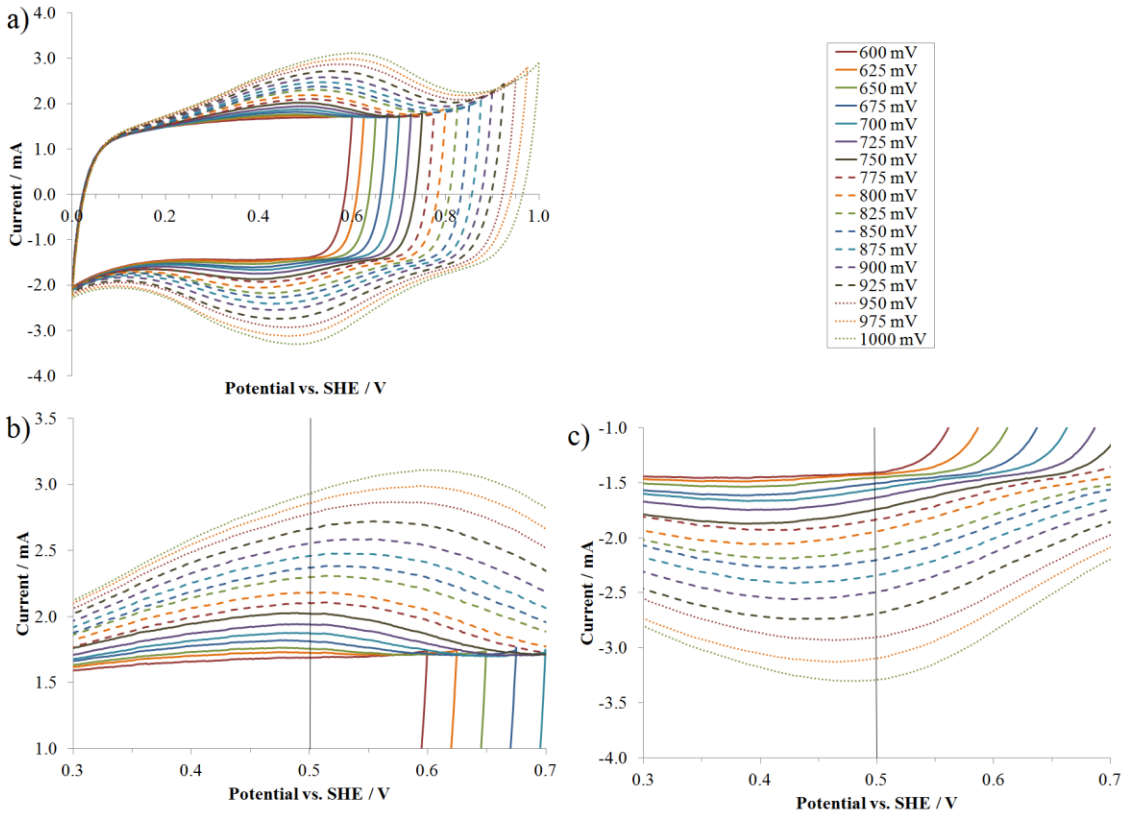

Figure 7.6: Cyclic voltammograms for Spectracarb 2225 carbon cloth electrode (10.96 mg) cycled to steady-state with various upper potentials in 1.0 M H_2SO_4 at 1 mV s^{-1}. b) magnified anodic region from a) and c) magnified cathodic region from a). Note the solid black line in b and c at 0.5 V are a visual aid.

The cyclic voltammogram data presented in Figure 7.6 shows a growth in the quinone/hydroquinone redox peak with increasing upper potential. The line at 0.5 V in Figure 7.6b and c allows the small separation of the quinone/hydroquinone redox peaks to be easily seen with increasing upper potentials. With increasing applied potentials (*i.e.* increasing the upper potential limit of the cyclic voltammogram) there is a positive shift in potential of the peak maximum in the anodic peak (Figure 7.6b) and a negative shift to lower potentials in the cathodic sweep (Figure 7.6c). The shift in other pseudocapacitive materials is generally attributed to a drop in kinetic reversibility.[11] It might be expected that pseudocapacitive surface groups would have a similar pattern to pseudocapacitive

materials, which is in fact seen in the cyclic voltammogram peaks shown in Figure 7.6b and c. Alternatively, it is possible that quinoid groups are developing farther down the pores resulting in increased pore resistance, and shifting the peak potential.

Similar incremental cyclic voltammograms as those shown in Figure 7.6 were run, where the cyclic voltammograms began at 0.0 – 0.15 V and increased in 10 mV increments. These electrodes were cycled only twice at each potential window and were not cycled to steady-state, as were the electrodes resulting in the previous data. These data were of interest to determine the charge in each region of the cyclic voltammogram throughout the entire potential window rather than just in potential increments above 0.6 V as shown in Figure 7.6. The length of the experiment to cycle an electrode to steady-state in 10 mV increments would be many months, and it is unlikely the electrode would last long enough with reproducible results in that time frame. As a result, only two cycle voltammograms were collected. Because the potential step of the upper potential limit was only 10 mV, it is likely the carbon electrode does not require as many cycles to reach steady-state as previously shown with larger incremental potential steps (25 mV).

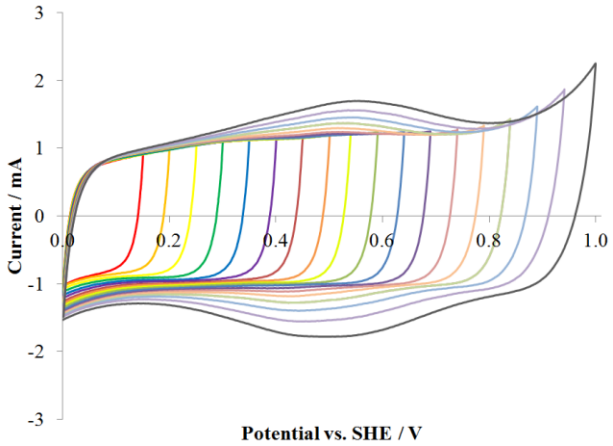

Figure 7.7: Incremental cyclic voltammograms of a Spectracarb 2225 carbon cloth electrode (7.06 mg) in 1.0 M H_2SO_4 at 1 mV s^{-1} with N_2, starting at 0 – 0.15 V and increasing in 10 mV increments. Only every fifth cyclic voltammogram is shown for graphical clarity.

The anodic and cathodic charge of Figure 7.7 was plotted versus the upper potential limit, shown in Figure 7.8a. From these data it can be seen that the amount the charge increases depends on the upper potential limit. Various regions of Figure 7.8a were plotted in Figure 7.8b-c and the slopes of these regions were found, where appropriate. The slope of Figure 7.8 corresponds to capacitance, and therefore, if the slope is constant, it suggests constant capacitance. If the slope changes with potential then there are two possibilities: either there is an increase in the double-layer charging at a given potential, or there is now a Faradaic reaction occurring at the electrode. Therefore a change in the slope would suggest a change in capacitance and a contribution from another possible charge storage mechanism.

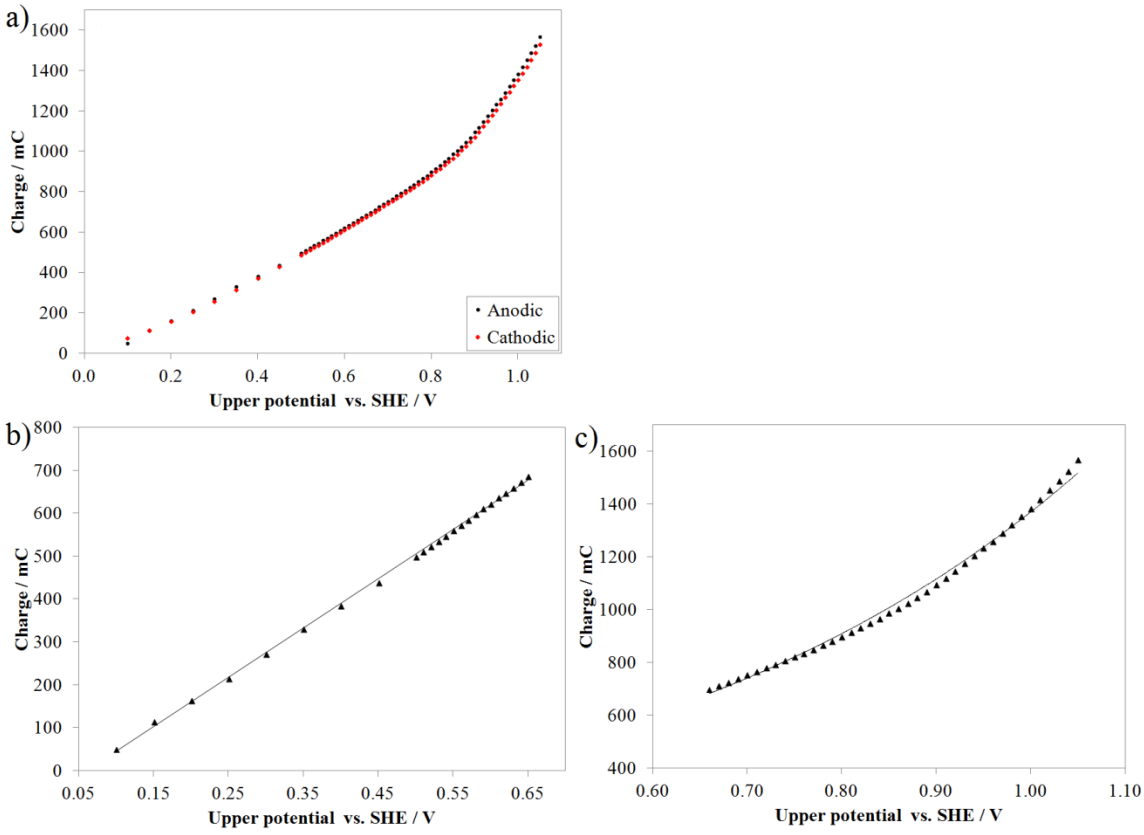

Figure 7.8: a) anodic and cathodic charge of incremental cyclic voltammograms of a Spectracarb 2225 carbon cloth electrode (7.47 mg) in 1.0 M H_2SO_4 at 1 mV s^{-1} with N_2 in electrolyte. Magnified regions of the anodic curves from b) 0 – 0.65 V, c) 0.65 – 1.05 V.

At potentials up to 0.65 V (Figure 7.8b), the data are nearly linear (with a small deviation away from linearity and purely double-layer charging possibly due to carbon oxidation to CO_2 adding a small contribution of Faradaic charge) the capacitance from the slope is 1140 ± 50 mF for the anodic sweep of the cyclic voltammogram and 1020 ± 60 mF for the cathodic sweep. By examining the cyclic voltammograms in Figure 7.7 it appears that the cyclic voltammograms are quite rectangular without any peaks, suggesting this region is due to mostly double-layer charging. To determine the double-layer charging, the slope of 1140 mF, typical mass of an electrode (10 mg) and the Spectracarb 2225 carbon cloth BET surface area (2500 $m^2\ g^{-1}$) were used, giving a value of *ca.* 5 μF cm^{-2}. Typical values of carbon double-layer charging at planar electrodes are *ca.* 30 μF cm^{-2}.[11] The value calculated for the Spectracarb 2225 carbon cloth is *ca.* six times smaller than the reported values in the literature, suggesting it is possible that not all the surface area is being used in double-layer formation. Interestingly, the capacitance of the cathodic sweep is not the same as the capacitance (slope) of the anodic sweep using a t-test with 95% confidence. The smaller slope seen for the cathodic sweep suggests there is an irreversible oxidation reaction in the anodic region which is then not reduced in the cathodic sweep. The standard reduction potential of carbon to CO_2 is seen at potentials above 0.207 (see reaction 10),[59, 151, 152] and therefore it is possible the difference seen between the anodic and cathodic sweeps is due to carbon oxidation.

Table 7.2: Summary of slopes found from Figure 7.8b, for six Spectracarb 2225 carbon cloth electrodes with N_2 in electrolyte, and similar eight electrodes with CO_2 in the electrolyte.

	Slope ±1σ / mF	
Potential region / V	Anodic	Cathodic
N_2: 0.00 – 0.65	1140 ± 50	1020 ± 60
CO_2: 0.00 – 0.65	1180 ± 80	1160 ± 60

The data between 0.65 – 1.05 V was unable to be linearly fit suggesting a combination of multiple processes, or possibly a reaction that is dependent on different reaction mechanism, such as an exponential growth. At upper potential limits above 0.65 V, the data are better fit with an exponential function, however the agreement is still not good. An exponential function would suggest an activation-controlled reaction as another form of charging now adding to the overall cyclic voltammogram. The increase in slope and change of capacitance growth might be due to an increase in double-layer charging at higher potentials, or Faradaic process(es). It is likely due to the beginning of a Faradaic process since a small peak is evident in these cyclic voltammograms, suggesting another charge storage mechanism through Faradaic reactions. Though, since the fit with the exponential curve still is not good, it is not currently possible to propose or identify if it is one Faradaic reaction or multiple reactions.

The faster increase of charge is likely due to the combination of double-layer charging, Faradaic conversion/charging, and possibly an irreversible reaction, such as carbon oxidation. Since the charge is integrated over the entire cyclic voltammogram, the quinone peaks are fairly well developed by these upper potential limits, adding to the overall charge increase, and suggesting a Faradaic or pseudocapacitive charging mechanism. Additionally, at higher potentials it has been shown in the literature that

there may be an irreversible oxidation of the carbon electrode to carbon dioxide at potentials above 0.9 V.[17, 153, 155] An irreversible reaction, such as carbon oxidation, would be seen only in the anodic data since the CO_2 would not then be reduced back onto the electrode. It is likely that there is a conversion process of electrochemical surface oxidation with the higher applied potentials which results in the higher rate of charge growth (higher capacitance) which is in line with the extra charge discussed above.

To test the hypothesis of CO_2 evolution causing the increased charge at higher potentials, the same incremental cyclic voltammograms were run as before, however CO_2 was bubbled into the electrolyte. Assuming CO_2 is being formed from carbon oxidation, using a CO_2 saturated electrolyte was expected to result in a shift in the equilibrium potential, resulting in less CO_2 formed from the electrode oxidation. The results of the experiment are shown in Figure 7.9. The cyclic voltammograms are similar in shape to those in Figure 7.7, with the development of a peak due to the quinone/hydroquinone redox couple, and capacitive behaviour as evidenced by the mirror image about the zero current axis.

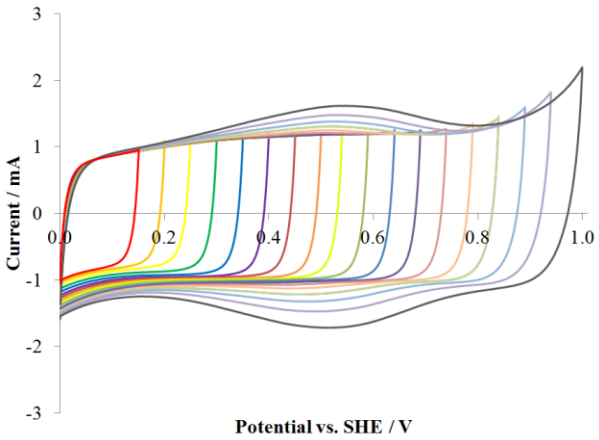

Figure 7.9: Incremental cyclic voltammograms of a Spectracarb 2225 carbon cloth electrode (7.85 mg) in 1.0 M H_2SO_4 at 1 mV s^{-1} with CO_2 in the electrolyte, starting at 0.00 – 0.15 V and increasing in 10 mV increments. Only every fifth cyclic voltammogram is shown for graphical clarity.

For the data with CO_2 in the electrolyte, the slopes for the anodic and cathodic sweep, shown in Table 7.2, were calculated in the region of 0.00 – 0.65 V. In this case, both the anodic and cathodic capacitance is the same (using a t-test). It is interesting to note that the N_2-saturated anodic capacitance and the CO_2-saturated anodic capacitance are also the same, but the N_2 cathodic capacitance is significantly different. Kinoshita and Bett[153, 155] suggested that the reactions occurring on the carbon electrode's surface are independent of carbon dioxide concentration and therefore it is surprising that the addition of CO_2 does affect the cathodic slope (capacitance) value calculated when CO_2 was present in the electrolyte.

7.6 Exposure to Caffeine to Identify Quinones

Since the quinone/hydroquinone redox couple is at a potential close to the oxidation wave onset, it would be advantageous to be able to separate these two processes. It was previously presented in the literature that benzoquinone-soaked graphite electrodes were able to detect caffeine concentrations in coffee via cyclic voltammetry.[164] A decrease in the benzoquinone redox peaks was related to the concentration of caffeine,[164] and therefore it was thought the same effect may be possible when the quinone/hydroquinone surface groups on the electrode were exposed to caffeine. Electrodes that had been continuously cycled to steady-state were exposed to 1.0 M H_2SO_4 with 0.01 M caffeine in the electrolyte, with the cyclic voltammetry results shown in Figure 7.10a. From these results it is apparent there is a noticeable decrease in current when the carbon electrode was exposed to caffeine-containing electrolyte; however the decrease is not specific to the quinone/hydroquinone redox peak *ca*. 0.5 V as

might be expected from the literature,[164] but is evident over the entire potential range. In fact, it appears the entire cyclic voltammograms current has been decreased yet the overall shape is retained. To determine whether the decrease in current is due to a decrease in quinone surface functionalities, the cyclic voltammograms were normalized using the current in a known double-layer region (0.15 V). When the data are normalized using the double-layer current, there appears to be no significant difference between the cyclic voltammograms collected in both the absence and presence of caffeine.

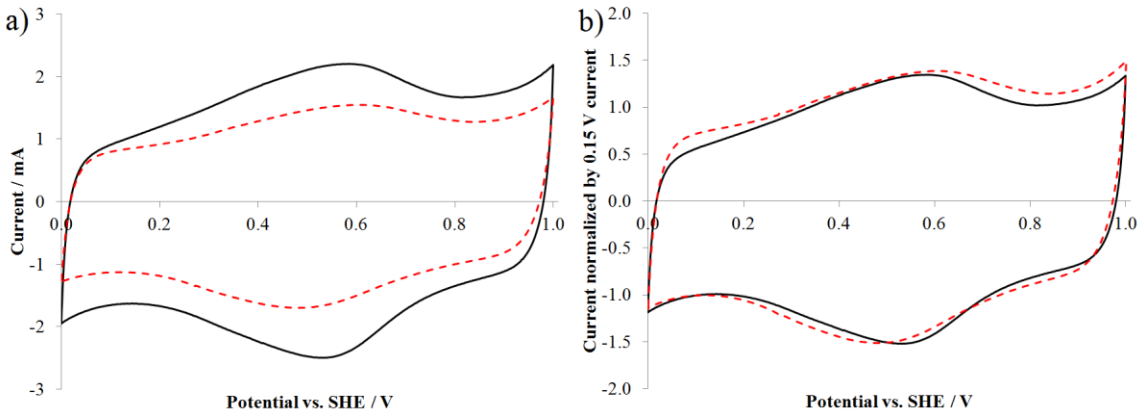

Figure 7.10: a) Cyclic voltammograms of the same Spectracarb 2225 carbon cloth electrode (6.91 mg) in 1.0 M H_2SO_4 at 1 mV s^{-1} (—), and also in the presence of 0.01 M caffeine in 1.0 M H_2SO_4 (— —). b) data in (a) normalized by the cathodic current at 0.15 V.

The addition of caffeine does not appear to specifically target the quinone/hydroquinone surface groups as predicted; it does, however, appear to block the electrode's surface, resulting in less current from the electrode and less charge storage. The reduction in current could be due to multiple possibilities including a change in the wettability of the carbon with the addition of caffeine to the electrolyte, the caffeine blocking parts of the electrodes surface directly, or similarly that the caffeine blocks the mouths of smaller pores of the carbon electrode. From the ratio of the peak current at 0.5

V and the current at 1.0 V, the values are similar, with 0.93 ± 0.01 for no caffeine and 0.96 ± 0.01 in the presence of caffeine. If the ratios were significantly different for these two experiments it might suggest that there was in fact a specific interaction with the quinone/hydroquinone functionalities. From a t-test with 95% confidence, there is no significant difference between the two experimental conditions. With no significant difference between these ratios, as well as the data presented in Figure 7.10b, this suggests the caffeine indiscriminately blocks the carbon electrode's surface area whether there are surface groups present or only carbon. Due to the fact that the caffeine molecule is unable to specifically interact only with the quinone/hydroquinone groups, this work was not further investigated, and other methods were considered to identify surface functionalities electrochemically.

7.7 Open-circuit Potential Measurements

Open-circuit potential measurements have been previously studied in carbon aqueous systems with varying results. According to both Tobias and Soffer,[166] and Bayram and Ayranci,[167] with increased oxidation (via applied potential) there was an increase in open-circuit potential of carbon materials. Assuming the opposite is also true, then reducing a carbon surface would result in a decrease in open-circuit potential. Another possibility presented by Goldin *et. al*[165] suggests that an increase in open-circuit potential is related to the amount of an organic species in aqueous media which has adsorbed on the surface. Goldin and co-workers also found the potential shifted negatively with desorption of the organic species, proportional to the amount of the organic contaminant leaving the surface.[165] Results presented by Kastening and co-

workers proposed carbon corrosion in the form of carbon oxidiation to carbonate in alkaline aqueous media to be responsible for a decrease in open-circuit potential.[195]

Changes in open-circuit measurements can be attributed to changes in the surface chemistry, such as redox processes, the overall oxidation or reduction of the carbon surface, or adsorption processes occurring at the surface. Therefore, open-circuit potential measurements were collected between many of the data shown in the chapter's previous sections. First, open-circuit potential measurements were collected of an electrode soaked in 1.0 M H_2SO_4 over roughly one week to determine how the open-circuit potential changes over time without the application of potential (see Figure 7.11). The open-circuit potential measured has a significant potential climb over the first *ca.* 3 hours. After the initial potential climb the change in potential slows greatly, though always with a positive trend. The data shows a potential increase at a slow rate of less than 10 mV per day.

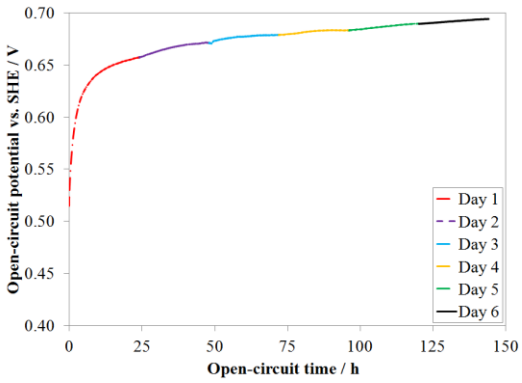

Figure 7.11: Representative open-circuit potential measurements over six days for a Spectracarb 2225 carbon cloth electrode (9.74 mg) immersed in 1.0 M H_2SO_4. Note that no potential was applied to this electrode.

The overall increase in potential with time could be attributed to either an increase in oxidation,[166, 167] though both of those references had anodic polarization applied to the carbon surface, or through the adsorption of inorganic species.[165] Since N_2 was

continuously bubbled during data collection, the open-circuit potential increase is unlikely due to adsorption of an inorganic species such as CO_3^- or HCO_3^- from CO_2 dissolution, or HSO_4^- from the electrolyte. Trace O_2 in the pores of the carbon may be responsible for the slow increase in potential over time. Oxygen reduction would result in a positive shift in potential where the electrode would donate electrons to the O_2 when in contact with the electrode's surface. Assuming the potential climb (*ca.* 0.22 V) is solely due to oxygen reduction, the concentration of O_2 responsible for the potential increase can be calculated. Using the capacitance of a not-previously cycled electrode at 0.5 V (150 F g^{-1}), a two electron transfer to H_2O_2, and the pore volume (1.2 mL g^{-1}) of a 10 mg electrode, the O_2 concentration is *ca.* 0.14 mol L^{-1}. Even in an electrode that has not been previously exposed to electrochemistry, this O_2 concentration is too high, suggesting the potential increase is not solely due to O_2-reduction. It is also a possibility that the increase in potential over one week was due to a shift in the reference electrodes potential. The SHE reference electrode is used due to its stable potential and, therefore, it is unlikely due to a drift in the potential over time. Since the electrochemical systems under study are in acidic media it is likely the carbon is becoming more oxidized over time, or O_2 reduction, is the cause of the increase in open-circuit potential.

After identifying the overall trend in open-circuit potential over a one week time period without applied electrochemistry, it was of interest to determine the open-circuit potential at various times during the process of cycling the electrode to steady-state. Cyclic voltammograms run from 0.5 – 1.0 – 0.0 – 0.5 V for 45 cycles, followed by a two hour open-circuit potential measurement resulted in the data presented in Figure 7.12. The "Day 0" open-circuit profile in Figure 7.12a also has an initial potential climb like

the open-circuit potential measurement in Figure 7.11, though on a much different time scale. The open-circuit potential then plateaus to *ca.* 0.65 V in Figure 7.12a. Since the "Day 0" data (Figure 7.12a) had not yet been exposed to electrochemistry it would be expected that both those open-circuit measurements would be similar, though this is not seen experimentally. The differences seen in the shape as well as the actual potential values might be due to variations between the carbon electrode surface (the experiments were run one year apart and it is likely the carbon was not taken from the same carbon cloth sample), how well wetted the surface was prior to immersion in the electrolyte, or the rate of nitrogen sparging to remove oxygen. It is also important to note the time scales as the week long experiment was collected over a full day whereas the measurement prior to cycling to steady-state was only two hours.

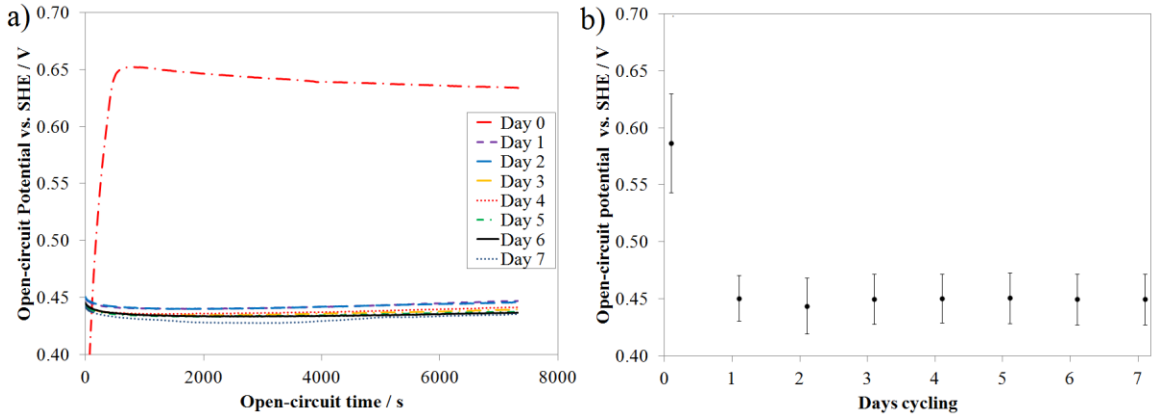

Figure 7.12: Representative curves of a) open-circuit potential measurements of Spectracarb 2225 carbon cloth electrodes (6.39 mg), taken after multiples of 45 cyclic voltammograms (which requires one day of cycling) from 0.5 - 1.0 - 0.0 - 0.5 V at 1 mV s^{-1} in 1.0 M H_2SO_4. b) averaged open-circuit potential measurements of seven *(N)* electrodes. The error bars represent one standard deviation (σ).[§]

The data for Day 1 – 7 open-circuit potential measurements (see Figure 7.12a) are all similar (*i.e.* a relatively flat profile at *ca.* 0.45 V), though this may in fact be

[§] Note that the average value for "Day 0" was taken after the initial potential climb, over the last 6000 seconds.

influenced by the way the experiment was set-up. The cyclic voltammograms' initial and final potential was 0.5 V, as this was the estimated open-circuit potential. When the experiment was switched from a cyclic voltammogram to open-circuit potential measurements, had the open-circuit potential of the electrode been 0.5 V then the potential would have been a flat line at 0.5 V. From the data of Days 1 – 7, it can be seen that the potential measurement begins at *ca.* 0.45 V, suggesting an immediate loss of potential when the electrode was switched from cyclic voltammograms to open-circuit potential measurements. After the initial potential loss from 0.5 to 0.45 V, the potential is nearly flat, though there is a slight trend upwards (Figure 7.12a). Had the potential chosen for the end of the cyclic voltammogram been significantly different than the natural open-circuit potential of the electrode then there would be a visible increase or decrease in the potential after switching to open-circuit, which is not evident in these data.

Since there is a continual change in the shape of the cyclic voltammogram over continuous cycling to steady-state (Figure 7.1), it might be expected the open-circuit potential would also show a change, dependent on the electrode's degree of oxidation[166, 167] or the adsorption onto the carbon's surface.[165] Because there is no change in the open-circuit potential with continued cycling (after the first measurement) it is likely open-circuit potentials do not give information on the changes evident in the cyclic voltammogram (*i.e.* the increase in the quinoid redox peak, and the decrease in the oxidation wave).

To determine whether the decrease in open-circuit potential is related to the application of applied anodic potential (like Tobias and Soffer,[166] and Bayram and

Ayranci[167]), open-circuit measurements were collected during incremental cyclic voltammograms similar those in Figure 7.3 and Figure 7.6. Rather than the potential window beginning at 0.0 V, the window was changed to accommodate for the open-circuit measurements between cyclic voltammograms and these cyclic voltammograms were run from 0.5 – X – 0.0 – 0.5 V, where X was the upper potential limit. For the incremental data, the open-circuit potential begins at a lower potential (*ca.* 0.5 V as seen in Figure 7.13) compared to the open-circuit potential measurements (*ca.* 0.65 V) from continuous cycling data (Figure 7.12). It is interesting to note these differences between data since the initial open-circuit potential should be similar between the two experiments as this measurement was taken prior to electrochemistry, and therefore should not be influenced by the difference in the electrochemical experimentation. Since the data presented in Figure 7.12 was run months prior to the data presented in Figure 7.13, there is a possibility of different levels of adsorbed species on the electrode's surface resulting in a different starting open-circuit potential. The difference in open-circuit potential between overall experiments could support the idea that an adsorbed organic species is desorbing from the carbon electrode surface between the first open-circuit potential measurement (prior to electrochemistry) and the second open-circuit potential measurement (post electrochemistry).

After the first open-circuit potential measurement at 0.5 V in Figure 7.13, the open-circuit potential is consistently *ca.* 0.45 V. Again this is counterintuitive since the x-axis in this graph is an increasing upper potential limit, and therefore is applying a larger anodic polarization. According to the literature[166, 167] the open-circuit potential should increase with increasing anodic polarization and carbon oxidation, which is not

seen. Again, changes were visible in the cyclic voltammograms, however the open-circuit potential does not show similar changes with increasing applied potential. Therefore it suggests that open-circuit potential measurements are not sensitive to the changes in the quinone groups and oxidation wave seen in the cyclic voltammogram.

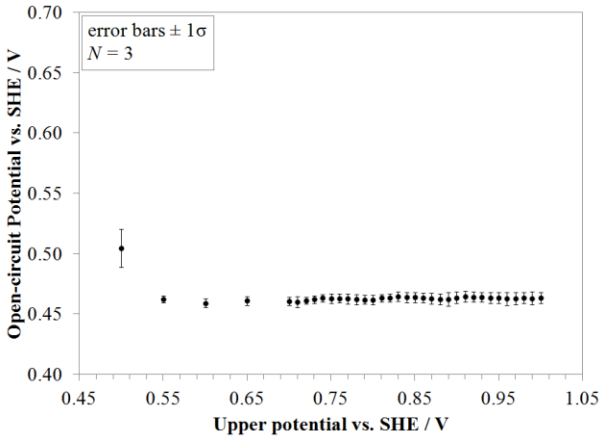

Figure 7.13: Averaged open-circuit potential taken for two hours between incremental stepwise cyclic voltammograms run from 0.5 – X – 0.0 – 0.5 V, where X is the upper potential limit, at 1 mV s^{-1} of three (*N*) Spectracarb 2225 carbon cloth electrode (*ca.* 10 mg) in 1.0 M H_2SO_4. The error bars represent one standard deviation (σ).

7.8 Conclusions

This chapter focused on electrochemical understanding and general examination of surface functionalities electrochemically active in the cyclic voltammograms and open-circuit potential measurements.

It was found that continuous potential cycling of Spectracarb 2225 carbon cloth electrodes results in a significant change in current and then the cyclic voltammogram current reaches a steady-state. The largest visible change in the cyclic voltammogram shape is the growth of a quinone/hydroquinone redox couple *ca.* 0.5 V and it was determined that potentials above 0.65 V were necessary for significant development of these quinoid groups. Incremental cyclic voltammograms run to steady-state from 0.0 –

0.6 V with increasing 25 mV steps found growth of the quinone/hydroquinone redox couple increased after the applied potentials were higher than 0.65 V. The 0.65 V corresponds with the onset of a large oxidation wave present in the first cyclic voltammogram when electrodes are cycled only between 0.0 – 1.0 V, and suggest there is a link between this higher oxidation wave and the development of the quinone/hydroquinone redox peak.

Although previous results (Chapter 5) and the literature suggested the development of H_2O_2 occurred at lower potentials, which would in turn act as an oxidizing agent, it was found that truncating the potential window above 0.4 V had no significant impact on the cyclic voltammograms, and therefore the oxidation wave *ca.* 0.7 V in the first cyclic voltammogram from 0.0 – 1.0 V was not caused by the presence of an increased concentration of H_2O_2 (a strong oxidizing agent).

Open-circuit potential measurements showed a possible reduction in the surface chemistry of the carbon electrode, though it is more likely open-circuit potential measurements were not sensitive to the changes in the electrode's surface during continuous potential cycling. It is also possible that there is an organic species being desorbed from the surface through continuous cycling, although further work must be done to conclusively determine the cause of open-circuit potential changes.

Chapter 8 EFFECT OF CYCLING ON SELF-DISCHARGE OF CARBON ELECTRODES

8.1 Introduction

In all previous self-discharge experiments presented the electrodes were continuously cycled prior to the collection of self-discharge profiles, meaning the potential of the electrode was cycled until the resulting cyclic voltammogram reached steady-state. This was to ensure any changes in the self-discharge profile was due to a change in the experimental conditions (*i.e.* change in $Fe^{2+/3+}$ concentration in Chapter 4, or partial pressures of dissolved gases in Chapter 5) rather than a change in the carbon electrode itself. It was previously shown there are significant differences in the cyclic voltammogram of Spectracarb 2225 carbon cloth over continued cycling (Chapter 7). Therefore, this chapter will examine the effect of the cycling pre-conditioning step on the positive (1.0 V) electrode self-discharge and float current measurements of Spectracarb 2225 carbon cloth electrodes. Only the positive electrode was examined as the negative electrode self-discharge mechanism has already been identified in Chapter 5.

8.2 Self-discharge of Previously Cycled Electrodes

All self-discharge data shown in previous chapters had been conducted on electrodes which had been electrochemically cycled to steady-state (Figure 7.1) prior to the self-discharge measurement. The results for self-discharge on a previously cycled electrode can be seen in Figure 8.1. Representative raw data is shown for ten self-

discharge profiles run consecutively on the same electrode in Figure 8.1a. A magnified region of (a) was plotted in (b) to show the final potential after two hours. Panel (c) shows a single representative self-discharge profile with the average potential (and error) every 500 s. By taking the potential every 500 s and then plotting the error bars (± 3σ), a representative curve that best fits the average potential versus time values was chosen. When the electrodes were previously cycled to steady-state, the self-discharge profiles are highly reproducible with a spread in the data of ± 10 mV (± 3σ), and therefore ± 3σ is the limit used to determine whether self-discharge profiles are different. It is important to note that although the self-discharge profiles are reproducible after cycling there is still substantial potential loss which must be minimized. It is likely that there is a portion of the potential lost due to charge redistribution; however the full effect is unknown.

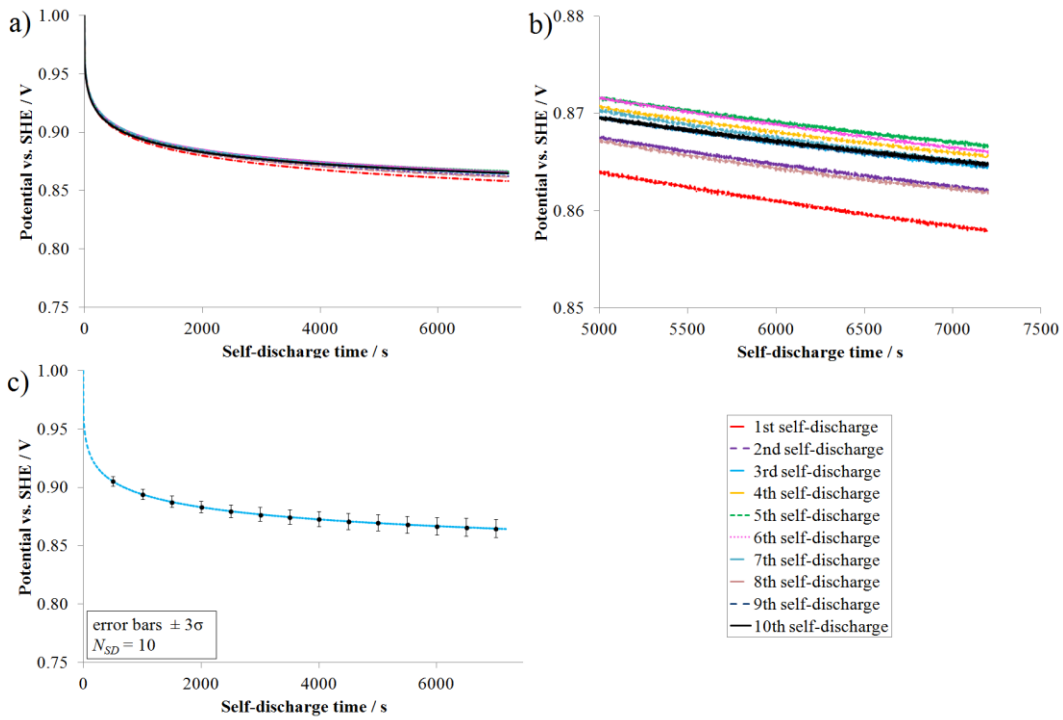

Figure 8.1: Self-discharge profiles of a Spectracarb 2225 carbon cloth electrode (*ca.* 10 mg), previously cycled to steady-state, after a potential ramp from 0.5 – 1.0 V at 1 mV s^{-1} in 1.0 M H_2SO_4, with no potential hold. Raw data are shown in (a), (b) is a magnified region of (a), and (c) shows a self-discharge profile with averaged potentials and error bars (± 3σ).

8.3 Self-discharge Profiles of As-received Electrodes

There are significant changes in the cyclic voltammograms over cycling time (namely the quinone/hydroquinone peak development and the decrease in the oxidation wave, as seen in Figure 7.1), and it was of interest to examine whether the development of the quinoid carbon surface functionality effects the self-discharge profile. Self-discharge profiles were collected on electrodes which had not undergone any previous electrochemistry to compare with the results in the previous section (section 8.2). Both the ramp of the self-discharge experiments and cyclic voltammograms vary the applied potential at a given rate (the sweep rate), and are electrochemically equivalent. Therefore, it was important that the first application of electrochemistry was a ramp rather than a cyclic voltammogram since there is a decrease in the current at 1.0 V over continued cycling which may affect the magnitude of self-discharge.

As can be seen in Figure 8.2, there is a significant difference in the loss of potential over time between the self-discharge profiles with the first self-discharge resulting in the largest potential drop. The largest difference between two consecutive self-discharge profiles was between the first and second self-discharge profiles; however with repeated measurements the loss of potential decreases and the self-discharge profiles become reproducible after the tenth self-discharge profile, within the same standards as the previously cycled electrodes (within $\pm 3\sigma$ variation).

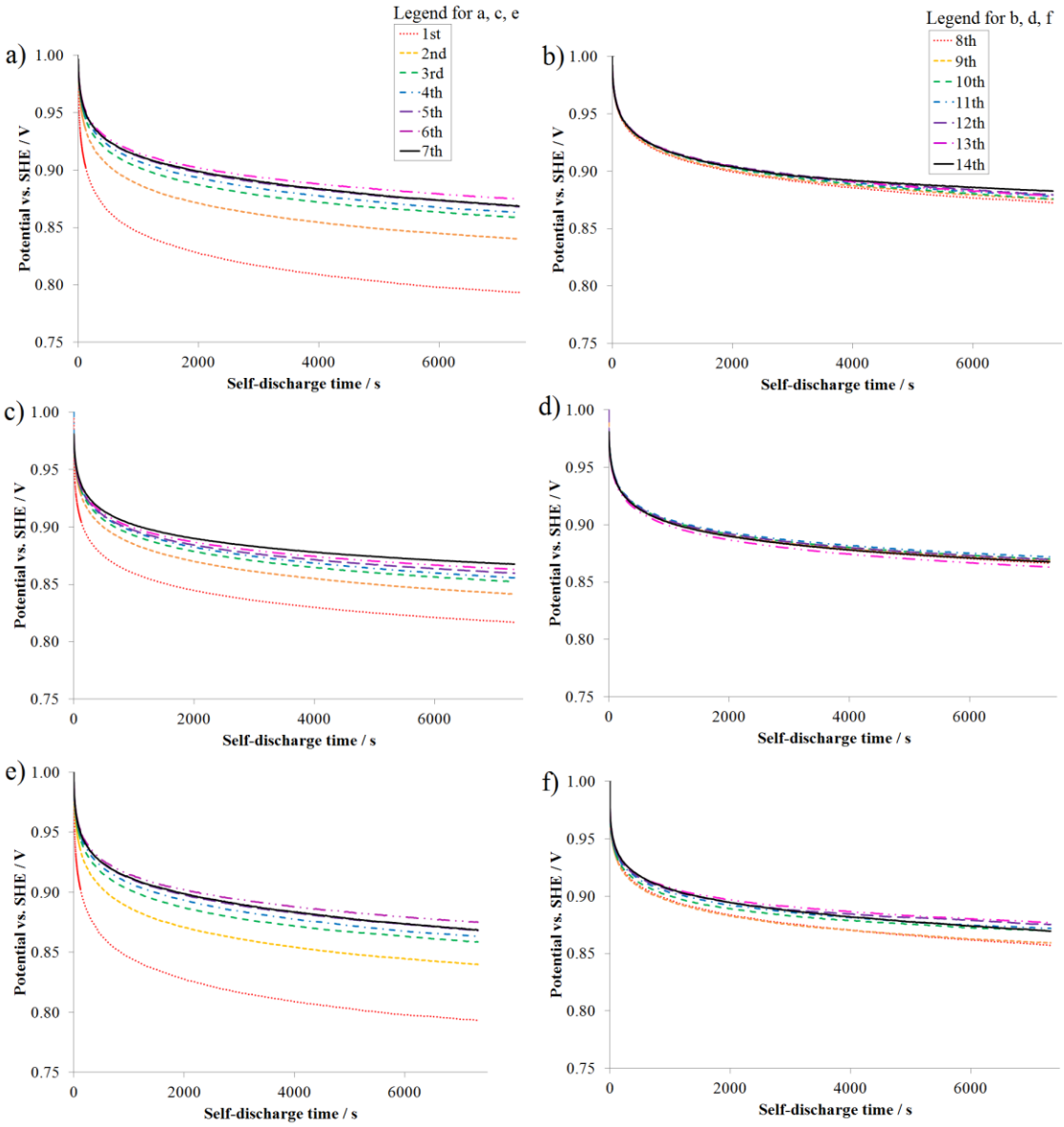

Figure 8.2: Self-discharge profiles an uncycled (as-received) Spectracarb 2225 carbon cloth electrode (*ca.* 10 mg) after a potential ramp from 0.5 – 1.0 V at 1 mV s^{-1} in 1.0 M H_2SO_4 with no potential hold. Self-discharge profiles were collected either directly (a, b); after one week immersed in 1.0 M H_2SO_4 (c, d); or after one week immersed in 18.2 MΩ·cm H_2O (e, f). Note the difference in the y-axis scale between (a, c, e) and (b, d, f).

As mentioned above, ramping the potential is equivalent to the anodic sweep of a cyclic voltammogram as both vary the applied potential at a given rate. Therefore, it is important to ensure that the magnitude of the self-discharge is not directly due to the high

current at 1.0 V flowing in the first cycle of Figure 7.1, causing an iR-drop. With the high current in the oxidation wave of the first cyclic voltammogram (and therefore also the ramp prior to open-circuit configuration) there will be a loss of potential due to the iR-drop, where the current and the resistance of the electrode result in a decrease in potential from the applied potential (1.0 V) when switched to open-circuit configuration. The data in Table 8.1 is from multiple experiments under the same conditions as Figure 8.2. The high current seen at the end of the ramp prior to the first self-discharge could correspond to the increased self-discharge; however, after the first self-discharge, the currents are all similar though the degree of self-discharge continues to decrease. This suggests that the current at the end of the ramp (or cyclic voltammogram) is not the cause of the increased self-discharge during the earlier self-discharge measurements.

Table 8.1: Summary of currents and voltages for self-discharge profiles of three (N) uncycled (as-received) Spectracarb 2225 carbon cloth electrodes. Also includes applied potential and the difference between the applied potential and the overall potential drop over two hours (V_{final}). Note that the $V_{applied}$ should be 1000 mV (1.0 V).

	Potential ± 1σ / mV		
Self-discharge number	I at end of ramp	$V_{applied}$	$V_{applied} - V_{final}$
1	8.7 ± 0.5	985 ± 1	188 ±3
2	5.1 ± 0.6	992 ± 1	153 ± 2
3	4.5 ± 0.5	993 ± 1	137 ± 4
4	4.3 ± 0.4	993 ± 1	129 ± 3
5	4.3 ± 0.5	993 ± 1	124 ± 4
6	4.2 ± 0.5	993 ± 1	121 ± 4
7	4.2 ± 0.5	993 ± 1	125 ± 4
8	4.2 ± 0.6	996 ± 5	124 ± 5
9	4.2 ± 0.6	993 ± 1	119 ± 3
10	4.2 ± 0.6	993 ± 1	118 ± 4
11	4.2 ± 0.6	994 ± 1	116 ± 4
12	4.1 ± 0.6	993 ± 1	115 ± 3
13	4.2 ± 0.6	993 ± 1	114 ± 3

Another method of analyzing the iR-drop data is to identify the potential drop when the potentiostat switched the ramped electrode to open-circuit configuration. It is therefore possible that the differences between the self-discharge profiles might be due to a difference in applied potential and not all the self-discharge profiles starting at the same potential value. The column labeled "$V_{applied}$" in Table 8.1 shows the first potential measurement during self-discharge for the self-discharge profiles collected from Figure 8.2 and should theoretically be 1.0 V as the electrode was ramped to this potential. The $V_{applied}$ is lower for the first self-discharge profile than for the self-discharge profiles that follow; however a 7 mV difference in applied potential does not explain the significantly larger potential loss over two hours. Also, for the second self-discharge profile there is no difference in the applied potential than the self-discharge profiles following, yet there is a significantly larger potential loss. The self-discharge data does not become reproducible though the $V_{applied}$ and current do; therefore, from Table 8.1, it is unlikely the increase in self-discharge on an as-received electrode compared to a previously cycled electrode is due to the higher current flowing prior to switching to open-circuit configuration.

There are two variables which are different between the self-discharge profiles shown in Figure 8.1 and Figure 8.2: the electrochemistry during continuous cycling and also the exposure to electrolyte (1.0 M H_2SO_4) for one week during the continuous cycling process. To test whether the difference might be due to electrolyte exposure, an electrode was immersed in 1.0 M H_2SO_4 for one week without applied electrochemistry. After the one week exposure to electrolyte (minus electrochemistry) the self-discharge profiles were collected, and are presented in Figure 8.2c-d.

The first self-discharge profile in Figure 8.2c again results in the largest loss of potential and the consecutive self-discharge profiles have a smaller loss of potential, comparable to the trend seen in Figure 8.2a. There is a difference between the magnitude (*ca.* 20 mV) of the self-discharge profiles when comparing the soaked electrodes to self-discharge profiles of the cycled electrode. It is interesting to note that the difference between the two conditions might be partly due to the slight increase in open-circuit potential over one week (see Figure 7.1). However the difference is within experimental error between two different electrodes, and therefore these two experimental conditions are not different. Therefore, the exposure to electrolyte does not appear to be responsible for the difference seen between Figure 8.2a and b and Figure 8.2 c and d.

It has been previously suggested that inorganic species, such as HSO_4^- adsorb to the carbon surface over time, resulting in a change in potential.[165] To remove the possible interaction with sulphuric acid, but still thoroughly wet the carbon surface, electrodes were immersed in 18.2 MΩ·cm water for one week prior to the collection of self-discharge profiles. The self-discharge profiles can be seen in Figure 8.2e-f. Again, as in Figure 8.2a-d, the same overall trend is visible where the first self-discharge profile has the largest potential loss. The potential loss evident when the electrode is immersed for one week prior to the collection of self-discharge profiles is the same for both 1.0 M H_2SO_4 and 18.2 MΩ·cm water as the solution (Figure 8.2c-d and Figure 8.2e-f). As a result, it is unlikely that an adsorption process with ions from sulphuric acid is resulting in the increased self-discharge visible. Since the two conditions where the electrodes were immersed for one week yield the same results as the data immediately collected after electrolyte exposure (shown in Figure 8.2a-b), the difference in self-discharge seen

is not due to the wetting of the electrode surface. It is likely the larger change in the first self-discharge is due to the application of potential changing the electrode's surface.

Continuous potential cycling of Spectracarb 2225 carbon cloth electrodes results in significantly more consistent self-discharge profiles than the as-received carbon cloth. Although the current at the end of the first ramp (comparable to the high current in the oxidation wave in the continuously cycled cyclic voltammograms) is larger in the first self-discharge profile, it is not the direct cause of the increased self-discharge in the first cyclic voltammogram. The changes evident in the cyclic voltammograms (*i.e.* the development of the quinoid groups and the decrease in the oxidation wave) appear to be related to the decrease in self-discharge, since when the cyclic voltammograms have reached a steady-state so too have the self-discharge profiles. Though the direct correlation between the cyclic voltammogram and the self-discharge profile is not known, cycling is beneficial to decreasing the magnitude of self-discharge. Further work needs to be done to better understand the chemistry occurring at the electrode and its link to self-discharge.

8.4 Float Current Measurements Pre- and Post-Continuous Cycling

Float currents measure the current that must be applied to hold the potential at a given value. A float current is the current that would otherwise flow in self-discharge profiles resulting in potential decay.[119, 163] These measurements are run until the float currents reach a near steady-state, evidenced by a slow rate of change over time (*i.e.* a constant current in the data). After an electrode is fully charged it is important to know how much current is necessary to hold the electrode at that charged state, since

electrochemical capacitors will be continually fed current to keep the device at a given state-of-charge.

Float current measurements were collected on as-received carbon electrodes, at a polarization potential of 0.0 V, presented in Figure 8.3. The current begins at a large negative potential, *ca.* -60 mA and sharply climbs over the first 100 seconds where the current begins to plateau. A negative current this large is the result of a significant reduction, likely oxygen reduction as the electrode was not previously exposed to electrochemistry and the pores of the carbon electrode likely contain oxygen.

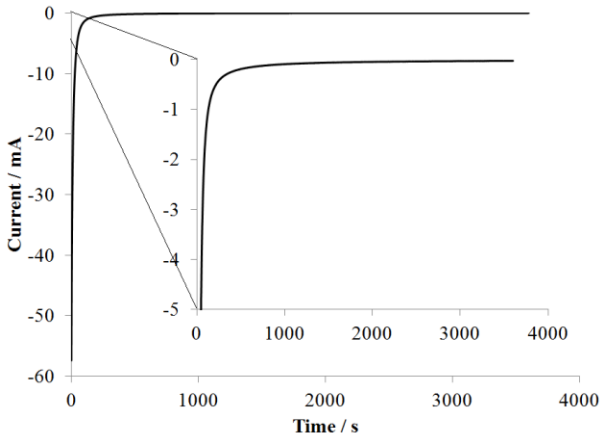

Figure 8.3: Float current measurements at 0.0 V for a Spectracarb 2225 carbon cloth electrode (*ca.* 10 mg) before continuous cycling in 1.0 M H_2SO_4. The inset graph shows a magnified region of the 0.0 V float current measurement.

Integrating the area under the float current curve results in the charge passed: in this experiment, *ca.* 1300 mC of charge was passed over 30 minutes. Assuming the charge of the double-layer is 750 mC (calculated from the double-layer current of 1.5 mA in a cyclic voltammogram and the change from open-circuit potential to the applied potential (0.5 V)) O_2 reduction to H_2O_2 (a two electron process), and using Faraday's constant, and the Spectracarb 2225 carbon cloth pore volume (1.2 mL g^{-1}), a pore

concentration of O_2 can be calculated to be 2.4 x 10^{-5} mol L^{-1}. The O_2 concentration value appears to be lower than values previously seen in Chapter 5 of 1.3 x 10^{-4} mol L^{-1} for an N_2 sparged electrolyte; therefore, the calculated O_2-content for the electrode in Figure 8.3 is reasonable, though it might have been expected to be higher than the electrode previously cycled to steady-state. When the first polarization potential applied was 0.05 V rather than 0.0 V a similar reduction current was evident, which shows that the lower potential range results in a large negative current when first exposed to electrochemistry, suggesting there is a species being reduced in the electrochemical cell.

Float current measurements were run on electrodes prior to and then immediately following continuous cycling to steady-state between 0.0 – 1.0 V. As can be seen in Figure 8.4 for both before and after continuous cycling, increasing the polarization potential results in an increase in the float current, which is expected based on the literature.[119, 163] Increasing the polarization potential results in more self-discharge reactions occurring and therefore a higher current.[119, 163] The current is likely comprised of a combination of double-layer charging, some amount of charge redistribution and the same process as the oxidation wave in the cyclic voltammograms (Figure 7.1).

Both pre- and post- continuous cycling, the 1.0 V float current data have the highest float current, *ca.* 0.20 mA for the as-received electrode compared to a cycled electrode at *ca.* 0.10 mA. It is important to note that although these float current measurements were collected for one hour due to literature precedent,[119, 163] the higher polarization potentials (0.80 V and above) for the electrode prior to continuous cycling do not ever reach a steady-state measurement (*i.e.* a near constant current). At the higher polarization potentials it is likely there is the addition of another electrochemical process

such as carbon oxidation (discussed in Chapter 7), which also may give rise to the magnitude of current decay in the float current measurements.

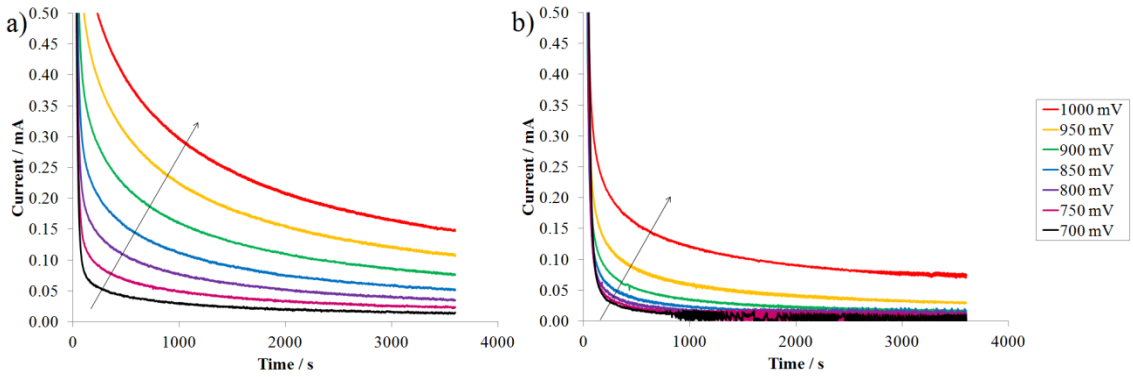

Figure 8.4: Float current measurements of a Spectracarb 2225 carbon cloth electrode (*ca.* 10 mg) in 1.0 M H_2SO_4 with data (a) before continuous cycling and (b) after continuous cycling. Note the noise in the 0.7 V polarization potential line (b) is due to the small currents being measured.

There is a large difference in the shapes of the float current measurements before and after continuous cycling. Prior to continuous cycling the initial drop in current becomes more gradual with increasing polarization potential (see Figure 8.4a), as is expected for porous electrodes due to uneven charging of the electrodes surface takes longer times for the applied voltage to reach farther down the pores.[119] In addition to the porous effect, a combination of Faradaic currents (both self-discharge and the oxidation wave) on the electrode result in the more gradual drop in current.[119] After continuous cycling (Figure 8.4b) the initial current decay are consistent for all the polarization potentials, possibly due to the full charging of the electrode and there are no longer as large a distribution of pore effects effecting the current drop. The decrease in the oxidation wave seen in the cyclic voltammograms in Figure 7.1 also corresponds to the smaller float current values after continuous cycling, suggesting it may be due to the

magnitude of the oxidation wave process. The results shown in Figure 8.4b are more consistent with those for a glassy carbon planar electrode which would not suffer as significantly from pore effects and have a faster decline in current, though the time scale is still different.[163] The steep decline suggests the electrode is more fully charged and therefore charge redistribution is not occurring to as large an extent. Also, it is possible a Faradaic reaction that was initially present in the electrochemical system was depleted over the course of float current measurements and cyclic voltammograms, such as the oxidation wave. As a result, the float current would be lower after continuous cycling and the float current value is then related directly to the self-discharge process.

Integrating under the current versus time curves presented in Figure 8.4 (and also lower polarization potentials which are not shown) results in the charge passed, shown in Figure 8.5. The charge passed to reach a steady-state float current is important since that charge is necessary to reach a steady-state double-layer charging without pore effects, and also a steady, reproducible self-discharge.[119] The data presented in Figure 8.5 shows many differences between the float currents prior to continuously cycling and those float current measurements after continuous cycling. At polarization potentials less than 0.4 V there is no significant difference between the float currents before and after continuous cycling. Additionally, the charge required to reach the specified potentials up to 0.4 V are not different. Above 0.4 V there in an increase in the charge passed for the float currents after continuous cycling, likely due to the Faradaic contributions of the quinone/hydroquinone redox couple. At 0.7 V the charge passed is the same both before and after continuous cycling; however above 0.7 V polarization potentials more charge is passed prior to continuous cycling. The increase in charge passed prior to continuous

cycling aligns well with the large carbon oxidation wave evident in the cyclic voltammograms above 0.7 V, suggesting that continuous cycling of the Spectracarb 2225 carbon cloth electrodes is necessary to result in less self-discharge current, consistent with the comparison of self-discharge data in section 8.2 and 8.3.

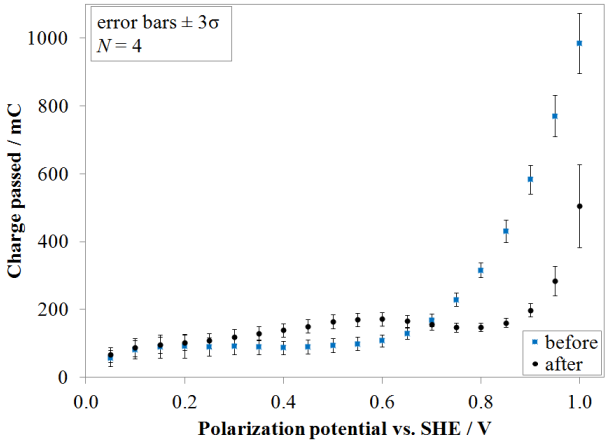

Figure 8.5: Average charge passed during 1 hour float current measurements of four (N) Spectracarb 2225 carbon cloth electrodes (*ca.* 10 mg) in 1.0 M H_2SO_4.

The self-discharge current corresponds to the float current value after a steady-state has been reached. Figure 8.6 shows the final current values for the Spectracarb 2225 carbon cloth before and after continuous cycling. At polarization potentials up to 0.65 V the currents are all close to 0 μA, meaning small currents are necessary to keep the electrode at the given potential. The 0.65 V polarization potential corresponds to the development of the quinone/hydroquinone redox peak in the incremental cyclic voltammograms (see Chapter 7). The redox process results in a higher current to keep the electrode at potentials above 0.65 V. Again at 0.7 V there is a difference in the data from before and after continuous cycling where the data obtained from before continuous cycling results in a larger final float current compared to the data collected after continuous cycling, which suggests that continuous cycling is necessary to minimize the continual feed of current necessary to keep the electrode at a given state-of-charge.

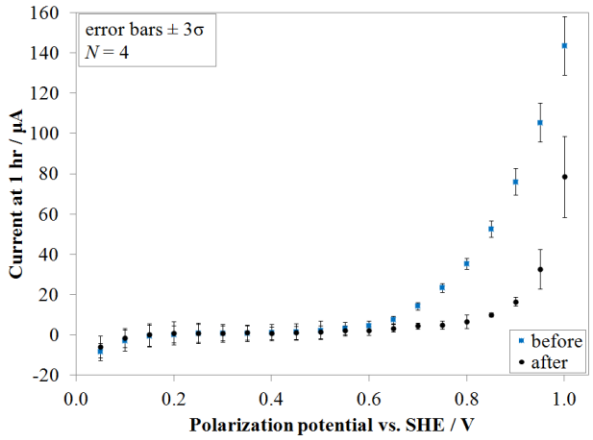

Figure 8.6: Average final current of one hour float current measurements for four (N) Spectracarb 2225 carbon cloth electrodes (*ca.* 10 mg) in 1.0 M H_2SO_4.

8.5 Conclusions

The self-discharge data presented in this chapter showed the significant effect cycling has on the self-discharge and float current measurements data for Spectracarb 2225 carbon cloth electrodes. It was shown that data from the positive (1.0 V) electrode is more reproducible when continuously cycled to steady-state prior to self-discharge experiments. It was also shown that there was no difference between self-discharge profiles of as-received electrodes when exposed to the 1.0 M H_2SO_4 electrolyte, or 18.2 MΩ·cm water. The depth of the self-discharge profiles does not result from the current flowing prior to switching to open-circuit potential. Continuous cycling prior to self-discharge profiles was found to be necessary, for Spectracarb 2225 carbon cloth systems, to remove possible irreversible Faradaic reactions.

Float current measurements show that the current flowing in an as-received electrode is much higher than the cycled electrodes. The potentials for given charges of the float current measurements align well with the cyclic voltammetry data previously presented in Chapter 7. The final currents (*i.e.* the current necessary to hold an electrode

at a given state-of-charge due to the self-discharge reaction) was found to be less for continuously cycled electrodes above 0.7 V compared to electrodes not previously cycled, consistent with the oxidation wave present in the first cyclic voltammogram.

Chapter 9 CONCLUSIONS

9.1 Thesis Summary

This research focused on understanding the self-discharge mechanisms in symmetric carbon-based, aqueous electrolyte electrochemical capacitors. Self-discharge profiles were collected from Spectracarb 2225 carbon cloth electrodes in a variety of experimental conditions to examine electrode and electrolyte properties and their effects on charge loss. It was shown that, in pure sulphuric acid with no additional redox-active species, electrodes that were previously potentially cycled to steady-state (no change in the cyclic voltammogram between consecutive cycles) showed different self-discharge mechanism on the two electrodes; self-discharge on the positive electrode was due to an activation-controlled self-discharge mechanism, and the self-discharge on the negative electrode was due to a diffusion-controlled self-discharge mechanism.

Self-discharge profiles were collected on Spectracarb 2225 carbon cloth electrodes previously cycled to steady-state, in sulphuric acid containing 0 – 10^{-1} M $Fe^{2+/3+}$ to examine the Fe-shuttle self-discharge mechanism. It was found that self-discharge on the positive electrode was consistent with 0 M Fe self-discharge profiles up until concentrations of 10^{-5} M $Fe^{2+/3+}$, and exhibited an activation-control/charge redistribution loss of potential, suggesting Fe-contamination is not causing the self-discharge at these $Fe^{2+/3+}$ concentrations. At concentrations greater than 10^{-5} M $Fe^{2+/3+}$, the potential loss increased significantly, and the mechanism of self-discharge has changed to diffusion-control. Therefore, at concentrations above 10^{-5} M $Fe^{2+/3+}$ self-discharge will be enhanced on the positive electrode.

The change of rate-determining steps from activation-control to diffusion-control suggests the $Fe^{2+/3+}$ which is causing the self-discharge has been depleted in the pores and self-discharge is occurring only on the planar face of the electrode. As a result, the Conway kinetic models are still able to be used although they were originally derived for a planar surface. The depletion of the $Fe^{2+/3+}$ is confirmed using leakage (float) current measurements.

Self-discharge on the negative electrode in the presence of Fe-contamination results in no increase in self-discharge until 10^{-3} M $Fe^{2+/3+}$. Interestingly, the loss of potential does not change self-discharge mechanism in the presence of Fe, and is always diffusion-controlled. The diffusion-controlled profile was expected for Fe-caused self-discharge (at Fe concentrations greater than 10^{-3} M) based on the positive electrode research. The diffusion-controlled self-discharge at Fe concentrations less than 10^{-3} M, where Fe is not causing self-discharge suggests a low concentration species controlling self-discharge, such as O_2.

For both the positive and negative electrodes, at high Fe concentrations (*e.g.* 10^{-1} M) Fe-induced self-discharge is the main self-discharge mechanism; however, at these concentrations, the system is no longer diffusion-controlled but rather is under mixed control (both activation- and diffusion-control). The change in control mechanism suggests that at these high Fe concentrations the rate-limiting step is the reaction of Fe on the carbon surface, rather than diffusion to the surface.

To identify the self-discharge mechanism in the absence of Fe-contamination (*i.e.* to identify the self-discharge evident at zero or low Fe-contamination), self-discharge profiles were also collected with sulphuric acid electrolyte with various partial pressures

of O_2, H_2, N_2. Varying the partial pressures of dissolved gases was used to examine whether water decomposition, in the form of oxygen evolution or hydrogen evolution, was the cause of self-discharge. Positive electrode self-discharge profiles in the presence of O_2 showed no significant difference in potential loss than those self-discharge profiles in N_2, and still retained a profile consistent with activation-control/charge redistribution. Therefore water oxidation to oxygen was deemed to not be the cause of positive electrode self-discharge. Self-discharge profiles from the negative electrode in the presence of H_2 also resulted in no significant change from the self-discharge profile with N_2-sparging. Self-discharge was therefore determined to not be caused by electrolyte decomposition.

Self-discharge was seen to increase dramatically on the negative electrode in the presence of O_2, due to the oxygen reduction to H_2O_2 or H_2O. It was found that self-discharge on the negative electrode, in the presence of O_2 resulted in mixed kinetic control (both activation and diffusion-control). Self-discharge on the negative electrode is likely due to O_2-reduction and therefore the removal of O_2 is a key factor to minimizing this self-discharge.

Carbon surface oxides are important to identify as some surface groups (quinone/hydroquinone) have been known to increase the capacitance through pseudocapacitive contributions. It was of interest to standardize a commonly used technique to identify surface groups, called the Boehm titration, as the procedures in the literature varied significantly between research groups, and also the procedure was not always explicitly stated. Standardization with regard to the use of dilute titrant, effect of base standardization, filtering, and the method of agitation were examined. It was determined that the former three conditions did not make a significant difference;

however, the method of agitation has a significant effect on the macroscopic surface of the carbon sample and must be selected appropriately.

Carbon oxidation was examined both electrochemically, and with the addition of CO_2 to the sulphuric electrolyte. Electrochemical oxidation was examined in regards to the potential at which the large oxidation wave evidenced in the cyclic voltammogram of Spectracarb 2225 carbon cloth begins, the possible relationship with surface group development, and also on self-discharge itself. Self-discharge on electrodes which had not previously been cycled to steady-state (*i.e.* electrodes which exhibited the large oxidation wave in the cyclic voltammogram) resulted in a larger self-discharge than those continuously cycled to steady-state (*i.e.* those electrodes in which the oxidation wave had been essentially removed through continuous cycling). It was thought the exposure to electrolyte during the continuously cycling procedure may have been the cause of the difference in self-discharge; however, when electrodes were immersed in electrolyte for the same length of time as during continuous cycling, and no electrochemistry was conducted, the same trend of larger self-discharge was seen. Therefore, the difference in the self-discharge profiles was not due to a change in exposure to electrolyte or water, but rather the continuous cycling to steady-state. It appears as though the cycling to steady-state also results in a steady-state in the self-discharge profile.

An attempt was made to correlate the development of the quinone/hydroquinone redox couple and the oxidation wave, and both of their effects on self-discharge. The overall trend in the oxidation wave and self-discharge are the same (*i.e.* a decrease in the magnitude of the oxidation wave occurs with a decrease in self-discharge), but there is not a direct correlation due to the charge passed. The oxidation wave also cannot be

directly linked to the development of the quinone/hydroquinone redox couple, though the oxidation wave may be, in part, a conversion of one surface species to another. Incremental cyclic voltammograms showed that potentials higher than the redox couple centre potential (0.65 V) are necessary for development of quinoid groups (0.55 V). For potentials up to 0.65 V, the cyclic voltammograms had an almost constant capacitance suggesting mainly double-layer charge with a possibility of a very small Faradaic contribution as well. At potentials above 0.65 V the data could no longer be fit linearly, suggesting additional Faradaic reactions. The data above 0.65 V did not fit an exponential curve as might be expected for an activation-controlled reaction, and therefore this suggests a mixture of Faradaic processes occurring at the positive electrode. These Faradaic processes have not yet been identified.

9.2 Future Work

The work presented in this thesis focused on the self-discharge processes of a high-surface-area carbon electrode (Spectracarb 2225 carbon cloth). Rather than starting with a purchased carbon that has varied pore structures (which may affect the charge redistribution and therefore makes analysis of the data more difficult), it would be interesting to carry out similar self-discharge experiments on carbons with lower surface-area, but also more defined surface-areas, such as a templated carbon, or even a glassy carbon surface with milled pores using a focused ion beam. Through this bottom-up approach, the effect of charge redistribution process could be more effectively separated from self-discharge process(es).

The Spectracarb 2225 carbon cloth also contains surface oxide groups which had advantageous increases in capacitance due to Faradaic processes (*i.e.* the quinone/hydroquinone redox couple results in increased pseudocapacitance). It is therefore possible that the electrode surface can be selectively oxidized and functionalized to individually determine the effect of each carbon surface oxide group on self-discharge.

Examining the effect of self-discharge in a full-cell set-up would expand the knowledge of an optimized system and how the self-discharge is effected by the removal of the reference electrode. It would be interesting to examine how two electrodes (with known and different self-discharge mechanisms) would interact for the two electrode set-ups self-discharge. Additionally, determining which self-discharge mechanism controls the cells self-discharge would be worth examining (or whether it is a combination of both self-discharge processes).

To gain more insight into oxygen reduction as a cause of self-discharge, the examination of multiple oxygen concentrations would add to the understanding of the charge loss due to oxygen. By extrapolating the data back to an electrolyte void of oxygen, it would then be possible to discern whether multiple processes were responsible for the negative electrodes self-discharge, or if it was solely due to oxygen reduction.

Further work on the self-discharge pH study would expand on the different possible self-discharge mechanisms at both high proton and hydroxide concentrations. Both carbon oxidation and oxygen reduction are pH dependent, and therefore it would be of interest to continue with this work. Difficulties of titrating the electrolyte resulted from: keeping the potential window constant over the entire pH range, as well as the

addition of a supporting electrolyte which complicated the data analysis in the middle of the pH range since the supporting electrolyte was now more concentrated than the protons or hydroxide ions.

Due to the significant variation seen in carbon samples using *ex situ* methods for carbon surface functionality identification and quantification (such as the Boehm titration), an *in situ* method would be necessary for a direct understanding of the electrode processes (*i.e.* the possible conversion of one carbon surface functionalities to quinone).

Further work on the relationship between carbon corrosion and the oxidation wave evident in the cyclic voltammograms of Spectracarb 2225 carbon cloth is necessary to definitively link the oxidation wave to the production of carbon dioxide. Head-space gas chromatography and mass spectrometry could be used to quantify the different concentrations in the electrochemical cell throughout the potential cycling process. Carbon dioxide measurements can also be taken in the electrolyte solution itself using a carbon dioxide probe to quantify the CO_2 produced in an N_2-saturated solution during both incremental cyclic voltammograms and cycling to steady-state.

Once the effect of carbon surface groups on self-discharge has been probed more significantly with electrochemistry, spectroscopic techniques could be used to support the electrochemical results. Spectroscopic techniques such as XPS could be used to support the differences seen in carbon surface electrochemically, such as a possible change in the different carbon-oxygen peaks.

REFERENCES

1. Becker, H.I.; Ferry, V. Low Voltage Electrolytic Capacitor. U.S. Patent 2,800,616, July 23, 1957.

2. Davies, A.; Yu, A. Material Advancements in Supercapacitors: From Activated Carbon to Carbon Nanotube and Graphene. *Can J Chem Eng.* **2011**, *89*, 1342-1357.

3. Zhang, J. On the Configuration of Supercapacitors for Maximizing Electrochemical Performance. *ChemSusChem.* **2012**, *5*, 818-841.

4. Conway, B.E.; Pell, W.G. Double-layer and Pseudocapacitance Types of Electrochemical Capacitors and Their Applications to the Development of Hybrid Devices. *J Solid State Electrochem.* **2003**, *7*, 637-644.

5. Frackowiak, E. Carbon Materials for Supercapacitor Application. *Phys. Chem. Chem. Phys.* **2007**, *9*, 1774-1785.

6. Miller, J.R.; Butler, S.M. Electrochemical Capacitor Performance in Energy Harvesting Applications. *ECS Trans.* **2008**, *16*, 3-11.

7. Kotz, R.; Carlen, M. Principles and Applications of Electrochemical Capacitors. *Electrochim Acta.* **2000**, *45*, 2483-2498.

8. Miller, J.R.; Simon, P. Electrochemical Capacitors for Energy Management. *Science* **2008**, *321*, 651-652.

9. Miller, J.R.; Burke, A.F. Electrochemical Capacitors: Challenges and Opportunities for Real-World Applications. *Electrochem Soc Interface.* **2008,** *17*, 53-57.

10. Winter, M.; Brodd, R.J. What are Batteries, Fuel Cells, and Supercapacitors? *Chem Rev.* **2004**, *104*, 4245-4269.

11. Conway, B.E. *Electrochemical Supercapacitors*. Kluwer Academic: New York, 1999.

12. Boehm, H.P. Surface Oxides on Carbon. *High Temperatures - High Pressures.* **1990**, *22*, 275-288.

13. Kazaryan, S.A.; Kharisov, G.G.; Litvinenko S.V.; Kogan, V.I. Self-discharge Related to Iron Ions and its Effect on the Parameters of HES $PbO_2|H_2SO_4|C$ Systems. *J Electrochem Soc.* **2007**, *154*, A751-A759.

14. Andreas, H.A.; Lussier, K.; Oickle, A.M. Effect of Fe-contamination on Rate of Self-Discharge in Carbon-based Aqueous Electrochemical Capacitors. *J Power Sources.* **2009**, *187*, 275-283.

15. Pillay, B.; Newman, J. The Influence of Side Reactions on the Performance of Electrochemical Double-layer Capacitors. *J Electrochem Soc.* **1996**, *143*, 1806-1814.

16. Oickle, A.M.; Andreas, H.A. Examination of Water Electrolysis and Oxygen Reduction as Self-discharge Mechanisms for Carbon-based, Aqueous Electrolyte Electrochemical Capacitors. *J Phys Chem C.* **2011**, *115*, 4283-4288.

17. Willsau, J.; Heitbaum, J. The Influence of Platinum Activation on the Corrosion of Carbon in Gas Diffusion Electrodes - a DEMS Study. *J Electroanal Chem.* **1984**, *161*, 93-101.

18. Boehm, H.P. Functional Groups on the Surface of Solids. *Angew.Chem., Intern. Ed*. **1966**, *5*, 533-544.

19. Boehm, H.P. Some Aspects of the Surface Chemistry of Carbon Blacks and Other Carbons. *Carbon.* **1994**, *32*, 759-769.

20. Bandosz, T.J; Jagiello, J.; Schwarz, J.A. Comparison of Methods to Assess Surface Acidic Groups on Activated Carbons. *Anal Chem.* **1992**, *64*, 891-895.

21. Guo, Y.; Rockstraw, D.A. Activated Carbons Prepared from Rice Hull by One-step Phosphoric Acid Activation. *Microporous Mesoporous Mater.* **2007**, *100*, 12-19.

22. Seredych, M.; Hulicova-Jurcakova, D.; Lu, G.Q.; Bandosz T.J. Surface Functional Groups of Carbons and the Effects of Their Chemical Character, Density and Accessibility to Ions on Electrochemical Performance. *Carbon.* **2008**, *46*, 1475-1488.

23. Goertzen, S.L.; Theriault, K.D.; Oickle, A.M.; Tarasuk, A.C.; Andreas, H.A. Standardization of the Boehm Titration. Part I. CO2 Expulsion and Endpoint Determination. *Carbon.* **2010**, *48*, 1252-1261.

24. Oickle, A.M.; Goertzen, S.L.; Hopper, K.R.; Abdalla, Y.O.; Andreas, H.A. Standardization of the Boehm Titration: Part II. Method of Agitation, Effect of Filtering and Dilute Titrant. *Carbon.* **2010**, *48*, 3313-3322.

25. Barker, J.R.; An Introduction to Global Warming. *Am J Phys.* **1999**, *67*, 1216-1226.

26. Brodd, R.J. Carbon in Batteries and Energy Conversion Devices. In *Carbons for Electrochemical Energy Storage and Conversion Systems;* Béguin, F.; Frackowiak, E., Ed.; CRC Press, 2009. p 411.

27. Lincoln, S. Fossil Fuels in the 21st Century. *Ambio.* **2005**, *34*, 621-627.

28. Simon, P.; Gogotsi, Y. Materials for Electrochemical Capacitors. *Nat Mater.* **2008**, *7*, 845-854.

29. Burke, A. Ultracapacitors: Why, How, and Where is the Technology. *J Power Sources.* **2000**, *91*, 37-50.

30. Burke, A. R&D Considerations for the Performance and Application of Electrochemical Capacitors. *Electrochim Acta.* **2007**, *53*, 1083-1091.

31. Bockris, J.O.; Reddy, A.K.N, Gamboa-Aldeco, M.E. Modern Electrochemistry 2A, Second Edition: Fundamentals of Electrodics. 2nd ed.; Kluwer Academic: New York, 1999.

32. Zhang, Y.; Feng, H.; Wu, X.; Wang, L.; Zhange, A.; Xia, Z.; Dong, H.; Li, X.; Zhang, L. Progress of Electrochemical Capacitor Electrode Materials: A Review. *Int J Hydrogen Energy.* **2009**, *34*, 4889-4899.

33. Conway, B.E.; Birss, V.; Wojtowicz, J. The Role and Utilization of Pseudocapacitance for Energy Storage by Supercapacitors. *J Power Sources.* **1997**, *66*, 1-14.

34. Miller, J.; Dunn, B.; Tran, T.D.; Pekala, R.W. Deposition of Ruthenium Nanoparticles on Carbon Aerogels for High Energy Density Supercapacitor Electrodes. *J Electrochem Soc.* **1997**, *144*, L309-L311.

35. Kim, I.; Kim, K. Ruthenium Oxide Thin Film Electrodes for Supercapacitors. *Electrochem Solid St.* **2001**, *4*, A62-A64.

36. Hu, C.; Chang, K. Cyclic Voltammetric Deposition of Hydrous Ruthenium Oxide for Electrochemical Supercapacitors: Effects of the Chloride Precursor Transformation. *J Power Sources.* **2002**, *112*, 401-409.

37. Frackowiak, E.; Khomenko, V.; Jurewicz, K.; Lota, K.; Béguin, F. Supercapacitors Based on Conducting Polymers/Nanotubes Composites. *J Power Sources.* **2006**, *153*, 413-418.

38. Frackowiak, E.; Beguin, F. Carbon Materials for the Electrochemical Storage of Energy in Capacitors. *Carbon.* **2001**, *39*, 937-950.

39. Hadzi-Jordanov, S.; Angerstein-Lozlowska, H.; Vukoviff, M.; Conway, B.E. Reversibility and Growth Behavior of Surface Oxide Films at Ruthenium Electrodes. *J Electrochem Soc.* **1978**, *125*, 1471-1480.

40. Long, J.W.; Swider, K.E.; Merzbacher, C.I.; Rolison, D.R. Voltammetric Characterization of Ruthenium Oxide-based Aerogels and Other RuO_2 Solids: The Nature of Capacitance in Nanostructured Materials. *Langmuir.* **1999**, *15*, 780-785.

41. Wen, J.; Zhou, Z. Pseudocapacitance Characterization of Hydrous Ruthenium Oxide Prepared via Cyclic Voltammetric Deposition. *Mater Chem Phys.* **2006**, *98*, 442-446.

42. Liang, Y.; Li, H.L.; Zhang, X. Solid State Synthesis of Hydrous Ruthenium Oxide for Supercapacitors. *J Power Sources.* **2007**, *173*, 599-605.

43. Lee, H.Y., Goodenough, J.B. Supercapacitor Behavior with KCl Electrolyte. *J Solid State Chem.* **1999**, *144*, 220-223.

44. Toupin, M.; Brousse, T.; Belanger, D. Charge Storage Mechanism of MnO_2 Electrode Used in Aqueous Electrochemical Capacitor. *Chem Mater.* **2004**, *16*, 3184-3190.

45. Reddy, R.N.; Reddy, R.G. Synthesis and Electrochemical Characterization of Amorphous MnO_2 Electrochemical Capacitor Electrode Material. *J Power Sources.* **2004**, *132*, 315-320.

46. Malak-Polaczyk, A.; Matei-Ghimbeu, C.; Vix-Guterl, C.; Frackowiak, E. Carbon/λ-MnO_2 Composites for Supercapacitor Electrodes. *J Solid State Chem.* **2010**, *183*, 969-974.

47. Pickup, P.G.; Birss, V.I. The Influence of the Aqueous Growth Medium on the Growth Rate, Composition, and Structure of Hydrous Iridium Oxide Films. *J Electrochem Soc.* **1988**, *135*, 126-133.

48. Conway, B.E.; Mozota, J. Surface and Bulk Processes at Oxidized Iridium Electrodes—II. Conductivity-switched Behaviour of Thick Oxide Films. *Electrochim Acta.* **1983**, *28*, 9-16.

49. Andreas, H.; Elzanowska, H.; Serebrennikova, I.; Birss, V. Hydrous Ir Oxide Film Properties at Sol-Gel Derived Ir Nanoparticles. *J Electrochem Soc.* **2000**, *147*, 4598-4604.

50. Liu, X.; Pickup, P.G. Performance and Low Temperature Behaviour of Hydrous Ruthenium Oxide Supercapacitors with Improved Power Densities. Energy Environ Sci. **2008**, *1*, 494-500.

51. Bélanger, D.; Ren, X.; Davey, J.; Uribe, F.; Gottesfeld, S. Characterization and Long-term Performance of Polyaniline-based Electrochemical Capacitors. *J Electrochem Soc.* **2000**, *147*, 2923-2929.

52. Fusalba, F.; Gouerec, P.; Villers, D.; Bélanger, D. Electrochemical Characterization of Polyaniline in Non-aqueous Electrolyte and its Evaluation as Electrode Material for Electrochemical Supercapacitors. *J Electrochem Soc.* **2001**, *148*, A1-A6.

53. Snook, G.A.; Kao, P.; Best, A.S. Conducting-Polymer-based Supercapacitor Devices and Electrodes. *J Power Sources.* **2011**, *196*, 1-12.

54. Khomenko, V.; Frackowiak, E.; Béguin, F. Determination of the Specific Capacitance of Conducting Polymer/Nanotubes Composite Electrodes Using Different Cell Configurations. *Electrochim Acta.* **2005**, *50*, 2499-2506.

55. Ryu, K.S.; Lee, Y.; Kim, K.M.; Park, Y-J.; Hong, Y-S.; Wu, X.; Kang, M.G.; Park, N-G.; Song, R.Y.; Ko, J.M. Electrochemical Capacitor with Chemically Polymerized Conducting Polymer based on Activated Carbon as Hybrid Electrodes. *Synth Met.* **2005**, *153*, 89-92.

56. Li, Y.; Zhao, X.; Xu, Q.; Zhang, Q.; Chen, D. Facile Preparation and Enhanced Capacitance of the Polyaniline/Sodium Alginate Nanofiber Network for Supercapacitors. *Langmuir.* **2011**, *27*, 6458-6463.

57. Winter, M.; Moeller, K-C.; Besanhard, J.O. Carbonaceous and Graphitic Anodes. In *Lithium Batteries;* Nazri, G.; Pistoia, G., Ed.; Spinger US, 2003; p 145.

58. Liu, H.; Song, C.; Zhang, L.; Zhang, J.; Wang, H.; Wilkinson, D.P. A Review of Anode Catalysis in the Direct Methanol Fuel Cell. *J Power Sources.* **2006**, *155*, 95-110.

59. Kinoshita K. *Carbon: Electrochemical and Physicochemical Properties.* 1st ed.; John Wiley and Sons: New York, 1988.

60. Guo, Y.; Qi, J.; Jiang, Y.; Yang, S.; Wang, Z.; Xu, H. Performance of Electrical Double Layer Capacitors with Porous Carbons Derived from Rice Husk. *Mater Chem Phys.* **2003**, *80*, 704-709.

61. Kalderis, D.; Bethanis, S.; Paraskeva, P.; Diamadopoulos, E. Production of Activated Carbon from Bagasse and Rice Husk by a Single-stage Chemical Activation Method at Low Retention Times. *Bioresour Technol.* **2008**, *99*, 6809-6816.

62. Matsis, V.M.; Grigoropoulou, H.P. Kinetics and Equilibrium of Dissolved Oxygen Adsorption on Activated Carbon. *Chem Eng Sci.* **2008**, *63*, 609-621.

63. Laine, J.; Calafat, A.; Labady, M. Preparation and Characterization of Activated Carbons from Coconut Shell Impregnated with Phosphoric Acid. *Carbon.* **1989**, *27*, 191-195.

64. Laine, J.; Yunes, S. Effect of the Preparation Method on the Pore Size Distribution of Activated Carbon from Coconut Shell. *Carbon.* **1992**, *30*, 601-604.

65. González, M.T.; Molina-Sabio, M.; Rodríguez-Reinoso, F. Steam Activation of Olive Stone Chars, Development of Porosity. *Carbon.* **1994**, *32*, 1407-1413.

66. El-Sheikh, A.H,.; Newman, A.P.; Al-Daffaee, H.K.; Phull, S.; Cresswell, N. Characterization of Activated Carbon Prepared from a Single Cultivar of Jordanian Olive Stones by Chemical and Physicochemical Techniques. *J Anal Appl Pyrolysis.* **2004**, *71*, 151-164.

67. Martínez, M.L.; Torres, M.M.; Guzmán, C.A.; Maestri, D.M. Preparation and Characteristics of Activated Carbon from Olive Stones and Walnut Shells. *Ind Crop Prod.* **2006**, *23*, 23-28.

68. Valix, M.; Cheung, W.H.; McKay, G. Preparation of Activated Carbon using Low Temperature Carbonisation and Physical Activation of High Ash Raw Bagasse for Acid Dye Adsorption. *Chemosphere.* **2004**, *56*, 493-501.

69. Demiral, H.; Demiral, I.; Tumsek, F.; Karabacakoglu, B. Pore Structure of Activated Carbon Prepared from Hazelnut Bagasse by Chemical Activation. *Surf Interface Anal.* **2008**, *40*, 616-619.

70. Machida, M.; Mochimaru, T.; Tatsumoto, H. Lead(II) Adsorption Onto the Graphene Layer of Carbonaceous Materials in Aqueous Solution. *Carbon.* **2006**, *44*, 2681-2688.

71. Pandolfo, A.G.; Hollenkamp, A.F. Carbon Properties and Their Role in Supercapacitors. *J Power Sources.* **2006**, *157*, 11-27.

72. Bleda-Martinez, M.J.; Macia-Agullo, J.A.; Lozano-Castello, D.; Morallon, E.; Cazorla-Amoros, D.; Linares-Solano, A. Role of Surface Chemistry on Electric Double Layer Capacitance of Carbon Materials. *Carbon.* **2005**, *43*, 2677-2684.

73. Sullivan, M.G.; Schnyder, B.; Bartsch, M.; Alliata, D.; Barbero, C.; Imhof, R.; Kotz, R. Electrochemically Modified Glassy Carbon for Capacitor Electrodes. Characterization of Thick Anodic Layers by Cyclic Voltammetry, Differential Electrochemical Mass Spectrometry, Spectroscopic Ellipsometry, X-ray Photoelectron Spectroscopy, FTIR, and AFM. *J Electrochem Soc.* **2000**, *147*, 2636-2643.

74. Gryglewicz, G.; Machnikowski, J.; Lorenc-Grabowska, E.; Lota, G.; Frackowiak, E. Effect of Pore Size Distribution of Coal-based Activated Carbons on Double Layer Capacitance. *Electrochim Acta.* **2005**, *50*, 1197-1206.

75. Bouchelta, C.; Medjram, M.S.; Bertrand, O.; Bellat, J. Preparation and Characterization of Activated Carbon from Date Stones by Physical Activation with Steam. *J Anal Appl Pyrolysis.* **2008**, *82*, 70-77.

76. Kierzek, K.; Frackowiak, E.; Lota, G.; Gryglewicz, G.; Machnikowski, J. Electrochemical Capacitors Based on Highly Porous Carbons Prepared by KOH Activation. *Electrochim Acta.* **2004**, *49*, 515-523.

77. Vinke, P.; van der Eijk, M.; Verbree, M.; Voskamp, A.F.; van Bekkum, H. Modification of the Surfaces of a Gas-activated Carbon and a Chemically Activated Carbon with Nitric Acid, Hypochlorite, and Ammonia. *Carbon.* **1994**, *32*, 675-686.

78. Moreno-Castilla, C.; Lopez-Ramon, M.V.; Carrasco-Marin, F. Changes in Surface Chemistry of Activated Carbons by Wet Oxidation. *Carbon.* **2000**, *38*, 1995-2001.

79. Park, S.; Jang, Y.; Shim, J.; Ryu, S. Studies on Pore Structures and Surface Functional Groups of Pitch-based Activated Carbon Fibers. *J Colloid Interface Sci.* **2003**, *260*, 259-264.

80. Guo, Y.; Rockstraw, D.A. Physical and Chemical Properties of Carbons Synthesized from Xylan, Cellulose, and Kraft Lignin by H_3PO_4 Activation. *Carbon.* **2006**, *44*, 1464-1475.

81. Matsumura, Y.; Hagiwara, S.; Takahashi, H. Automatic Potentiometric Titration of Surface Acidity of Carbon Black. *Carbon.* **1976**, *14*, 163-167.

82. Gomez-Serrano, V.; Acedo-Ramos, M.; Lopez-Peinado, A.J.; Valenzuela-Calahorro, C. Oxidation of Activated Carbon by Hydrogen Peroxide. Study of Surface Functional Groups by FT-IR. *Fuel.* **1994**, *73*, 387-395.

83. Ahmadpour, A.; Do, D.D. The Preparation of Activated Carbon from Macadamia Nutshell by Chemical Activation. *Carbon.* **1997**, *35*, 1723-1732.

84. Raymundo-Pinero, E.; Kierzek, K.; Machnikowski, J.; Beguin, F. Relationship Between the Nanoporous Texture of Activated Carbons and Their Capacitance Properties in Different Electrolytes. *Carbon.* **2006**, *44*, 2498-2507.

85. Chmiola, J.; Yushin, G.; Gogotsi, Y.; Portet, C.; Simon, P.; Taberna, P.L. Anomalous Increase in Carbon Capacitance at Pore Sizes Less Than 1 Nanometer. *Science.* **2006**, *313*, 1760-1763.

86. Boehm, H.P. Surface Oxides on Carbon and their Analysis: A Critical Assessment. *Carbon.* **2002**, *40*, 145-149.

87. Strickland-Constable, R.F. Part Played by Surface Oxides in the Oxidation of Carbon. *Trans Faraday Soc.* **1938**, *34*, 1074-1080.

88. Ishizaki, C.; Marti, I. Surface Oxide Structures on a Commercial Activated Carbon. *Carbon.* **1981**, *19*, 409-412.

89. Garten, V.A.; Weiss, D.E. Quinone-hydroquinone Character of Activated Carbon and Carbon Black. *Aust J Chem.* **1955**, *8*, 68-95.

90. Drushel, H.V.; Hallum, J.V. The Organic Nature of Carbon Black Surfaces. II. Quinones and Hydroquinones by Coulometry at Controlled Potential. *J Phys Chem.* **1958**, *62*, 1502-1505.

91. Hallum, J.V.; Drushel, H.V. The Organic Nature of Carbon Black Surfaces. *J Phys Chem.* **1958**, *62*, 110-117.

92. Boehm, H.P.; Diehl, E.; Heck, W.; Sappok, R. Surface Oxides of Carbon. *Angew Chem Int Ed.* **1964**, *76*, 742-751.

93. Hulicova-Jurcakova, D.; Kodama, M.; Shiraishi, S.; Hatori, H.; Zhu, Z.H.; Lu, G.Q. Nitrogen-enriched Nonporous Carbon Electrodes with Extraordinary Supercapacitance. *Adv Funct Mater.* **2009**, *19*, 1800-1809.

94. Biniak, S.; Szymanski, G.; Siedlewski, J.; Swiatkowski, A. The Characterization of Activated Carbons with Oxygen and Nitrogen Surface Groups. *Carbon.* **1997**, *35*, 1799-1810.

95. Chin, H.C. Preparation and Characterization of Carbon-Sulfur Surface Compounds. *Carbon.* **1981**, *19*, 175-186.

96. Dastgheib, S.A.; Rockstraw, D.A. Pecan Shell Activated Carbon: Synthesis, Characterization, and Application for the Removal of Copper from Aqueous Solution. *Carbon.* **2001**, *39*, 1849-1855.

97. Fuente, E.; Menendez, J.A.; Suarez, D.; Montes-Moran, M.A. Basic Surface Oxides on Carbon Materials: A Global View. *Langmuir.* **2003**, *19*, 3505-3511.

98. Montes-Moran, M.A.; Suarez, D.; Menendez, J.A.; Fuente, E. On the Nature of Basic Sites on Carbon Surfaces: An Overview. *Carbon.* **2004**, *42*, 1219-1225.

99. Yoshida, A.; Tanahashi, I.; Nishino, A. Effect of Concentration of Surface Acidic Functional Groups on Electric Double-layer Properties of Activated Carbon Fibers. *Carbon.* **1990**, *28*, 611-615.

100. Azais, P.; Duclaux, L.; Florian, P.; Massiot, D.; Lill-Rodenas, M.; Linares-Solano, A.; Peres, J-P.; Jehoulet, C.; Béguin, F. Causes of Supercapacitors Ageing in Organic Electrolyte. *J Power Sources.* **2007**, *171*, 1046-1053.

101. Cazorla-Amoros, D.; Lozano-Castello, D.; Morallon, E.; Bleda-Martinez, M.J.; Linares-Solano, A.; Shiraishi, S. Measuring Cycle Efficiency and Capacitance of Chemically Activated Carbons in Propylene Carbonate. *Carbon.* **2010**, *48*, 1451-1456.

102. Boehm, H.P. Chemical Identification of Surface Groups. *Advan.Catalysis.* **1966**, *16*, 179-274.

103. Contescu, A.; Contescu, C.; Putyera, K.; Schwarz, J.A. Surface Acidity of Carbons Characterized by Their Continuous pK Distribution and Boehm Titration. *Carbon.* **1997**, *35*, 83-94.

104. Salame, I.I.; Bandosz, T.J. Surface Chemistry of Activated Carbons: Combining the Results of Temperature-Programmed Desorption, Boehm, and Potentiometric Titrations. *J Colloid Interface Sci.* **2001**, *240*, 252-258.

105. Kim, C.; Pyun, S.; Shin, H. Kinetics of Double-layer Charging/Discharging of Activated Carbon Electrodes: Role of Surface Acidic Functional Groups. *J Electrochem Soc.* **2002**, *149*, A93-A98.

106. Fletcher, A.J.; Uygur, Y.; Thomas, K.M. Role of Surface Functional Groups in the Adsorption Kinetics of Water Vapor on Microporous Activated Carbons. *J Phys Chem C.* **2007**, *111*, 8349-8359.

107. McEwen, A. Electrochemical Properties of Imidazolium Salt Electrolytes for Electrochemical Capacitor Applications. *J Electrochem Soc.* **1999**, *146*, 1687-1695.

108. Ue, M. Application of Low-Viscosity Ionic Liquid to the Electrolyte of Double-layer Capacitors. *J Electrochem Soc.* **2003**, *150*, A499-A502.

109. Arulepp, M.; Permann, L.; Leis, J.; Person, A.; Rumma, K.; Janes, A.; Lust, E. Influence of the Solvent Properties on the Characteristics of a Double Layer Capacitor. *J Power Sources.* **2004**, *133*, 320-328.

110. Vix-Guterl, C.; Frackowiak, E.; Jurewicz, K.; Friebe, M.; Parmentier, J.; Beguin, F. Electrochemical Energy Storage in Ordered Porous Carbon Mmaterials. *Carbon.* **2005**, *43*, 1293-1302.

111. Largeot, C.; Portet, C.; Chmiola, J.; Taberna, P.; Gogotsi, Y.; Simon, P. Relation Between the Ion Size and Pore Size for an Electric Double-layer Capacitor. *J Am Chem Soc.* **2008**, *130*, 2730-2731.

112. Lide, D.R. (ed). *CRC Handbook of Chemistry and Physics. Internet Version* ed.; CRC Press: Boca Raton, 2005.

113. Andreas, H.A.; Conway, B.E. Examination of the Double-layer Capacitance of an High Specific-Area C-cloth Electrode as Titrated from Acidic to Alkaline pHs. *Electrochim Acta.* **2006**, *51*, 6510-6520.

114. Ue, M.; Ida, K.; Mori, S. Electrochemical Properties of Organic Liquid Electrolytes Based on Quaternary Onium Salts for Electrical Double-layer Capacitors. *J*

Electrochem Soc. **1994**, *141*, 2989-2996.

115. Frackowiak, E. Supercapacitors Based on Carbon Materials and Ionic Liquids. *J Braz Chem Soc.* **2006**, *17*, 1074-1082.

116. Sato, T.; Masuda, G.; Takagi, K. Electrochemical Properties of Novel Ionic Liquids for Electric Double Layer Capacitor Applications. *Electrochim Acta.* **2004**, *49*, 3603-3611.

117. Galiński, M.; Lewandowski, A.; Stępniak, I. Ionic Liquids as Electrolytes. *Electrochim Acta.* **2006**, *51*, 5567-5580.

118. Conway, B.E.; Pell, W.G.; Liu, T. Diagnostic Analyses for Mechanisms of Self-Discharge of Electrochemical Capacitors and Batteries. *J Power Sources.* **1997**, *65*, 53-59.

119. Niu, J.; Conway, B.E.; Pell, W.G. Comparative Studies of Self-discharge by Potential Decay and Float-current Measurements at C Double-layer Capacitor and Battery Electrodes. *J Power Sources.* **2004**, *135*, 332-343.

120. de Levie, R. Porous Electrodes in Electrolyte Solutions. I. Capacitance Effects. *Electrochim Acta.* **1963**, *8*, 751-780.

121. de Levie R. Porous Electrodes in Electrolyte Solutions. IV. *Electrochim Acta.* **1964**, *9*, 1231-1245.

122. Yaniv, M.; Soffer, A. The Transient Behavior of an Ideally Polarized Porous Carbon Electrode at Constant Charging Current. *J Electrochem Soc.* **1976**, *123*, 506-511.

123. Black, J.; Andreas, H.A. Effects of Charge Redistribution on Self-discharge of Electrochemical Capacitors. *Electrochim Acta.* **2009**, *54*, 3568-3574.

124. Bonnefoi, L.; Simon, P.; Fauvarque, J.F.; Sarrazin, C.; Sarrau, J.F.; Dugast, A. Electrode Compositions for Carbon Power Supercapacitors. *J Power Sources.* **1999**, *80*, 149-155.

125. Nian, Y.; Teng, H. Nitric Acid Modification of Activated Carbon Electrodes for Improvement of Electrochemical Capacitance. *J Electrochem Soc.* **2002**, *149*, A1008-A1014.

126. Hsieh, C.; Teng, H. Influence of Oxygen Treatment on Electric Double-layer Capacitance of Activated Carbon Fabrics. *Carbon.* **2002**, *40*, 667-674.

127. Nian, Y.; Teng, H. Influence of Surface Oxides on the Impedance Behavior of Carbon-based Electrochemical Capacitors. *J Electroanal Chem.* **2003**, *540*, 119-127.

128. Braun, A.; Bartsch, M.; Merlo, O.; Schnyder, B.; Schaffner, B.; Kotz, R.; Haas, O.; Wokaun, A. Exponential Growth of Electrochemical Double Layer Capacitance in Glassy Carbon During Thermal Oxidation. *Carbon*. **2003**, *41*, 759-765.

129. Okajima, K.; Ohta, K.; Sudoh, M. Capacitance Behavior of Activated Carbon Fibers with Oxygen-Plasma Treatment. *Electrochim Acta.* **2005**, *50*, 2227-2231.

130. Centeno, T.A.; Stoeckli, F. On the Specific Double-layer Capacitance of Activated Carbons, in Relation to their Structural and Chemical Properties. *J Power Sources.* **2006**, *154*, 314-320.

131. Yamada, H.; Nakamura, H.; Nakahara, F.; Moriguchi, I.; Kudo, T. Electrochemical Study of High Electrochemical Double Layer Capacitance of Ordered Porous Carbons with both Meso/Macropores and Micropores. *J Phys Chem C.* **2007**, *111*, 227-233.

132. Soudan, P.; Lucas, P.; Ho, H.A.; Jobin, D.; Breau, L.; Belanger, D. Synthesis, Chemical Polymerization and Electrochemical Properties of Low Band Gap Conducting Polymers for use in Super Capacitors. *J Mater Chem.* **2001**, *11*, 773-782.

133. Hong, M.S.; Lee, S.H.; Kim, S.W. Use of KCl Aqueous Electrolyte for 2 V Manganese Oxide/Activated Carbon Hybrid Capacitor. *Electrochem Solid-State Lett.* **2002**, *5*, A227-A230.

134. Liu, P.; Verbrugge, M.; Soukiazian, S. Influence of Temperature and Electrolyte on the Performance of Activated-Carbon Supercapacitors. *J Power Sources.* **2006**, *156*, 712-718.

135. Lota, G.; Centeno, T.A.; Frackowiak, E.; Stoeckli, F. Improvement of the Structural and Chemical Properties of a Commercial Activated Carbon for its Application in Electrochemical Capacitors. *Electrochim Acta.* **2008**, *53*, 2210-2216.

136. Pell, W.G.; Conway, B.E. Analysis of Power Limitations at Porous Supercapacitor Electrodes under Cyclic Voltammetry Modulation and dc Charge. *J Power Sources.* **2001**, *96*, 57-67.

137. Lewandowski, A.; Galinski, M. Practical and Theoretical Limits for Electrochemical Double-layer Capacitors. *J Power Sources.* **2007**, *173*, 822-828.

138. Ricketts, B.W.; Ton-That, C. Self-discharge of Carbon-based Supercapacitors with Organic Electrolytes. *J Power Sources.* **2000**, *89*, 64-69.

139. Hahn, M.; Bartsch, M.; Schnyder, B.; Kotz, R.; Haas, O.; Carlen, M.; Evard, D. Supercapacitors Based on Glassy Carbon and Sulfuric Acid - Mechanisms of Self-Discharge. *PSI Scientific Report.* **2001.** *5*, 67.

140. Hahn, M.; Wuersig, A.; Gallay, R.; Novak, P.; Koetz, R. Gas Evolution in Activated Carbon/Propylene Carbonate Based Double-layer Capacitors. *Electrochem Commun.* **2005**, *7*, 925-930.

141. Kazaryan, S.A.; Litvinenko, S.V.; Kharisov, G.G. Self-discharge of Heterogeneous Electrochemical Supercapacitor of $PbO_2|H_2SO_4|C$ Related to Manganese and Titanium ions. *J Electrochem Soc.* **2008**, *155*, A464-A473.

142. Diab,Y.; Venet, P.; Gualous, H.; Rojat, G. Self-discharge Characterization and Modeling of Electrochemical Capacitor used for Power Electronics Applications. *IEEE Trans Power Electron.* **2009**, *24*, 510-517.

143. Zhang, Q.; Rong, J.; Wei, B. A Divided Potential Driving Self-discharge Process for Single-Walled Carbon Nanotube Based Supercapacitors. *RSC Adv.* **2011,** 1 989-994.

144. Zhang, Q.; Rong, J.; Ma, D.; Wei, B. The Governing Self-discharge Processes in Activated Carbon Fabric-based Supercapacitors with Different Organic Electrolytes. *Energy Environ Sci.* **2011**, *4*, 2152-2159.

145. Dey, A.N.; Sullivan, B.P. Electrochemical Decomposition of Propylene Carbonate on Graphite. *J Electrochem Soc.* **1970**, *117*, 222-224.

146. Shu, Z.X.; McMillan, R.S.; Murray, J.J. Electrochemical Intercalation of Lithium into Graphite. *J Electrochem Soc.* **1993**, *140*, 922-927.

147. Besenhard, J.O. The Electrochemical Preparation and Properties of Ionic Alkali Metal- and Tetraalkylammonium-Graphite Intercalation Compounds in Organic Electrolytes. *Carbon.* **1976**, *14*, 111-115.

148. Yeager, E. Electrocatalysts for Molecular Oxygen Reduction. *Electrochim Acta.* **1984**, *29*, 1527-1537.

149. Feng, X.; Dementev, N.; Feng, W.; Vidic, R.; Borguet, E. Detection of Low Concentration Oxygen Containing Functional Groups on Activated Carbon Fiber Surfaces Through Fluorescent Labeling. *Carbon.* **2006**, *44*, 1203-1209.

150. Vaaler, L.E. Graphite-electrolytic Anodes. Electrochem Tech. **1967**, *May-June*, 170-174.

151. Fuller, T.F.; Gray, G. Carbon Corrosion Induced by Partial Hydrogen Coverage. *ECS Trans.* **2006**, *1*, 345-353.

152. Takeuchi, N.; Fuller, T.F. Modeling and Investigation of Design Factors and their Impact on Carbon Corrosion of PEMFC Electrodes. *J Electrochem Soc.* **2008**, *155*, B770-B775.

153. Kinoshita, K.; Bett, J. Electrochemical Oxidation of Carbon Black in Concentrated Phosphoric Acid at - 135.deg. *Carbon.* **1973**, *11*, 237-247.

154. Pyun, S.; Ryu, Y.; Choi, S. Corrosion Behavior of Platinum-catalyzed Carbon in Phosphoric Acid Solution. *Carbon.* **1994**, *32*, 161-164.

155. Kinoshita, K.; Bett, J. Potentiodynamic Analysis of Surface Oxides on Carbon Blacks. *Carbon.* **1973**, *11*, 403-411.

156. Choo, H.; Kinumoto, T.; Nose, M.; Miyazaki, K.; Abe, T.; Ogumi, Z. Electrochemical Oxidation of Highly Oriented Pyrolytic Graphite During Potential Cycling in Sulfuric Acid Solution. *J Power Sources.* **2008**, *185*, 740-746.

157. Ruiz, V.; Santamaria, R.; Granda, M.; Blanco, C. Long-term Cycling of Carbon-Based Supercapacitors in Aqueous Media. *Electrochim Acta.* **2009**, *54*, 4481-4486.

158. Ruiz, V.; Blanco, C.; Santamaria, R.; Ramos-Fernandez, J.M.; Martinez-Escandell, M.; Supulved-Escribano, A.; Rodriguez-Reinoso, F. An Activated Carbon Monolith as an Electrode Material for Supercapacitors. *Carbon.* **2009**, *47*, 195-200.

159. Borup, R.; Meyers, J.; Pivovar, B.; Kim, Y.; Mukundan, R.; Garland, N.; Myers, D.; Wilson, M.; Garzon, F.; Wood, D.; Zelenay, P.; More, K.; Stroh, K.; Zawadzinski, T.; Boncella, J.; McGrath, J.; Inaba, M.; Miyatake, K.;, Hori, M.; Ota, K.; Ogumi, Z.; Miyata, S.; Nishikata, A.; Siroma, Z.; Uchimoto, Y.; Yasuda, K.; Kimijima, K.; Iwashita, N. Scientific Aspects of Polymer Electrolyte Fuel Cell Durability and Degradation. *Chem Rev.* **2007**, *107*, 3904-3951.

160. Avasarala, B.; Moore, R.; Haldar, P. Surface Oxidation of Carbon Supports due to Potential Cycling under PEM Fuel Cell Conditions. *Electrochim Acta.* **2010**, *55*, 4765-4771.

161. Bard, A.J.; Faulkner, L.R. *Electrochemical Methods: Fundamentals and Applications.* 2nd ed.: John Wiley & Sons, United States of America, 2001.

162. Sawyer, D.T.; Sobkowiak, A.; Roberts, J.J. *Electrochemistry for chemists:* 2nd ed.: John Wiley & Sons, United States of America,1995.

163. Niu, J.; Pell, W.G.; Conway, B.E. Requirements for Performance Characterization of C Double-layer Supercapacitors: Applications to a High Specific-area C-cloth Material. *J Power Sources.* **2006**, *156*, 725-740.

164. Aklilu, M.; Tessema, M.; Redi-Abshiro, M. Indirect Voltammetric Determination of Caffeine Content in Coffee using 1,4-benzoquinone Modified Carbon Paste Electrode. *Talanta.* **2008**, *76*, 742-746.

165. Goldin, M.M.; Kolesnikov, V.A.; Khubutiya, M.S.; Volkov, A.G.; Blanchard, G.J.; Evseev, A.K. Goldin, M.M. Open Circuit Potential Shifts of Activated Carbon in Aqueous Solutions During Chemical and Adsorption Interactions. *J Appl Electrochem.* **2008**, *38*, 1369-1374.

166. Tobias, H.; Soffer, A. The Immersion Potential of High Surface Electrodes. *J Electroanal Chem Interfacial Electrochem.* **1983**, *148*, 221-232.

167. Bayram, E.; Ayranci, E. A Systematic Study on the Changes in Properties of an Activated Carbon Cloth upon Polarization. *Electrochim Acta.* **2011**, *56*, 2184-2189.

168. Boehm, H.P. Carbon Surface Chemistry. *World Carbon*. **2001**, 1, 141-178.

169. Lefevre, M.; Dodelet, J. Fe-based Electrocatalysts made with Microporous Pristine Carbon Black Supports for the Reduction of Oxygen in PEM Fuel Cells. *Electrochim Acta.* **2008**, *53*, 8269-8276.

170. Black, J. The Role of Charge Redistribution in the Self-discharge of Electrochemical Capacitor Electrodes. PhD Dissertation, Dalhousie University, Halifax, Nova Scotia, 2010.

171. Niu, J.; Conway, B.E. Development of Techniques for Purification of Waste Waters: Removal of Pyridine from Aqueous Solution by Adsorption at High-area C-cloth Electrodes using in situ Optical Spectroscopy. *J Electroanal Chem.* **2002**, *521*, 16-28.

172. Kapałka, A.; Fóti, G.; Comninellis, C. Determination of the Tafel Slope for Oxygen Evolution on Boron-doped Diamond Electrodes. *Electrochem Communs.* **2008**, *10*, 607-610.

173. Britto, P.J.; Santhanam, K.S.V.; Rubio, A.; Alonso, J.A.; Ajayan, P.M. Improved Charge Transfer at Carbon Nanotube Electrodes. *Adv Mater.* **1999**, *11*, 154-157.

174. Black, J.; Andreas, H.A. Prediction of the Self-discharge Profile of an Electrochemical Capacitor Electrode in the Presence of both Activation-controlled Discharge and Charge Redistribution. *J Power Sources*. **2010**, *195*, 929-935.

175. Seidel, A. (ed). *Kirk-Othmer Encyclopedia of Chemical Technology.* 5th ed.; John Wiley & Sons, Inc.: United States of America, 1992.

176. Burg, P.; Cagniant, D. Characterization of Carbon Surface Chemistry. *Chem.Phys.Carbon*. **2008**, *30*, 129-175.

177. Goertzen, S.L. Characterization of Electrode Materials for Aqueous-based Eletrochemical Capacitors using Spectroscopy, the Boehm Titration and Spectroelectrochemistry. MSc dissertation, Dalhousie University, Halifax, Nova Scotia, 2010.

178. Tennant, M.F.; Mazyck, D.W. The Role of Surface Acidity and Pore Size Distribution in the Adsorption of 2-methylisoborneol via Powdered Activated Carbon. *Carbon.* **2007**, *45*, 858-864.

179. Mestre, A.S.; Pires, J.; Nogueira, J.M.F.; Carvalho, A.P. Activated Carbons for the Adsorption of Ibuprofen. *Carbon.* **2007**, *45*, 1979-1988.

180. Kato, Y.; Machida, M.; Tatsumoto, H. Inhibition of Nitrobenzene Adsorption by Water Cluster Formation at Acidic Oxygen Functional Groups on Activated Carbon. *J Colloid Interface Sci.* **2008**, *322*, 394-398.

181. Hermans, S.; Diverchy, C.; Demoulin, O.; Dubois, V.; Gaigneaux, E.M.; Devillers, M. Nanostructured Pd/C Catalysts Prepared by Grafting of Model Carboxylate Complexes onto Functionalized Carbon. *J Catal.* **2006**, *243*, 239-251.

182. Kim, Y.; Mitani, T. Competitive Effect of Carbon Nanotubes Oxidation on Aqueous EDLC Performance: Balancing Hydrophilicity and Conductivity. *J Power Sources.* **2006**, *158*, 1517-1522.

183. Gonzalez-Guerrero, A.B.; Mendoza, E.; Pellicer, E.; Alsina, F.; Fernandez-Sanchez, C.; Lechuga, L.M. Discriminating the Carboxylic Groups from the Total Acidic Sites in Oxidized Multi-wall Carbon Nanotubes by Means of Acid-base Titration. *Chem.Phys.Lett.* **2008**, *462*, 256-259.

184. Laszlo, K. Adsorption from Aqueous Phenol and Aniline Solutions on Activated Carbons with Different Surface Chemistry. *Colloids Surf, A.* **2005**, *265*, 32-39.

185. Starck, J.; Burg, P.; Cagniant, D.; Tascon, J.M.D.; Martinez-Alonso, A. The Effect of Demineralisation on a Lignite Surface Properties. *Fuel.* **2004**, *83*, 845-850.

186. Lopez-Garzon, F.J.; Domingo-Garcia, M.; Perez-Mendoza, M.; Alvarez P.M.; Gomez-Serrano, V. Textural and Chemical Surface Modifications Produced by Some Oxidation Treatments of a Glassy Carbon. *Langmuir.* **2003**, *19*, 2838-2844.

187. Zhang, N.; Wang, L.; Liu, H.; Cai, Q. Nitric Acid Oxidation on Carbon Dispersion and Suspension Stability. *Surf Interface Anal.* **2008**, *40*, 1190-1194.

188. Horton, R.; Moran, L.A.; Scrimgeuor, G.; Perry, M.; and Rawn, D. *Principles of Biochemistry.* 4th ed.; Pearson Prentice Hall: United States of America, 2006.

189. Patni, A.G.; Ludlow, D.K.; Adams, C.D. Characteristics of Ground Granular Activated Carbon for Rapid Small-Scale Column Tests. *J Environ Eng*. **2008**, *134*, 216-221.

190. Otake, Y.; Jenkins, R.G. Characterization of Oxygen-Containing Surface Complexes Created on a Microporous Carbon by Air and Nitric Acid Treatment. *Carbon.* **1993**, *31*, 109-121.

191. Noh, J.S.; Schwarz, J.A. Effect of Nitric Acid Treatment on the Surface Acidity of Activated Carbons. *Carbon.* **1990**, *28*, 675-682.

192. Greenwood, N.N.; Earnshaw, A. *Chemistry of the Elements.* 2nd ed.; Butterworth Heinemann: Great Britain: 1997.

193. Compton, R.G.; Eklund, J.C.; Page, S.D.; Sanders, G.H.W.; Booth, J. Voltammetry in the Presence of Ultrasound. Sonovoltammetry and Surface Effects. *J Phys Chem.* **1994**, *98*, 12410-12414.

194. Guittonneau, F.; Abdelouas, A.; Grambow, B.; Huclier, S. The Effect of High Power Ultrasound on an Aqueous Suspension of Graphite. *Ultrason Sonochem.* **2010**, *17*, 391-398.

195. Kastening, B.; Heins, M. Properties of Electrolytes in the Micropores of Activated Carbon. *Electrochim Acta.* **2005**, *50*, 2487-2498.